AD-A191 747 FINITE ELEMENT ANALYSIS OF AN UNDERGROUND STRUCTURE(U) 1/2
FLORIDAUUNIV GAINESVILLE DEPT OF CIVIL ENGINEERING
M C MCVAY ET AL JAN 88 AFESC/ESL-TR-87-05
UNCLASSIFIED F08635-83-C-0136 F/G 13/13 NL

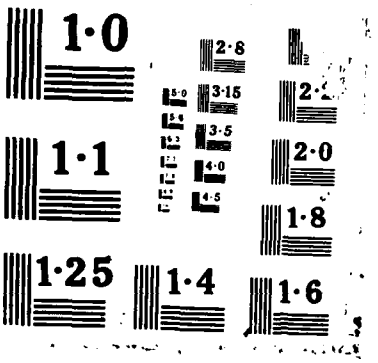
1·0
1·1
1·25
1·4
1·6
2·8
3·15
3·5
4·0
2·0
1·8

ESL-TR-87-05

FINITE ELEMENT ANALYSIS OF AN UNDERGROUND STRUCTURE

M.C. MCVAY, S. ZALZMAN

UNIVERSITY OF FLORIDA
DEPT OF CIVIL ENGINEERING
GAINESVILLE FL 32611

JANUARY 1988

FINAL REPORT

SEPTEMBER 1985 - SEPTEMBER 1986

AFESC

ENGINEERING & SERVICES LABORATORY
AIR FORCE ENGINEERING & SERVICES CENTER
TYNDALL AIR FORCE BASE, FLORIDA 32403

REPORT DOCUMENTATION PAGE

Form Approved
OMB No. 0704-0188

1a. REPORT SECURITY CLASSIFICATION UNCLASSIFIED	1b. RESTRICTIVE MARKINGS
2a. SECURITY CLASSIFICATION AUTHORITY	3. DISTRIBUTION / AVAILABILITY OF REPORT Approved for public release. Distribution unlimited.
2b. DECLASSIFICATION / DOWNGRADING SCHEDULE	
4. PERFORMING ORGANIZATION REPORT NUMBER(S)	5. MONITORING ORGANIZATION REPORT NUMBER(S) ESL-TR-87-05
6a. NAME OF PERFORMING ORGANIZATION UNIVERSITY OF FLORIDA DEPT OF CIVIL ENGINEERING 6b. OFFICE SYMBOL (If applicable)	7a. NAME OF MONITORING ORGANIZATION
6c. ADDRESS (City, State, and ZIP Code) GAINESVILLE, FL 32611	7b. ADDRESS (City, State, and ZIP Code)
8a. NAME OF FUNDING / SPONSORING ORGANIZATION AIR FORCE ENGINEERING AND SERVICES CENTER 8b. OFFICE SYMBOL (If applicable)	9. PROCUREMENT INSTRUMENT IDENTIFICATION NUMBER Contract #F08635-83-C-0136
8c. ADDRESS (City, State, and ZIP Code) AFESC Tyndall AFB FL 32404	10. SOURCE OF FUNDING NUMBERS PROGRAM ELEMENT NO: 6.2 / PROJECT NO.: 2673 / TASK NO: 0048 / WORK UNIT ACCESSION NO: N/A

11. TITLE (Include Security Classification)

FINITE ELEMENT ANALYSIS OF AN UNDERGROUND STRUCTURE

12. PERSONAL AUTHOR(S)
M.C. McVay and S. Zalzman-c

13a. TYPE OF REPORT	13b. TIME COVERED	14. DATE OF REPORT (Year, Month, Day)	15. PAGE COUNT
Final	FROM SEP 85 TO SEP 86	JAN 88	164

16. SUPPLEMENTARY NOTATION
Availability of this report is specified on reverse of front cover

17. COSATI CODES			18. SUBJECT TERMS (Continue on reverse if necessary and identify by block number)
FIELD	GROUP	SUB-GROUP	Finite Element Analysis NONSAP-C Scaled Structures Blast Loads
13	13		
13	02		

19. ABSTRACT (Continue on reverse if necessary and identify by block number)

The evaluation and design of underground structures subjected to blast loads are presently based upon empirical correlations of field studies and some numerical analysis of structural components. Recently, the United States Air Force initiated an investigation of the feasibility of implementing analytical procedures and computer models to evaluate the response of these structures.

This study was concerned with the evaluation of the finite element program NONSAP-C (nonlinerar elasto-dynamic finite element program) as a means to predict the response of a structure subjected to different loading conditions.

The evaluation was made by comparing the predicted responses with the observed responses from laboratory tests. These tests were performed on laboratory scaled structures with simple geometry. Three types of tests were

20. DISTRIBUTION / AVAILABILITY OF ABSTRACT	21. ABSTRACT SECURITY CLASSIFICATION
☒ UNCLASSIFIED/UNLIMITED ☐ SAME AS RPT ☐ DTIC USERS	Unclassified
22a. NAME OF RESPONSIBLE INDIVIDUAL 2LT STEVEN T. KUENNEN	22b. TELEPHONE (Include Area Code) (904) 283-6138 / 22c. OFFICE SYMBOL HQ AFESC/RDCS

DD Form 1473, JUN 86 *Previous editions are obsolete.* SECURITY CLASSIFICATION OF THIS PAGE

(Block 19. continued:)
conducted on the scaled structures. The first two tests consisted of the application of static dynamic loads to a scaled concrete structure. The third test consisted of the application of an explosive load to a scaled concrete structure buried in dry sand and subjected to a high gravity environment. The three types of tests were simulated with the program NONSAP-C.

This study concluded that the program NONSAP-C was adequate for predicting the response of a scaled structure subjected to simple static and dynamic loads. The study also concluded that the program NONSAP-C was adequate for predicting the general response of a scaled underground structure subjected to a blast load in a high gravity environment. However, the results were not accurate and further investigation is required

PREFACE

This report was prepared by the Department of Civil Engineering, University of Florida, Gainesville, Florida 32611 under Contract Number F08635-83-C-0136, Task 85-1, for the Air Force Engineering and Services Center, Engineering and Services Laboratory, Engineering Research Division, Tyndall AFB, Florida 32403-6001.

This report is published as submitted to the University of Florida by Miss Sarah de Los Angles Zalzman-Cendo, as her Master of Engineering thesis under the direction of Professors M.C. McVay, F.C. Townsend and D. Bloomquist and assistance from fellow graduate student Habibollah Tabatabai. Messrs. Paul L. Rosengren, Jr. and John R. Hayes, and Lt Steven T. Kuennen were the HQ AFESC/RDCS Project Officers. This report summarizes work performed between September 1985 and September 1986 and is published as submitted because of its interest to the USAF Scientific and Engineering Community.

This report evaluates finite element program NONSAP-C (nonlinear elasto-dynamic finite element program) to predict the response of buried structures subjected to blast loadings. Comparisons between NONSAP-C predictions and results observed from centrifugal model tests were lacking in quantitative agreement.

This report has been reviewed by the Public Affairs Office (PA) and is releasable to the National Technical Information Service (NTIS). At NTIS, it is available to the general public, including foreign nationals.

This technical report has been reviewed and is approved for publication.

STEVEN T. KUENNEN, 2LT, USAF
Project Officer

ROBERT R. COSTIGAN, Lt Col, USAF
Chief, Engineering Research Division

WILLIAM S. STRICKLAND, GM-14
Chief, Facilities and Systems

LAWRENCE D. HOKANSON, Col, USAF
Director, Engineering and Services Laboratory

(The reverse of this page is blank)

TABLE OF CONTENTS

Page

ACKNOWLEDMENTS....ii

LIST OF TABLES....vi

LIST OF FIGURES....vii

ABSTRACT....xiv

CHAPTERS

ONE INTRODUCTION....1

General....1
Objective....1
Scope....2

TWO LITERATURE REVIEW....7

THREE GENERAL STUDY....11

Material Modeling of Concrete....11
General....11
Chen and Chen Elastic Plastic Model....11
Orthotropic Variable-Modulus Model....13
Material Study....16
Design of the Finite Element Mesh....21

FOUR ANALYSIS OF THE SINGLE BAY STRUCTURE....33

Introduction....33
Static Analysis....34
Dynamic Analysis....35

FIVE ANALYSIS OF THE SOIL-STRUCTURE SYSTEM....43

General....43
Input Requirements....43
Finite Element Mesh Design....45
Calculation of Loading Functions....61
Description of Element Groups....63
Details of the Analysis....68

Page

SIX PRESENTATION AND DISCUSSION OF RESULTS.....71

Introduction.....71
Processing of the Results.....71
Static Analysis.....71
Dynamic Analysis.....74
Blast Analysis.....77
Presentation and Discussion.....78
Static Analysis.....78
Dynamic Analysis.....95
Blast Analysis.....116

SEVEN CONCLUSIONS AND RECOMMENDATIONS.....130

Review of Objectives.....130
Summary of Results.....130
Static Analysis.....130
Dynamic Analysis.....131
Blast Analysis.....131
Conclusions.....132
Recommendations.....133

APPENDIX

A CALCULATION OF THE MATERIAL CONSTANTS USED IN THE CHEN AND CHEN CONCRETE MODEL.....134

B MODAL ANALYSIS.....136

C CALCULATION OF THE STEEL REINFORCEMENT.....143

BIBLIOGRAPHY.....149

BIOGRAPHICAL SKETCH.....151

LIST OF TABLES

Table		Page
3.1	Properties of the Microconcrete Used in the Analysis of the Miniature Structure	12
3.2	Input Parameters Used in NONSAP-C With the Chen and Chen Elastic Plastic Model	15
3.3	Properties of the Standard Wire Gauges Used as Reinforcement in the Scaled Models	15
3.4	Load Function Used in NONSAP-C for the Material Study	19
5.1	Pressure Time Functions Used in NONSAP-C Characterize the Shock Wave of the Blast	67
5.2	Material Properties Used in NONSAP-C for the Blast Load Analysis	70
6.1	Summary of Results	72
6.2	Finite Element Numbers and Integration Point Numbers Used for Comparison of Strains With Static and Dynamic Tests	75
C.1	Cross Sectional Areas and Properties of Truss Bars Used With the Chen & Chen and Linear Models	146
C.2	Ratios of Steel Used With the Orthotropic Variable-Modulus Model	147

LIST OF FIGURES

Figure		Page
1.1	Dimensions of the Prototype Structure (after Gill, 1985)	3
1.2	Scaled Single Bay Structure Analyzed in the Static and Dynamic Analyses	5
1.3	Scaled Soil-Structure Analyzed in the Blast Load Analysis	6
2.1	Soil-Structure System Studied by Yovaish (1984)	8
3.1	Failure and Discontinuous Surfaces in Principal Stress Space (Chen, Chen, 1975)	14
3.2	Three-dimensional Element Representing the Concrete Block in the Material Study	17
3.3	Support of the Block Used in the Material Study	18
3.4	Results of the Material Study	20
3.5	Portion of the Structure (Strip) Discretized for the Static and Dynamic Analysis	23
3.6	Fine Discretization of the Strip (node number in parenthesis is on the back plane)	25
3.7	Coarse Discretization of the Strip (node number in parenthesis is on the back plane	26
3.8	Orientation of the Strip in Space	28
3.9	Comparison of the Average Bending Stresses Induced in the Top Slab in the Finite Element Mesh Study (stresses in psi)	29

Page

3.10 Comparison of the Average Bending Stresses Induced in the Wall in the Finite Element Mesh Study (stresses in psi).....30

3.11 Comparison of the Average Bending Stresses Induced in the Bottom Slab in the Finite Element Mesh Study (stresses in psi).....31

4.1 Typical Three-Dimensional Element in NONSAP-C with Eight Integration Point Numbers.....36

4.2 Typical Three-Dimensional Element in NONSAP-C with Twenty Seven Integration Point Numbers.....38

4.3 Loading Function Used in the Dynamic Analysis of the Non-Reinforced Structure.....40

4.4 Loading Function Used in the Dynamic Analysis of the Reinforced Structure.....41

5.1 Schematic of the Test Setup in the Centrifuge Bucket.....44

5.2 One Quarter of the Soil-Structure System Discretized.....47

5.3 Discretization of the System in the z-y Plane for x=0.....48

5.4 Discretization of the System in the z-y Plane for x=0.2.....49

5.5 Discretization of the System in the z-y Plane for x=0.4.....50

5.6 Discretization of the System in the z-y Plane for x=0.65.....51

5.7 Discretization of the System in the z-y Plane for x=0.9.....52

5.8 Discretization of the System in the z-y Plane for x=1.15.....53

5.9 Discretization of the System in the z-y Plane for x=1.4.....54

Page

5.10 Discretization of the System in the z-y Plane for x=1.7.....55

5.11 Discretization of the System in the z-y Plane for x=2.0.....56

5.12 Discretization of the System in the z-y Plane for x=3.0.....57

5.13 Discretization of the System in the z-y Plane for x=4.0.....58

5.14 Discretization of the System in the z-y Plane for x=5.5.....59

5.15 Discretization of the System in the z-y Plane for x=6.0.....60

5.16 Shock Wave Parameters for Spherical TNT Explosions in Free Air (after U.S. Army Engineer Waterways, 1982).....64

5.17 Reflected Pressure Coefficient versus Angle of Incidence (after U.S. Army Waterways, 1982).....65

5.18 Global Nodes (represented by numbers) Used to Calculate the Pressure Time Functions (f_i) for Loading the Burster Slab.....66

6.1 Location of Accelerometers and Strain Gages (numbers designate accelerometers and gage numbers).....73

6.2 Element Numbers in the Coarse Discretization of the Strip.....76

6.3 Comparison of Predicted and Observed Strains in the Static Analysis of the Nonreinforced Structure (gage #1).....79

6.4 Comparison of Predicted and Observed Strains in the Static Analysis of the Nonreinforced Structure (gage #2).....80

6.5 Comparison of Predicted and Observed Strains in the Static Analysis of the Nonreinforced Structure (gage #3).....81

Page

6.6 Comparison of Predicted and Observed Strains in the Static Analysis of the Nonreinforced Structure (gage #4).....82

6.7 Comparison of Predicted and Observed Strains in the Static Analysis of the Nonreinforced Structure (gage #5).....83

6.8 Comparison of Predicted and Observed Strains in the Static Analysis of the Nonreinforced Structure (gage #6).....84

6.9 Comparison of Predicted and Observed Strains in the Static Analysis of the Nonreinforced Structure (gage #8).....85

6.10 Comparison of Predicted and Observed Strains in the Static Analysis of the Reinforced Structure (gage #1).....87

6.11 Comparison of Predicted and Observed Strains in the Static Analysis of the Reinforced Structure (gage #2).....88

6.12 Comparison of Predicted and Observed Strains in the Static Analysis of the Reinforced Structure (gage #3).....89

6.13 Comparison of Predicted and Observed Strains in the Static Analysis of the Reinforced Structure (gage #4).....90

6.14 Comparison of Predicted and Observed Strains in the Static Analysis of the Reinforced Structure (gage #5).....91

6.15 Comparison of Predicted and Observed Strains in the Static Analysis of the Reinforced Structure (gage #6).....92

6.16 Comparison of Predicted and Observed Strains in the Static Analysis of the Reinforced Structure (gage #7).....93

6.17 Comparison of Predicted and Observed Strains in the Static Analysis of the Reinforced Structure (gage #8).....94

Page

6.18 Comparison of Predicted and Observed Accelerations at the Center of the Top Slab of the Nonreinforced Structure.....97

6.19 Comparison of Predicted and Observed Accelerations at the Center of the In-Wall of the Nonreinforced Structure.....98

6.20 Predicted Average Bending Stresses at the Center of the Inside Top Slab and at the Center of the Inside Wall (non-reinforced structure).....99

6.21 Comparison of Predicted and Observed Strains in the Dynamic Analysis of the Non-Reinforced Structure (gage #1).....101

6.22 Comparison of Predicted and Observed Strains in the Dynamic Analysis of the Nonreinforced Structure (gage #3).....102

6.23 Comparison of Predicted (time step of 0.015 ms) and Observed Accelerations at the Center of the Top Slab of the Reinforced Structure.....104

6.24 Comparison of Predicted (time step of 0.010 ms) Accelerations at the Center of the Top Slab of the Reinforced Structure.....106

6.25 Comparison of Predicted (time step of 0.010 ms) Accelerations at the Center of the Inside Wall of the Reinforced Structure.....107

6.26 Comparison of Predicted (time step of 0.010 ms) and Observed Accelerations at the Center of the Top Slab of the Reinforced Structure.....108

6.27 Comparison of Predicted (Variable-Modulus) and Observed Accelerations at the Center of the Top Slab of the Reinforced Structure.....109

6.28 Predicted Average Bending Stresses at the Center of the Inside Top Slab and at the Center of the Inside Wall (reinforced structure).....111

Page

6.29 Comparison of Predicted (time step of 0.010 ms) and Observed Accelerations at the Center of the Inside Wall of the Reinforced Structure.....112

6.30 Comparison of Predicted (Variable-Modulus) and Observed Accelerations at the Center of the Inside Wall of the Reinforced Structure.....113

6.31 Comparison of Predicted (linear) and Observed Accelerations at the Center of the Top Slab of the Reinforced Structure.....114

6.32 Comparison of Predicted (linear) and Observed Accelerations at the Center of the Inside Wall of the Reinforced Structure.....115

6.33 Comparison of Predicted and Observed Accelerations at the Center of the Top Slab (blast analysis).....117

6.34 Comparison of Predicted and Observed Accelerations at the Center of the Inside Wall (blast analysis).....118

6.35 Comparison of Predicted and Observed Strains in the Blast Analysis of the Soil-Structure System (gage #1).....120

6.36 Comparison of Predicted and Observed Strains in the Blast Analysis of the Soil-Structure System (gage #2).....121

6.37 Comparison of Predicted and Observed Strains in the Blast Analysis of the Soil-Structure System (gage #5).....122

6.38 Comparison of Predicted and Observed Strains in the Blast Analysis of the Soil-Structure System (gage #6).....123

6.39 Comparison of Predicted and Observed Strains in the Blast Analysis of the Soil-Structure System (gage #7).....124

Page

6.40 Comparison of Predicted and Observed Strains in the Blast Analysis of the Soil-Structure System (gage #8).....125

B.1 Lines A-B and C-D on the Top Slab of the Structure.....138

B.2 Bending Moment and Displacement Diagrams of Line A-B at Time Step 25.....139

B.3 Bending Moment and Displacement Diagrams of Line A-B at Time Step 35.....140

B.4 Bending Moment and Displacement Diagrams of Line C-D at Time Step 25.....141

B.5 Bending Moment and Displacement Diagrams of Line C-D at Time Step 35.....142

C.1 Location of Truss Bars in the Strip.....144

C.2 Elements for Which Steel Ratios Were Specified in the Orthotropic Variable-Modulus Model.....148

CHAPTER ONE
INTRODUCTION

General

The United States Air Force is involved in the economic design and survival of underground structures subjected to blast loadings. Numerical modeling of the response of this type of structures can greatly increase the ability of engineers to evaluate design and assess the vulnerability to various threats. In order to validate computer models, extensive testing of full-scale structures is necessary; however, this type of testing involves considerable cost and safety risk. As an alternative testing procedure for reducing cost and safety risk, centrifugal modeling of reduced-scale underground structures subjected to blast loads is being implemented (Gill, 1985). These scale models provide a viable method for evaluating numerical and computer models.

Objective

The primary objective of this research is to evaluate the finite element program NONSAP-C (nonlinear elasto-dynamic finite element program) as a means to predict

a) the response of a laboratory scaled concrete structure subjected to static loads;
b) the response of a laboratory scaled concrete structure subjected to dynamic loads; and
c) the response of a laboratory scaled concrete structure buried in sand subjected to a a blast load in a high gravity environment.

Comparisons between computer predictions and laboratory tests will be made to assess the capabilities of the program.

Scope

This research was conducted as Part V of a five-phase project. Part IV of the project involved static, dynamic, and explosive testing of laboratory scale models; and the results are documented in Centrifugal Modeling of a Subterranean Structure Subjected to Blast Loading by John J. Gill (Gill, 1985). The modeling scale used in the investigation was 1/60th of the prototype size. The dimensions of the prototype structure are depicted in Figure 1.1.

The finite element program NONSAP-C (nonlinear elasto-dynamic finite element program) (Anderson, Smith, Carruthers, 1982) was used in this research to evaluate the response of laboratory scale models subjected to different loading conditions. The predicted response of the structure

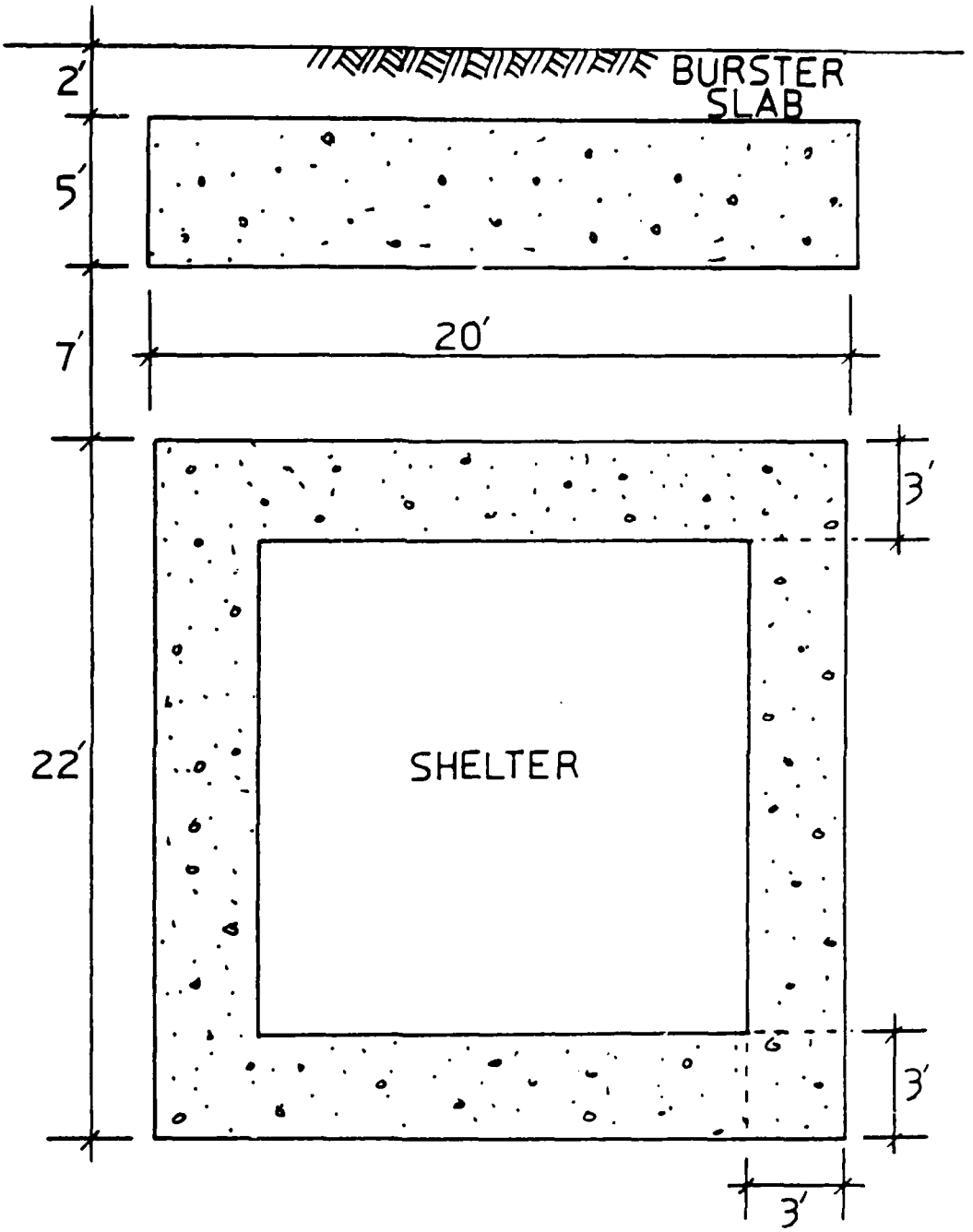

Figure 1.1. Dimensions of the Prototype Structure (after Gill, 1985)

with NONSAP-C was compared to the response of the models in the laboratory.

This investigation was divided into three major tasks:

1. Study of the material models used in NONSAP-C for evaluating concrete response, and the study of the finite element mesh effects;
2. Analysis of the response of the scaled single-bay structure (Figure 1.2) subjected to static and dynamic loads applied at the center of the top slab;
3. Analysis of the response of the scaled buried structure (Figure 1.3) subjected to an explosive load applied at the center and top of the burster slab in a 60-g environment.

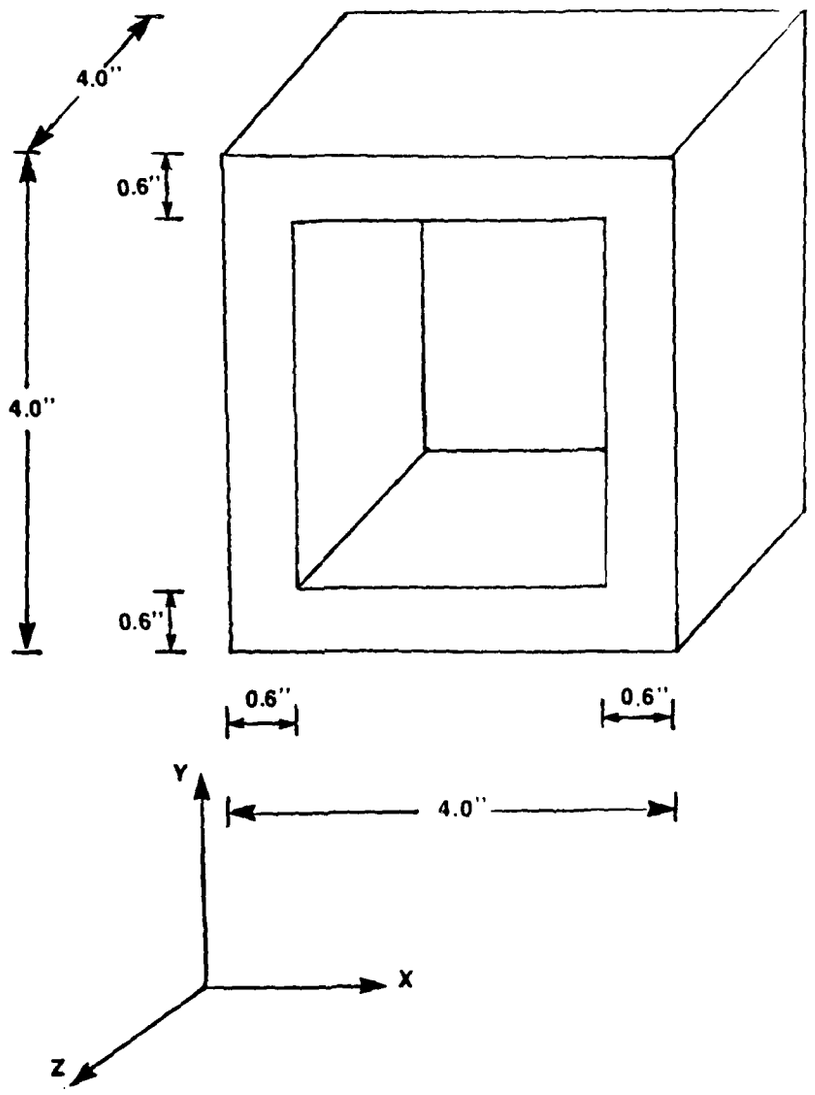

Figure 1.2. Scaled Single Bay Structure Analyzed in the Static and Dynamic Analyses

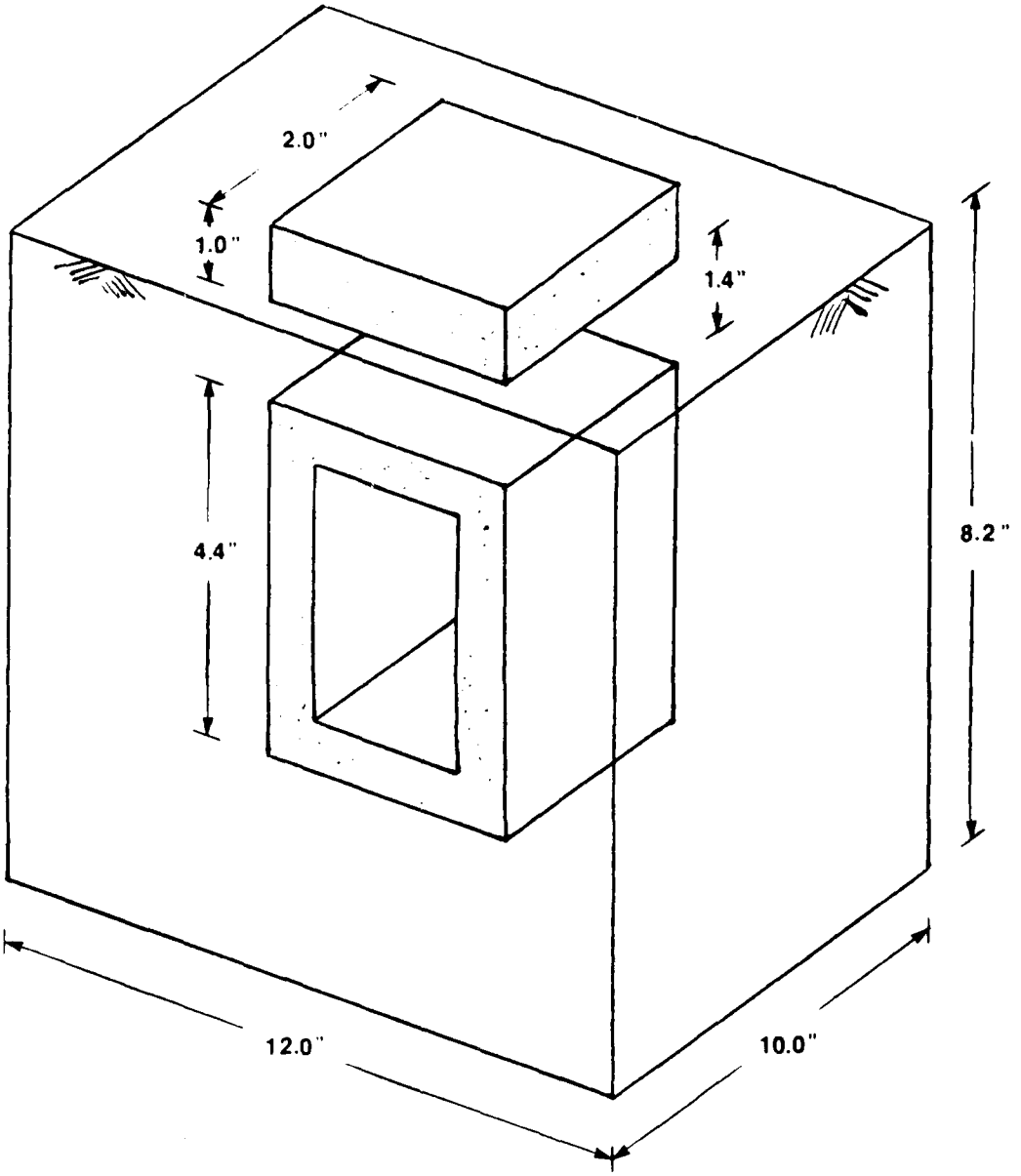

Figure 1.3. Scaled Soil-Structure Analyzed in the Blast Load Analysis

CHAPTER TWO
LITERATURE REVIEW

The design of a structure is based on its anticipated response to applied loadings. Presently, the evaluation and design of earth covered structures subjected to blast loads are based upon empirical correlations of field studies and some numerical analyses of structural components (Townsend et al., no date). Recently, the Air Force initiated an investigation of the feasibility of implementing analytical procedures and computer models to evaluate the response of an underground structure subjected to an explosive charge.

Douglas J. Yovaish (1984) investigated the ability to theoretically evaluate the response of these types of structures. He specifically studied the response of the soil-structure system shown in Figure 2.1 subjected to a near blast using the finite element program NONSAP-C for the analysis. He studied the stability and convergence of the program and the errors associated in the step-by-step solution scheme to solve the equation of motion in dynamic problems. Yovaish also added a nonlinear soil model (Modified Duncan Model) to the NONSAP-C code in order to incorporate the stress dependent behavior of soils into the analysis.

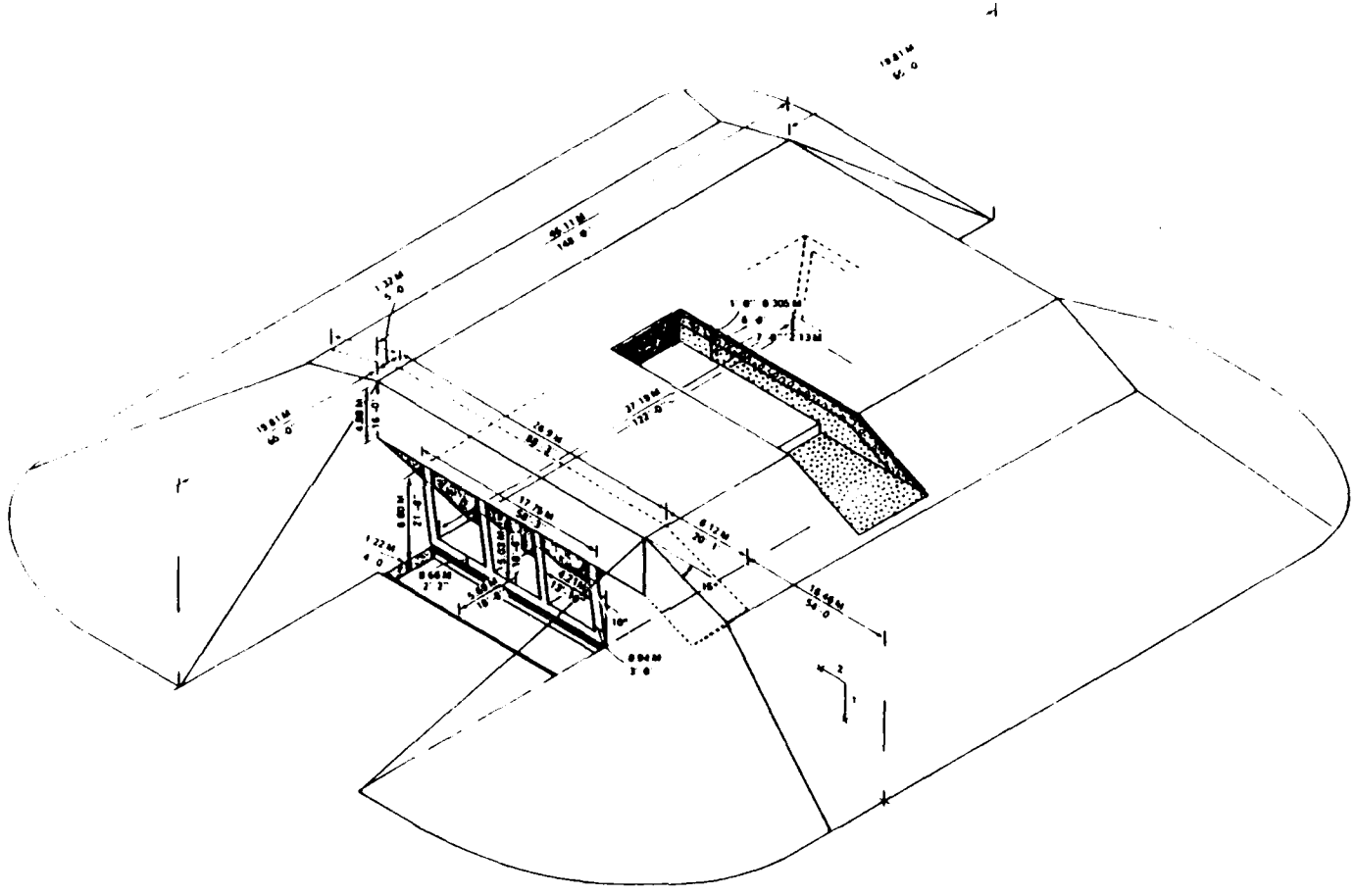

Figure 2.1. Soil-Structure System Studied by Yovaish (1984)

Yovaish studied the effects of using different time steps of integration in the analysis. He reported that smaller time steps produced the highest peak stresses, with the greatest effect near the area where the load was applied. This effect was due primarily to the nonlinear stress dependency of the soil in regions of high stress gradients. Also, he reported that at lower stress gradients (away from the point of detonation) time step sensitivity decreased. Likewise, he compared time displacements at different points of the soil-structure system and reported that displacements near the detonation increased with decreasing time steps, indicating that convergence had not been achieved.

Yovaish also studied the effects of material nonlinearity in the analysis of the blast problem. He reported that in general, the nonlinear analysis predicted higher stresses than the linear analysis, and as much as 10 times greater than those predicted by empirical design methods (Townsend et al., no date).

The accuracy of the predicted response for the soil structure system investigated by Yovaish could not be assessed due to the lack of actual test data. However, his study revealed several inadequacies in the finite element idealization with regard to node and element placement and the use of linear and nonlinear materials. He concluded that a finer discretization near the detonation was necessary,

and that the elements near that area should be modeled with nonlinear properties.

CHAPTER THREE
GENERAL STUDY

Material Modeling of Concrete

General

The objective of this phase of this research was to examine the numerical models in NONSAP-C used for describing concrete response and to investigate the effects of finite element mesh size on the predicted response. The program NONSAP-C uses different material models for simulating concrete response. Two of the nonlinear material models, the Chen and Chen Elastic Plastic Model and the Orthotropic Variable-Modulus Model (Anderson et al., 1982) were studied by predicting the stress-strain response characteristic in a laboratory compressive strength test. The compressive strength tests were performed on the microconcrete used in the laboratory scaled models (Gill, 1985); the properties of which are given in Table 3.1.

A brief explanation of the material models will follow.

Chen and Chen Elastic Plastic Model

The elastic plastic model of Chen and Chen (Chen, Chen, 1975) assumes the concrete to be a continuous, isotropic, and linearly elastic-plastic strain-hardening-fracture material. In this theory, the stress states are limited by a

Table 3.1. Properties of the Microconcrete Used in the Analysis of the Miniature Structure

Microconcrete Properties	
Compressive Strength	4085 psi
Tensile Strength	327 psi
Modulus of Elasticity	3.3×10^6 psi
Modulus of Rupture	601 psi
Unit Weight	130 pcf
Poisson's Ratio	0.15

Source: Cunningham et al., 1986.

failure surface (Figure 3.1) that is a function of the first invariant of the stress state tensor and the second invariant of the deviatoric stress tensor. Two other surfaces are defined: an initial discontinuous surface and a loading surface (Figure 3.1). The functions that describe these surfaces are defined for a compression region and a tension region thereby incorporating biaxial strength data. There are eight material constants used in the surface function equations which are determined from the concrete tensile and compressive strengths. These constants and three other concrete properties are the input parameters used in NONSAP-C for the Chen and Chen Elastic Plastic Model. The values used in the material analysis are listed in Table 3.2. The procedure to calculate these constants is described in Appendix A.

Orthotropic Variable-Modulus Model

The Orthotropic Variable-Modulus Model (Isenberg, Adham, 1970) defines a composite material which incorporates the concrete and reinforcing steel properties. This model allows for tensional cracking. Orthotropic axes are defined in the direction of principal stresses prior to the crack formation. The weakest direction is perpendicular to the crack. When the crack forms, the concrete stress is released and redistributed. The redistribution of the stresses is affected by the presence or absence of steel reinforcement across the crack. The input parameters for this model are

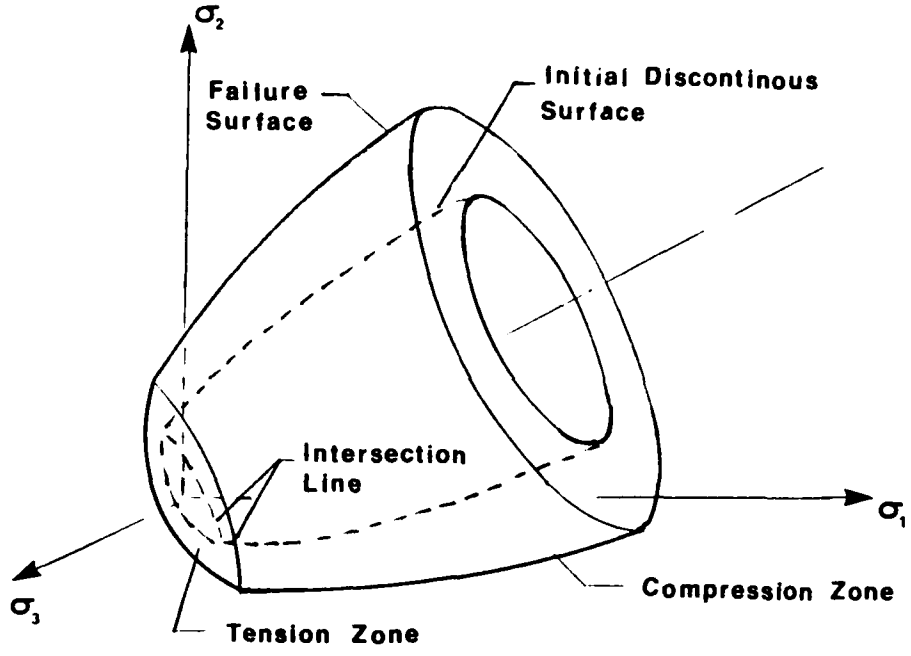

Figure 3.1. Failure and Discontinuous Surfaces in Principal Stress Space (Chen, Chen, 1975)

Table 3.2. Input Parameters Used in NONSAP-C With the Chen and Chen Elastic Plastic Model

Parameters	Compression Region	Tension-Compression Region
A_o	575.42	1037.50
τ_o	1120.68	256.17
A_u	1309.09	2305.00
τ_u	2480.23	570.09

Table 3.3. Properties of the Standard Wire Gauges Used as Reinforcement in the Scaled Models

Standard Wire Gauge Properties	
Modulus of Elasticity	2.9×10^7 psi
Yield Strength	5.1×10^4 psi
Plastic Modulus	2.9×10^5 psi

Source: Cunningham et al., 1986

the elastic properties of concrete and steel, the tensile and compressive strength of concrete, the steel yield strength and hardening modulus, and the percentages of the steel reinforcement.

The reinforcement in the laboratory scale structure was modeled with Standard Wire Gages of sizes 28, 24, and 22 (Cunningham et al., 1986). The properties of the reinforcement used in the miniature structures are listed in Table 3.3.

In the orthotropic model, the reinforcement is included as a ratio of the area of steel to the area of the concrete element.

Material Study

The material model study consisted of predicting the response of a laboratory compressive strength test of micro-concrete. For ease in developing the finite element grid a 3" × 3" × 6" block instead of a concrete cylinder was modeled. The block was modeled with a single three-dimensional continuum element with 20 nodes (see Figure 3.2) and it was supported at the bottom as shown in Figure 3.3. The pressure load in Table 3.4 was applied at the top of the block.

Two analyses of the response of the block were performed using the two different material models described previously. The results of the analyses are given in Figure 3.4 along with the results of a typical compressive strength test (Gill, 1985).

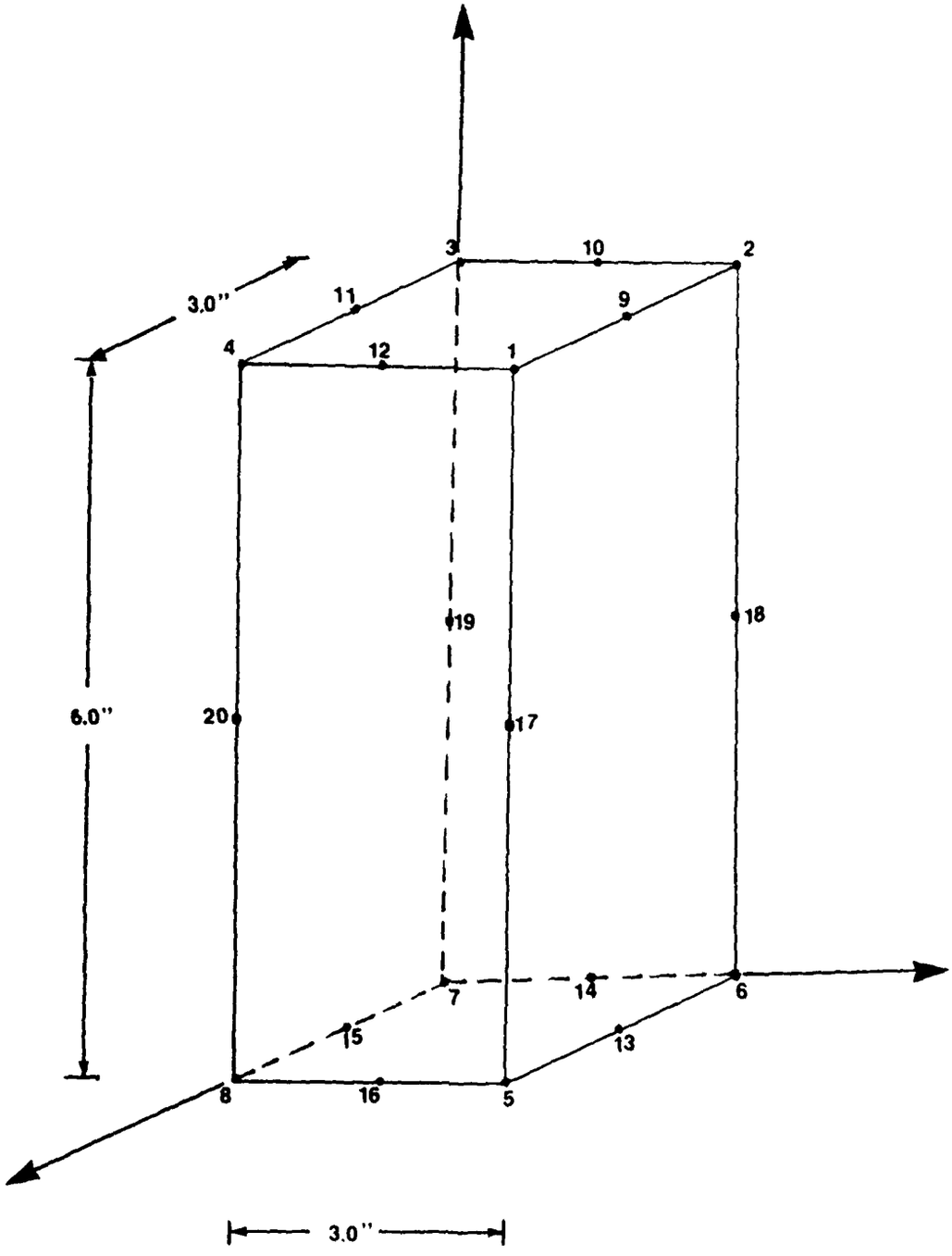

Figure 3.2. Three-dimensional Element Representing the Concrete Block in the Material Study

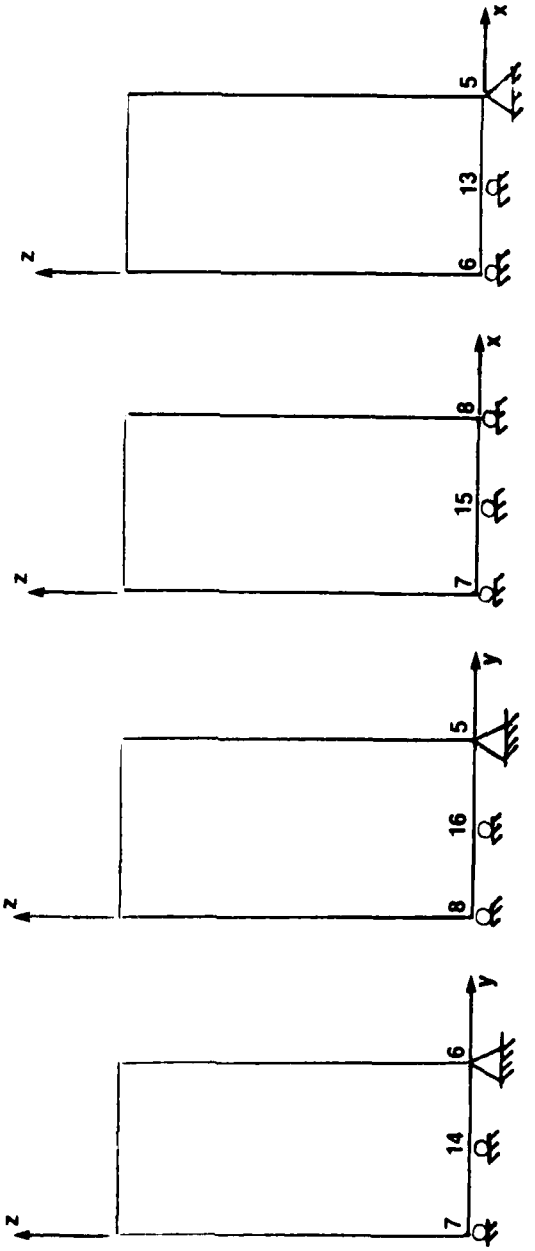

Figure 3.3. Support of the Block Used in the Material Study

Table 3.4. Load Function Used in NONSAP-C for the Material Study

Time Value (s)	Function Value (psi)
0.0	0.0
1.0	278.0
2.0	556.0
3.0	833.0
4.0	1111.0
5.0	1389.0
6.0	1667.0
7.0	1944.0
8.0	2222.0
9.0	2500.0
10.0	2778.0
11.0	3056.0
12.0	3333.0
13.0	3611.0
14.0	3889.0
15.0	4167.0
16.0	4444.0
17.0	4722.0
18.0	5000.0
19.0	5278.0
20.0	5556.0
29.0	8058.0

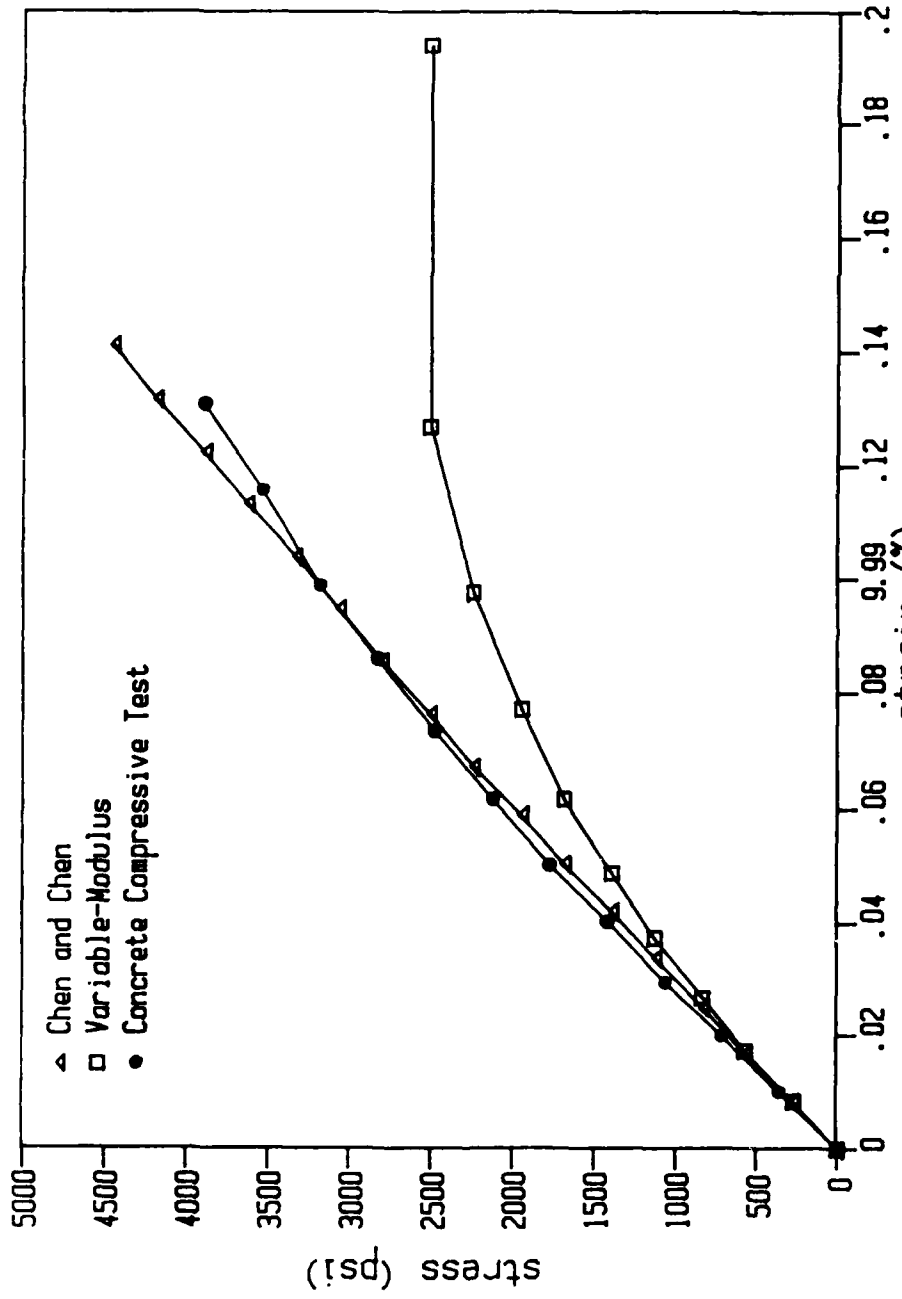

Figure 3.4. Results of the Material Study

As shown, a good correlation with the compressive strength test was obtained using the Chen and Chen model. The Orthotropic Variable-Modulus model predicted failure at a relatively low stress (2500 psi). However, it must be noted that the Orthotropic-Variable Modulus model uses a composite material of steel and concrete, and may not be suitable for predicting the response of nonreinforced concrete.

Following this study, it was decided to use the Chen and Chen model to represent the nonlinear nonreinforced concrete. However, for the reinforced model, both the Chen and Chen model and the Orthotropic Variable-Modulus model would be used. Truss elements would represent the reinforcement for the Chen and Chen model.

Design of the Finite Element Mesh

The goal of mesh design is to select the number and location of finite element nodes and element types so that the analysis will be sufficiently accurate (Melosh, Utku, 1983). The best mesh is simple to design yet fine enough to provide accurate results. The selection of element types and the design of the grid depend on the problem to be analyzed and the finite element models that are available for the analysis.

The structure in Figure 1.2 would be analyzed using static and dynamic loads applied at the center of the top slab. The finite element type selected for the analysis was

a three-dimensional continuum element. Symmetry of the structural geometry and of the loading indicated that only a quarter of the model needed to be discretized.

Prior to developing the finite element grid, the whole structure was analyzed using the finite element program SAP80 (Wilson, Habibullah, 1984) to determine the frequencies of vibration and the mode shapes of the structure. The results of the modal analysis were used to perform a dynamic analysis of the structure with the load applied at the center of the top slab. This analysis revealed that bending on the structure was basically in one direction, and that the behavior of the structure was essentially plain strain, see Appendix B. Consequently, only a strip (Figure 3.5) of one-half of the structure was discretized. The single strip was used to improve the finite element discretization and the accuracy of the results.

It was intended at the beginning of the research to use the discretization of the strip as the basis for developing the finite element mesh for the blast load analysis. In the blast load analysis, at least one-quarter of the model had to be discretized due to the nature of the load and the addition of the soil elements. Therefore, the finite element mesh for the strip had to be discrete enough to obtain accurate results and coarse enough to be used in the blast load analysis without requiring unreasonable computer time and storage.

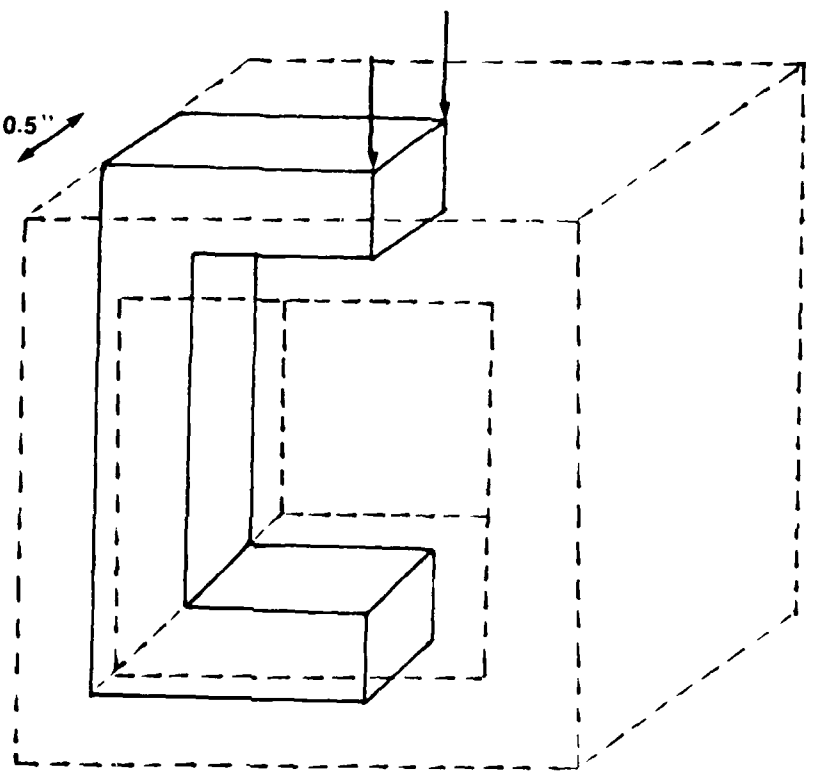

Figure 3.5. Portion of the Structure (Strip) Discretized for the Static and Dynamic Analyses

Two different discretizations of the strip were made: a fine grid with 144 elements and 1026 nodes (Figure 3.6), and a coarse grid with 90 elements and 674 nodes (Figure 3.7). Each element in both grids was modeled with 16 nodes.

The fine grid was divided into three element groups:

- First group (top slab) 52 elements
- Second group (wall) 48 elements
- Third group (bottom slab) 44 elements

The coarse grid was also divided into three element groups:

- First group (top slab) 30 elements
- Second group (wall) 30 elements
- Third group (bottom slab) 30 elements

For the purpose of studying the grid discretization, all elements were modeled with linear material properties, which included the modulus of elasticity and the Poisson's ratio of the material. The values used in the analysis were listed in Table 3.1.

The two models (finite element grids) were evaluated by applying an arbitrary static load at the top of the strip. This load had to be calculated to conform with the size of the strip. The actual load that would be applied to the whole structure was multiplied by the ratio of the width of the strip (0.5 in) to the width of the whole structure (4.0 in) and also by the ratio of the length of the strip (2.0 in) to the length of the whole structure (4.0 in). Two concentrated loads of 3 lb each were applied at the top of

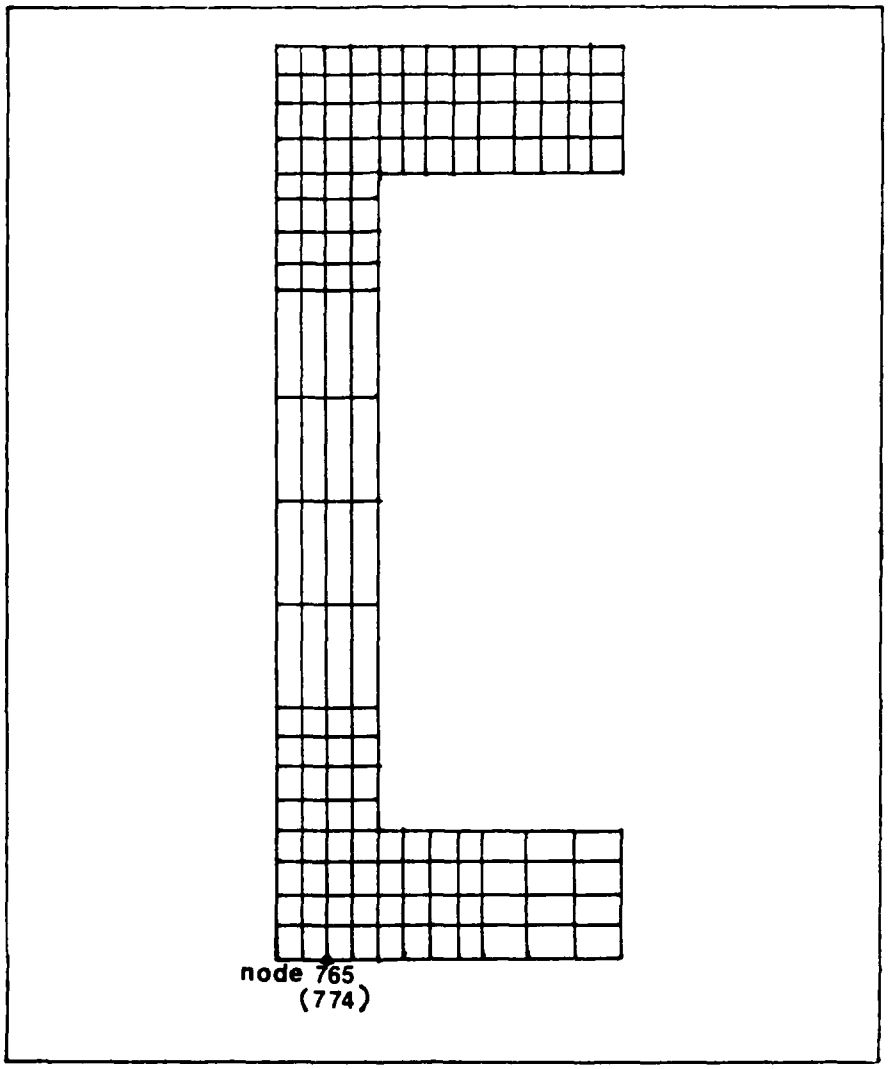

Figure 3.6. Fine Discretization of the Strip (node number in parenthesis is on the back plane)

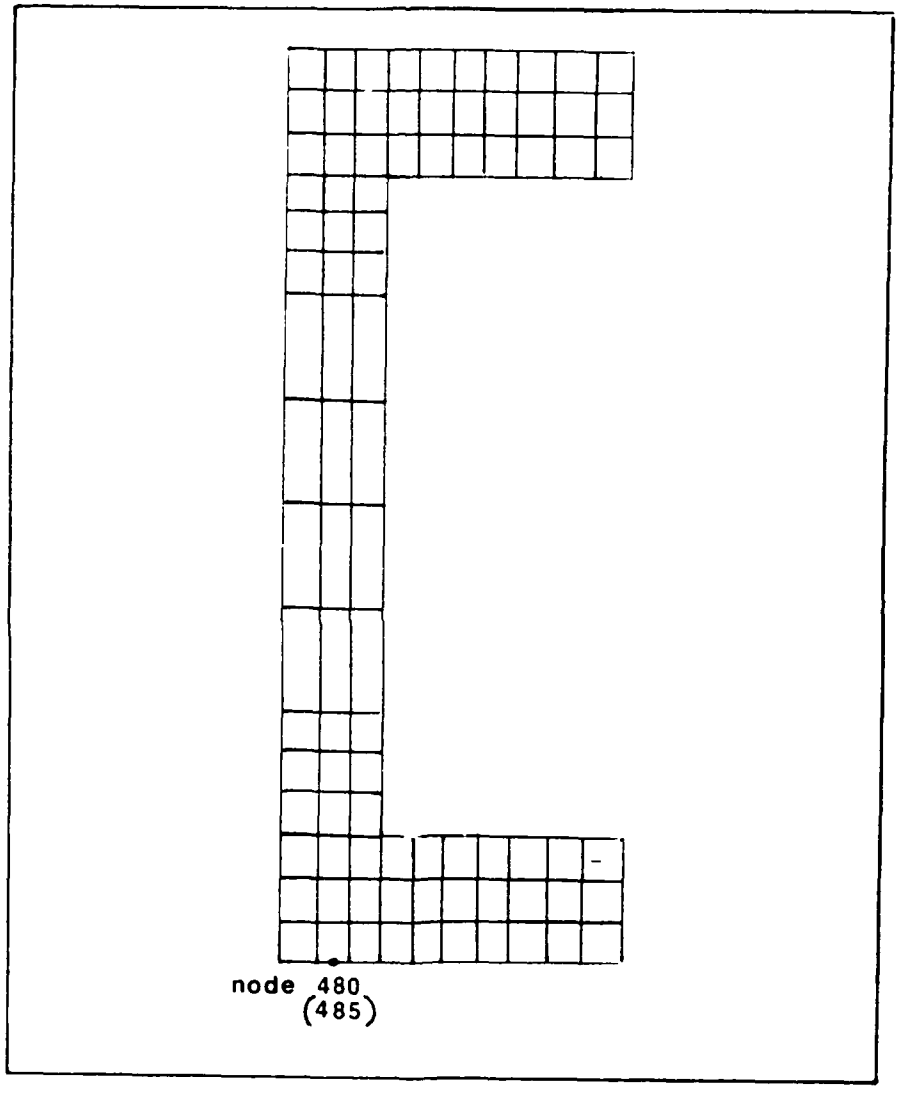

Figure 3.7 Coarse Discretization of the Strip (node number in parenthesis is on the back plane)

the strip as shown in Figure 3.5. The load was applied in one step only.

In order to satisfy symmetry, the translations of the nodes at the top and bottom slabs on the x-y plane (Figure 3.8) at z=0 were fixed in the z-direction. The strip was supported in the vertical direction by fixing the translations in the y-direction of nodes 765 and 774 of the fine grid (Figure 3.6), and of nodes 480 and 485 of the coarse grid (Figure 3.7). The translations of all the nodes in the x-direction were fixed in order to satisfy the plain strain condition.

The results of these analyses are shown comparatively in Figures 3.9, 3.10, and 3.11. Figures 3.9, 3.10, and 3.11 show the comparison of the predicted stresses in the elements of the top slab, the wall, and the bottom slab, respectively. The numbers represent the average bending stresses in those elements. The negative sign preceding the number indicates compression in that element. The stresses were calculated by averaging the stresses given at integration points in the element. A typical element with the integration points is depicted in Figure 4.1.

The results showed good agreement between the stresses predicted with both discretizations. The greatest difference was observed near the point of load application, near the corners, and near the support of the structure. This difference was expected due to the high stress gradient in these areas. The change in stresses between elements was

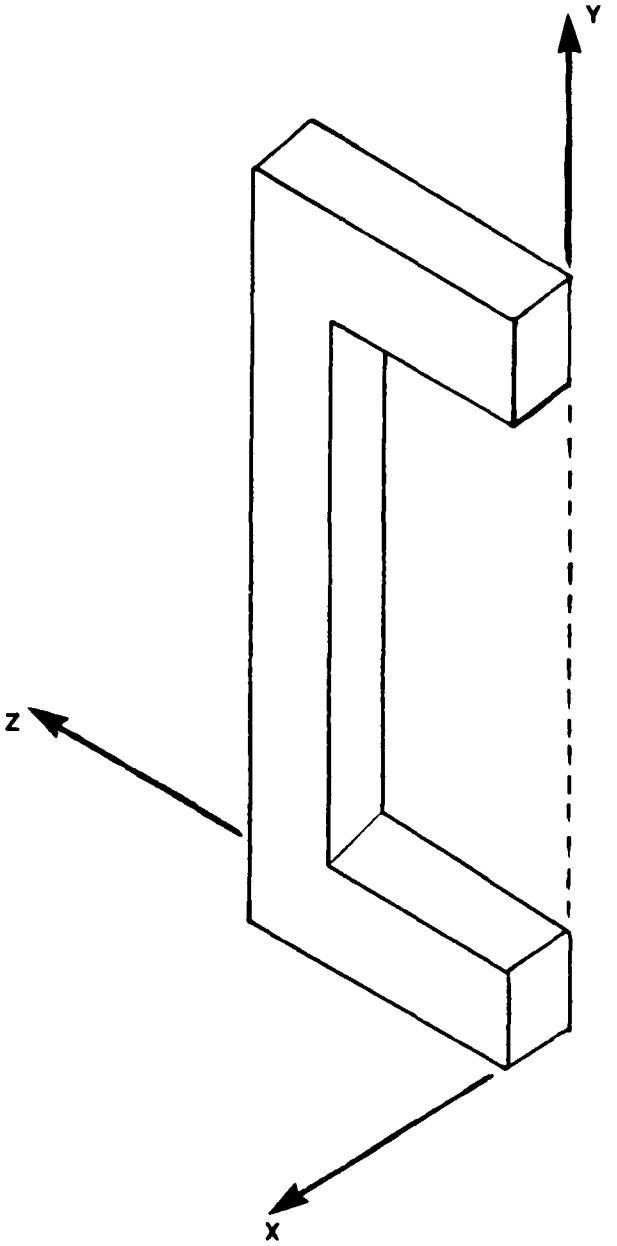

Figure 3.8. Orientation of the Strip in Space

TOP OF SLAB

6	42	90	109	82	12	26	169	272	371	450	525	722
-5	27	64	127	-176	-19	67	152	253	359	456	547	609

BOTTOM OF SLAB

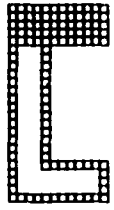

TOP OF SLAB

11	64	101	66	-31	-148	-264	-373	-473	-650
-8	-40	-98	-136	22	131	245	362	485	576

BOTTOM OF SLAB

Figure 3.9. Comparison of the Average Bending Stresses Induced in the Top Slab in the Finite Element Mesh Study

OUTSIDE WALL

-95	-84	-68	-51	-17	35	87	140	176	192	203	197
-28	-54	-68	-83	-115	-167	-219	-271	-303	-319	-339	-434

INSIDE WALL

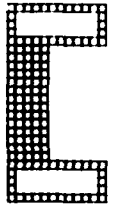

OUTSIDE WALL

-93	-76	-55	-19	33	83	134	171	190	188
-35	-61	-80	-115	-165	-216	-266	-300	-320	-395

INSIDE WALL

Figure 3.10. Comparison of the Average Bending Stresses Induced in the Wall in the Finite Element Mesh Study

TOP OF SLAB

3	17	32	61	109	89	83	81	81	81	81
- 8	- 77	- 91	- 30	- 41	- 51	- 55	- 58	58	- 58	- 58

BOTTOM OF SLAB

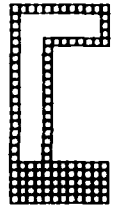

TOP OF SLAB

6	24	54	100	83	80	79	79	79	79
1	102	33	36	53	56	56	56	56	56

BOTTOM OF SLAB

Figure 3.11. Comparison of the Average Bending Stresses Induced in the Bottom Slab in the Finite Element Mesh Study

also similar in both grids, which indicated that the finer discretization was not necessary.

As a result of this study, the coarse mesh was selected for the finite element analysis of the structure. However, it must be noted that the selection of the coarse mesh was based only on the size of the discretization (number of nodal points and elements), which would reduce the requirements of computer time and computer storage. The selection of the mesh on this basis does not indicate it is the best mesh for the analysis. As it was revealed in the analysis of the grid (Figures 3.9, 3.10, and 3.11), the change in stresses between adjoining elements in some areas of the structure was very sharp. This dramatic change in stresses could have been reduced by increasing the discretization in those areas.

CHAPTER FOUR
ANALYSIS OF THE SINGLE-BAY STRUCTURE

Introduction

The purpose of this phase of the research was to analyze the scaled single-bay structure (Figure 1.2) subjected to static and dynamic loads. The analyses were performed for comparison with static and dynamic tests conducted on the scaled models in order to examine the capabilities of the program NONSAP-C. The analyses were performed on both the nonreinforced and reinforced structures. The dynamic analyses were performed using linear and nonlinear material properties.

In the analyses of the scaled reinforced structure, the reinforcing steel was modeled in two different ways depending on the material model used for concrete. As mentioned previously, the Orthotropic Variable-Modulus model includes the reinforcement in a composite element of concrete and steel. The amount of reinforcement for this model is included as a ratio of the area of steel in the element to the area of concrete in the same element. On the other hand, the Chen and Chen model does not include any reinforcement; therefore, truss bar elements were added to the finite element mesh to represent the steel. The same

truss bars were used with the linear model. The calculation and placement of the reinforcement in the model are presented in Appendix C.

Static Analysis

The purpose of the static analysis was to simulate static tests performed on the structure in order to assess the capabilities of the program NONSAP-C.

The static test consisted of the application of a static strip load along the longitudinal centerline of the top slab of the model (Gill, 1985). This load was equated to a point load ranging from 0 to 100 lb. The load was then reduced accordingly to the size of the strip. Two concentrated loads were applied at the top of the strip, as shown in Figure 3.5. The magnitude of each concentrated load ranged from 0 to 3.125 lb. This load was applied at increments of 0.156 lb, equivalent to a 5 lb increment on the whole structure. The same loading function was applied to the nonreinforced and the reinforced concrete models.

The support of the structure was modeled as in the finite element mesh study. However, the translation in the x-direction of the nodes on the z-y plane for x=0 (Figure 3.8) were released. Although this change does not satisfy the plane strain condition, it was necessary to free the movement of these nodes because high stresses were generated in this direction due to the small thickness of the strip.

The elements in the nonreinforced structure were modeled with the Chen and Chen material model. The elements in the reinforced structure were modeled with the Chen and Chen model and the Orthotropic Variable-Modulus model. The concrete material properties used in the analyses were listed in Table 3.2.

For the static analyses, a numerical integration of 8 (2 × 2 × 2) Gauss points was specified to calculate the stiffness matrix. The 8 integration points and their approximate location in a typical element are shown in Figure 4.1.

Dynamic Analysis

The dynamic analyses were performed to evaluate the capability of the program NONSAP-C to predict the dynamic response of the scaled structures. The dynamic tests consisted on the application of an impulse load at the center of the top slab. The load was applied with a PCB piezoelectric hammer (Gill, 1985). The dynamic tests included the measurement of dynamic strains and the measurement of accelerations at the center of the bottom of the top slab and at the center of the inside wall.

For the dynamic analyses, the translations of the nodes and the support of the strip were modeled as in the static test. The strip was dynamically loaded at the top with two concentrated loads.

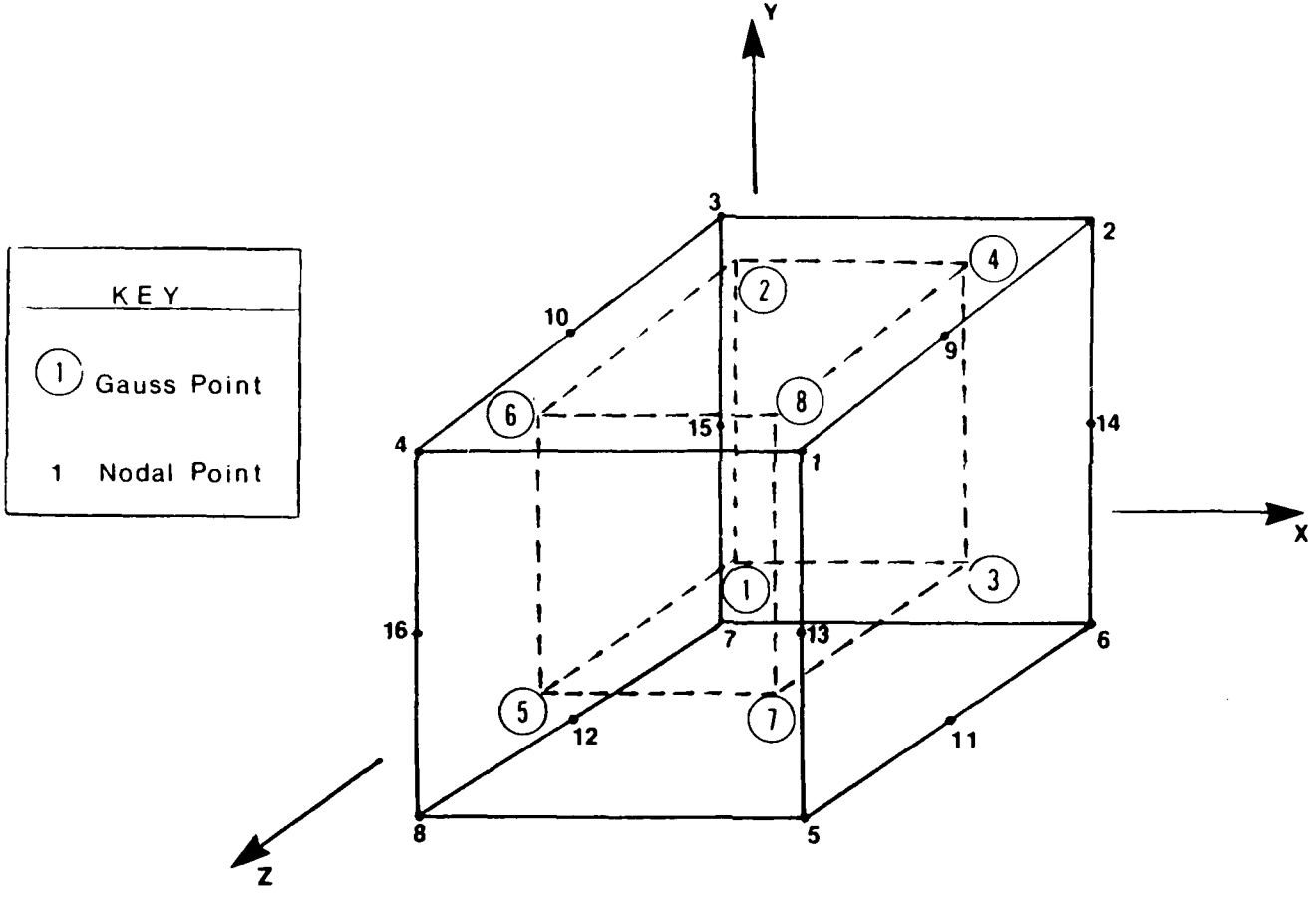

Figure 4.1. Typical Three-Dimensional Element in NONSAP-C With Eight Integration Point Numbers

The dynamic analyses were performed without damping. In general, damping coefficients are difficult to determine because the energy-loss mechanisms in practical structure are seldom understood. Also, it has been determined that for impulse-type loadings, the influence of damping on maximum response of a structure is small (Clough, Penzien, 1975, and Rebora, Zimmermann, 1976).

The program NONSAP-C has the capability of performing a dynamic analysis using either a lumped mass matrix (diagonal matrix) or a consistent mass matrix. For the dynamic analyses of the scaled structures a consistent mass matrix was specified although it increases the computational effort. Previous investigations by Yovaish (1984) using the program NONSAP-C showed that at different integration time steps there was less variation of the predicted response with a consistent mass matrix than with the lumped mass matrix. Also, it has been reported that the consistent mass matrix compensates for the errors introduced in the implicit integration scheme used in NONSAP-C (Belytschko, 1976). In the program NONSAP-C the consistent mass matrix is always calculated with a 27 ($3 \times 3 \times 3$) Gauss point integration (Anderson, et al., 1982). For consistency, a $3 \times 3 \times 3$ point integration was specified in the analyses to calculate the stiffness matrix. The 27 Gauss points and their approximate location in a typical element are shown in Figure 4.2.

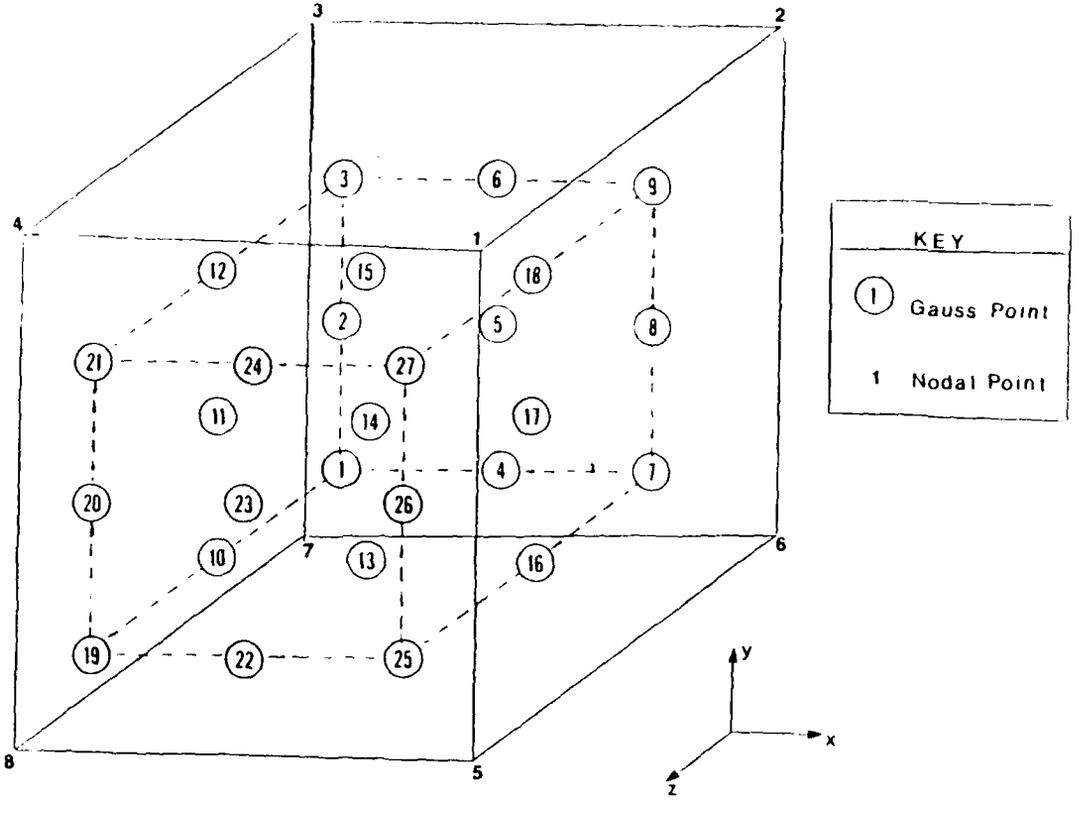

Figure 4.2. Typical Three-Dimensional Element in NONSAP-C With Twenty Seven Integration Point Numbers

The integration method used in the analyses was the Wilson-Theta Method. This integration method is unconditionally stable for linear systems (Belytschko, 1975). Yovaish (1984) discussed the effects of this method in the amplitude and the period of the structural response.

The analyses were performed on both the nonreinforced and reinforced models.

The nonreinforced model was loaded with the loading function shown in Figure 4.3. This load is the same applied on the structure in the dynamic test. The load in the figure is the reduced load corresponding to the strip size. Two analyses were performed with the nonreinforced model: a linear analysis and a nonlinear analysis. In the linear analysis all elements were modeled with the concrete properties used in the finite element mesh study. In the nonlinear analysis all elements were modeled with the Chen and Chen model. The dynamic analyses of the nonreinforced structure were performed with an integration time step of 0.020 ms; and the analyses were conducted through 50 time steps.

The reinforced model was loaded with the loading function shown in Figure 4.4, which is the same applied to the reinforced model in the dynamic test. The load shown in the figure is the reduced load corresponding to the thickness of the strip. Five analyses were performed with the reinforced model: two linear analyses and three nonlinear analyses. In the linear analyses the concrete

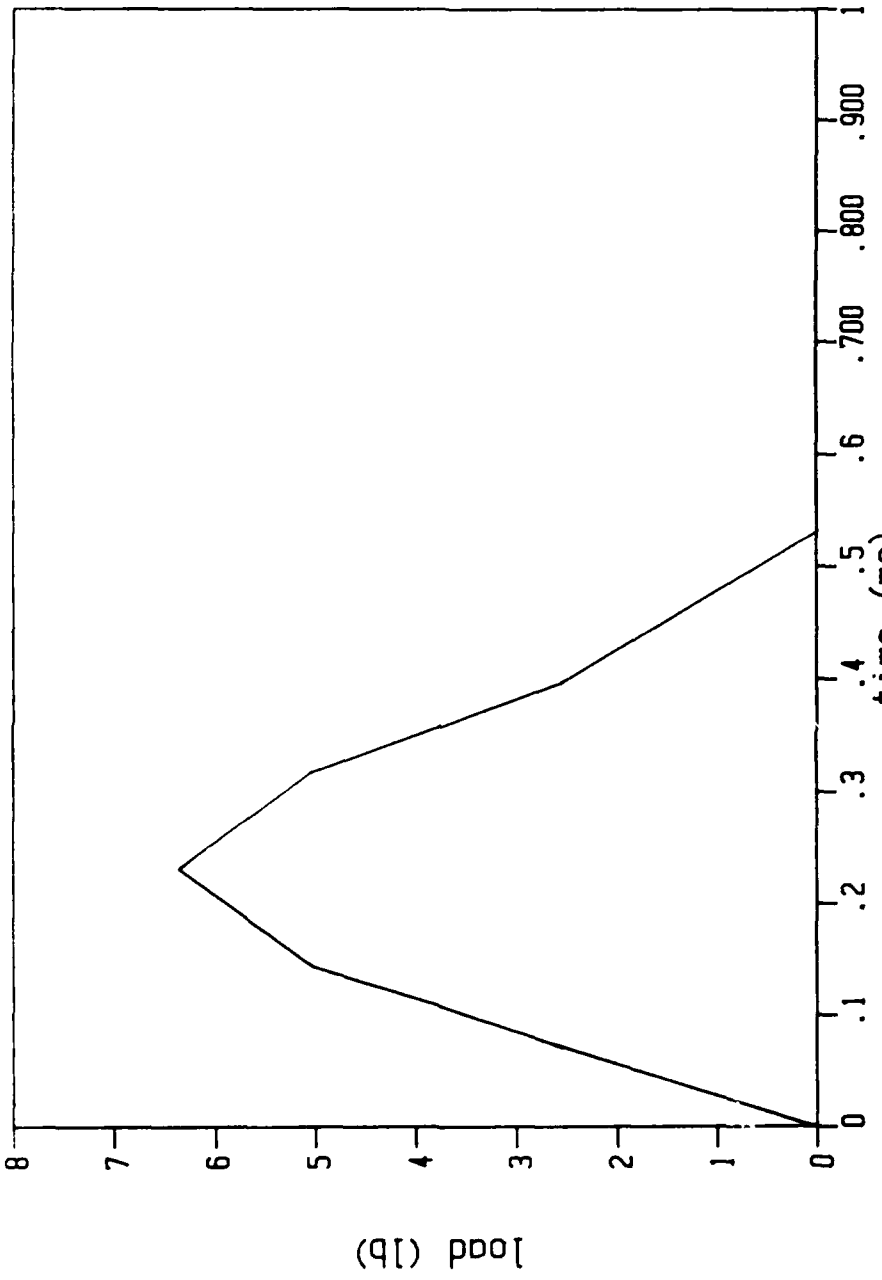

Figure 4.3. Loading Function Used in the Dynamic Analysis of the Non-Reinforced Structure

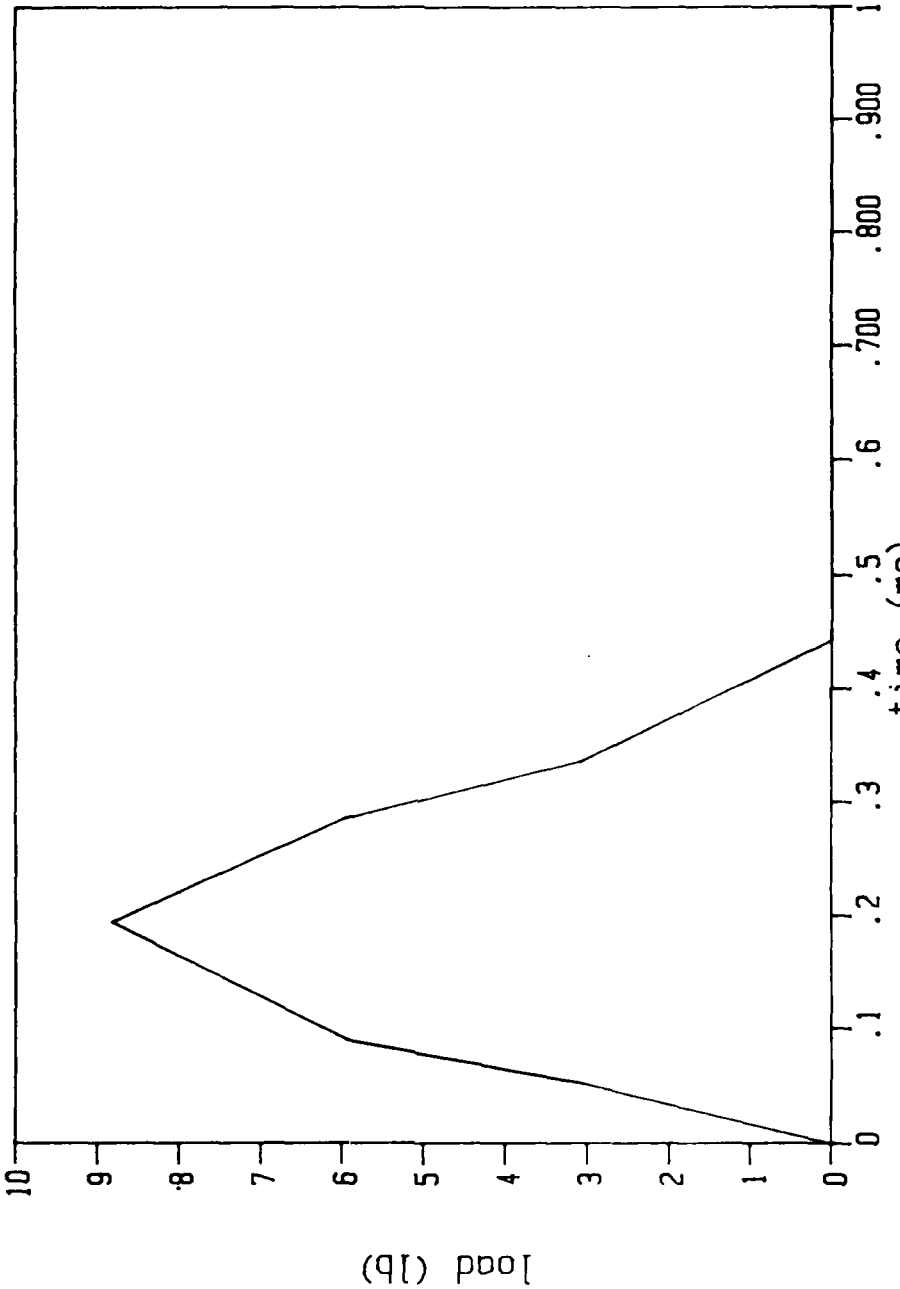

Figure 4.4. Loading Function Used in the Dynamic Analysis of the Reinforced Structure

elements were modeled with the properties listed in Table 3.2. In two of the nonlinear analyses the concrete elements were represented with the Chen and Chen model. These two analyses were performed with integration time steps of 0.010 ms and 0.015 ms. The reinforcement in the linear analyses and the Chen and Chen nonlinear analyses was represented by truss bars. In the third nonlinear analysis, all elements were represented with the Orthotropic Variable-Modulus model and the reinforcement was included in the appropriate elements. This nonlinear analysis was performed with an integration time step of 0.010 ms.

CHAPTER FIVE
ANALYSIS OF THE SOIL-STRUCTURE SYSTEM

General

This chapter includes the design of the finite element mesh and the calculation of the loading functions necessary for the analysis of the soil-structure system shown in Figure 1.3. The objective of this analysis was to simulate an explosive test performed in the University of Florida centrifuge. In this test, the soil structure system was subjected to a 60-g environment and was exposed to a blast load simulating a 500 lb bomb on the prototype structure. A schematic of the testing set-up in the centrifuge bucket is presented in Figure 5.1. The explosive test included the measurement of dynamic strains at different points of the structure; the measurement of accelerations at the center of the bottom of the top slab and at the center of the inside wall; and the measurement of pressures at different points of the structure.

Input Requirements

Three major steps were followed to develop the input requirements for the solution of the problem with NONSAP-C:

1. The design of the finite element mesh.

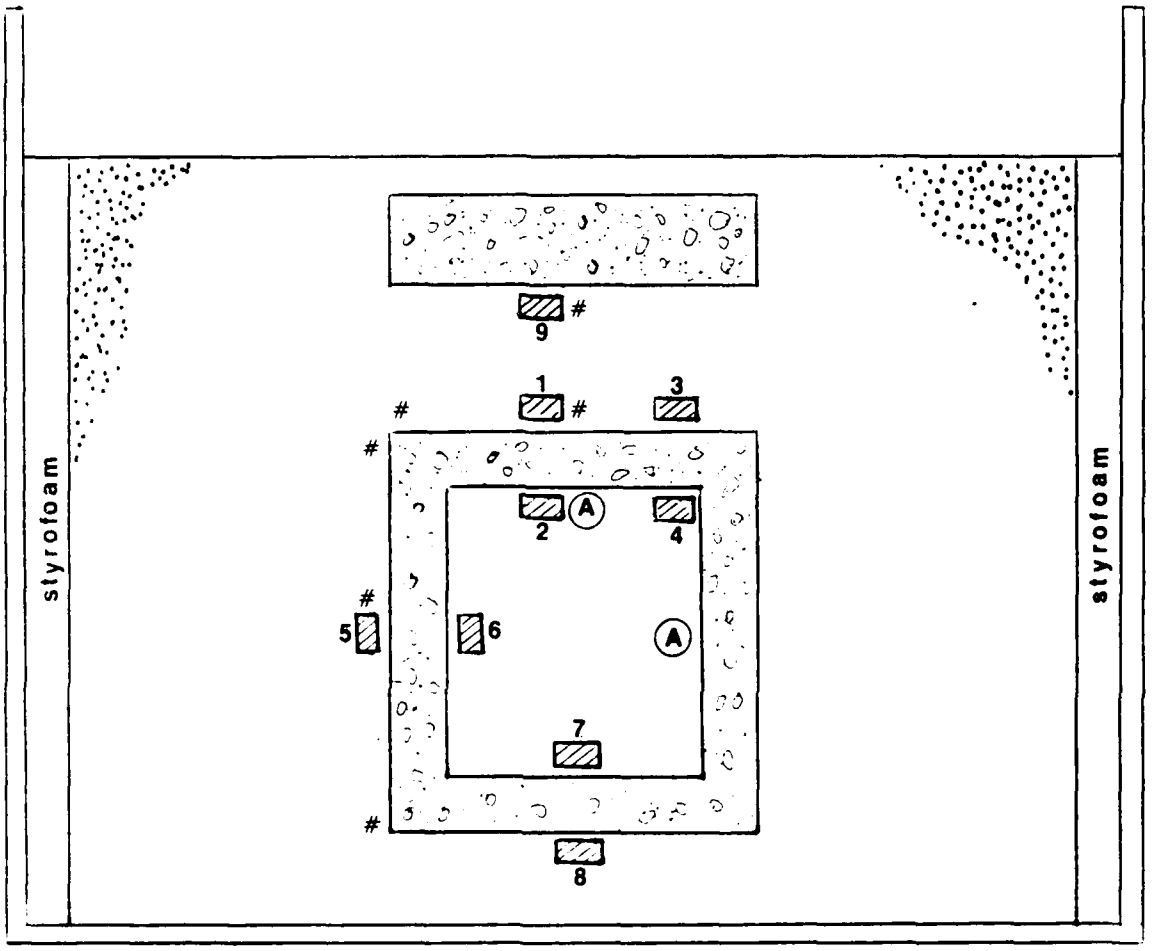

Scale 1"

INSTRUMENTATION KEY

- # Pressure Gages
- Strain Gages
- (A) Accelerometers

Figure 5.1. Schematic of the Test Set-up in the Centrifuge Bucket

2. The calculation of the load-time histories.
3. The division of the system into element groups according to material type and their location in the system.

Finite Element Mesh Design

The design of the finite element mesh for the soil-structure system required the consideration of several factors:

- The limitations in cpu time and storage requirements.
- The nature and location of the load.
- The desired accuracy of the analysis at points of interest in the system.

For the analysis of the soil-structure system, it was important to optimize the discretization of the structure in order to minimize the cpu time and the mass storage requirements. Previous analyses with the static and dynamic loads required large amounts of cpu time and mass storage. The nonlinear dynamic analyses required an average of 50 hours to complete with 24 to 26 hours of cpu time in an IBM 4341 computer. The addition of soil elements and other concrete elements to model the soil-structure system would impose even larger requirements. Therefore, the previous mesh developed for the static and dynamic analyses could not be used as a basis for the mesh of the soil-structure system as it was originally intended.

The nature and location of the load (top and center of the burster slab) and the symmetry of the system geometry

required that only a quarter of the model be discretized (Figure 5.2). The system was discretized using three-dimensional continuum elements.

Accuracy of the results required a finer discretization in the areas of interest and in the areas of greatest response (near the detonation). Previous analyses of the single-bay structure with static and dynamic loads showed that a fine discretization was required in the areas near the point of application of the load. These analyses also revealed that the bottom slab of the single bay structure did not require as many elements as the top slab.

Figures 5.3 through 5.15 show the discretization of the system in the z-y plane of symmetry. Each figure indicates the x-coordinate of the plane. In order to satisfy the quarter symmetry of the problem, the translations of the nodes on the z-y plane for x=0 were fixed in the x-direction; and the translations of the nodes on the x-y plane for z=0 were fixed in the z-direction. In order to model the configuration of the system in the centrifuge bucket, the translations of the nodes at the bottom of the system were fixed in the y-direction; the translations of the nodes on the x-y plane for z=5 (at the wall of the bucket) were fixed in the z-direction; and the translations of the nodes on the z-y plane for x=6 (at the wall of the bucket) were fixed in the x-direction.

The closest spacing of the nodes was near the intersection of the two planes of symmetry and in the

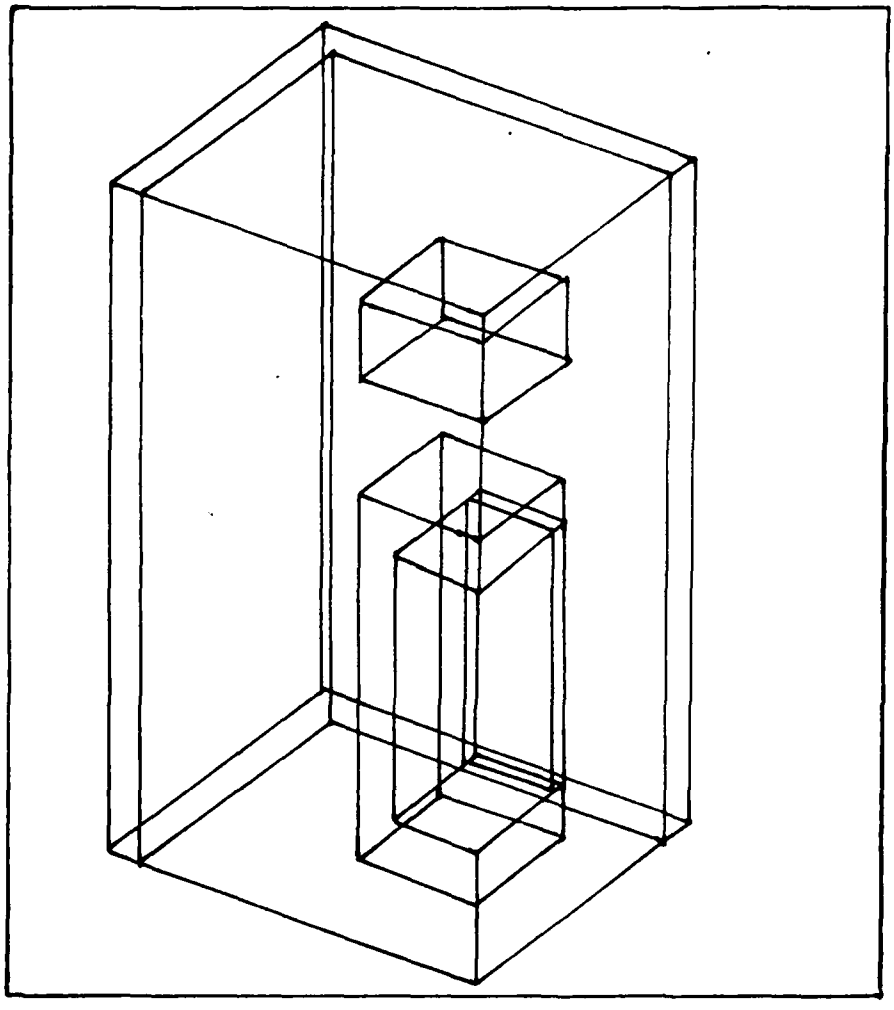

Figure 5.2. One Quarter of the Soil-Structure System Discretized

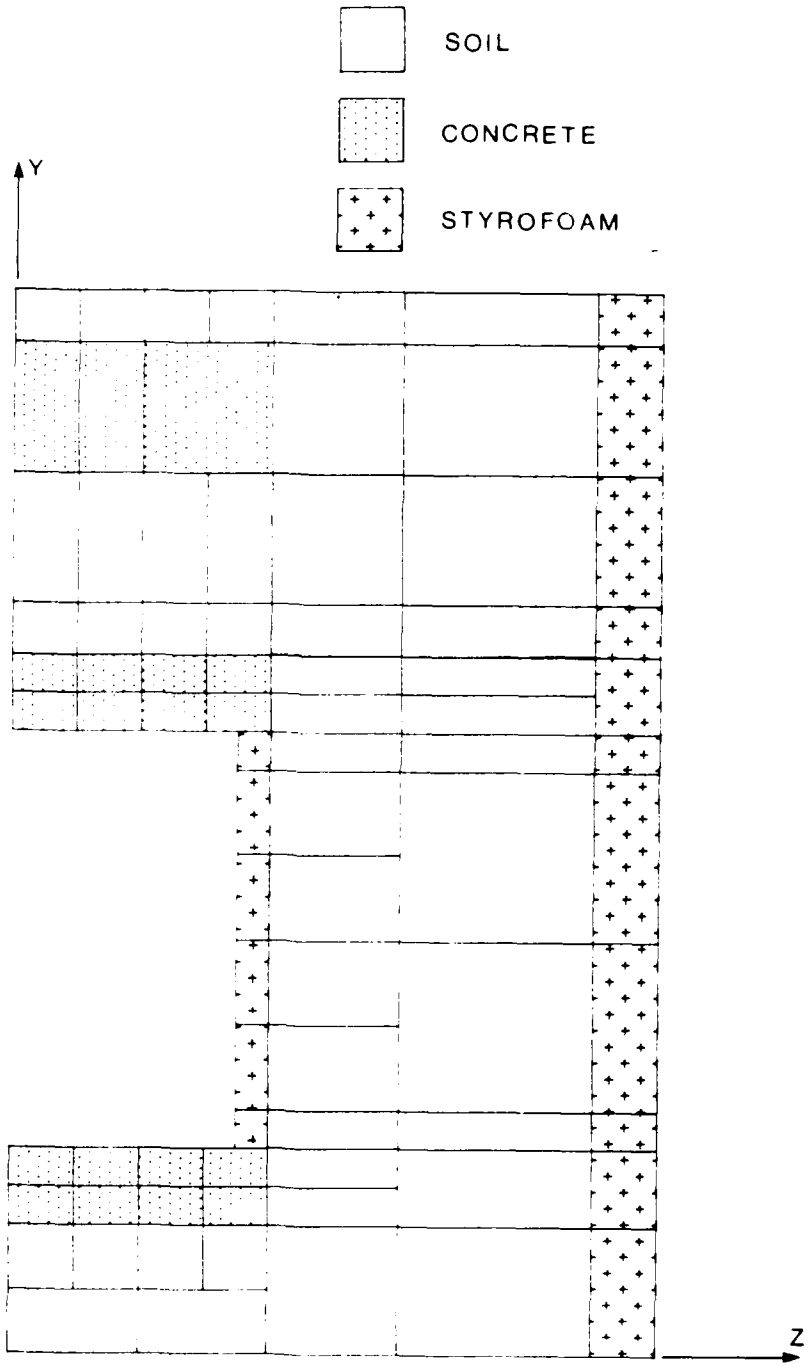

Figure 5.3. Discretization of the System in the z-y Plane for x=0

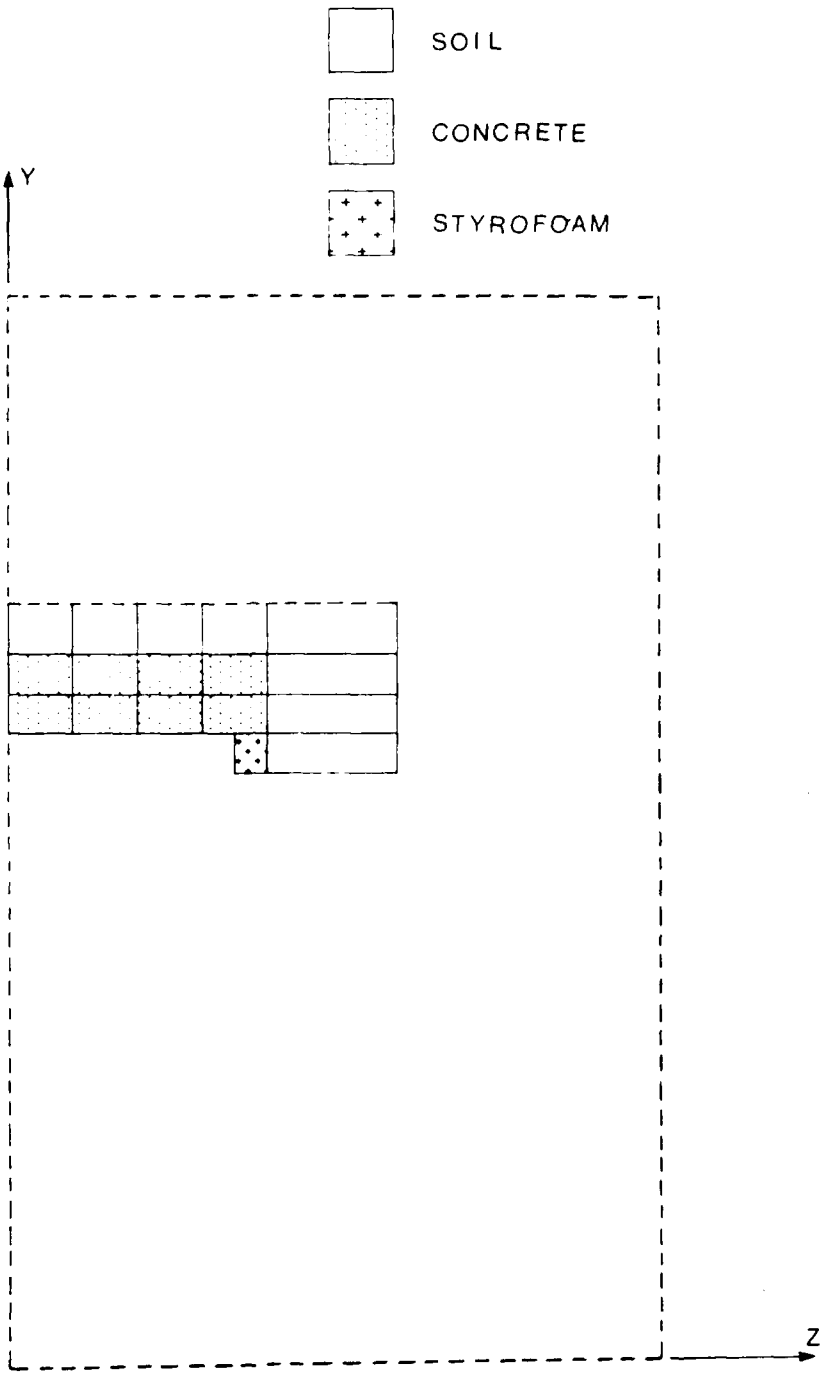

Figure 5.4. Discretization of the System in the z-y Plane for x=0.2

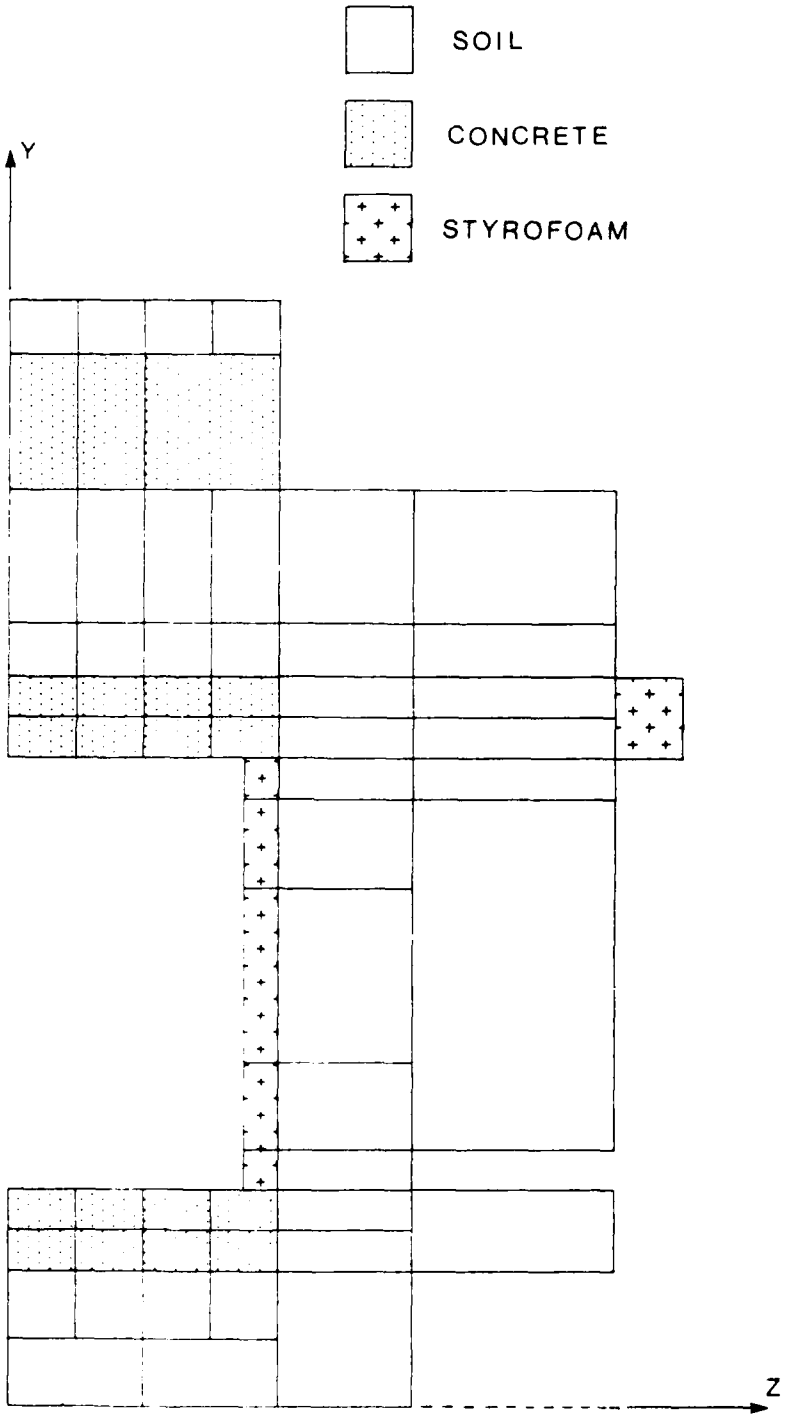

Figure 5.5. Discretization of the System in the z-y Plane for x=0.4

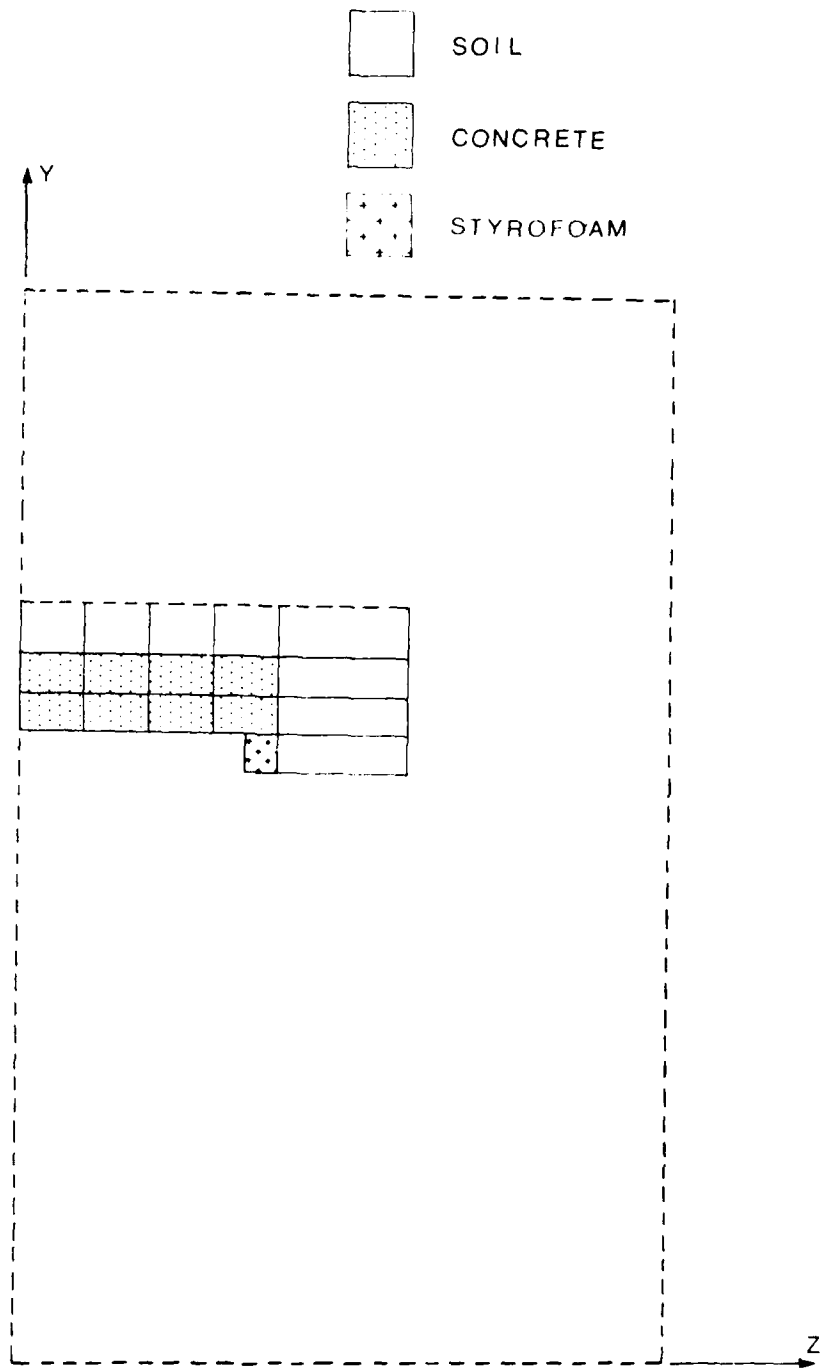

Figure 5.6. Discretization of the System in the z-y Plane for x=0.65

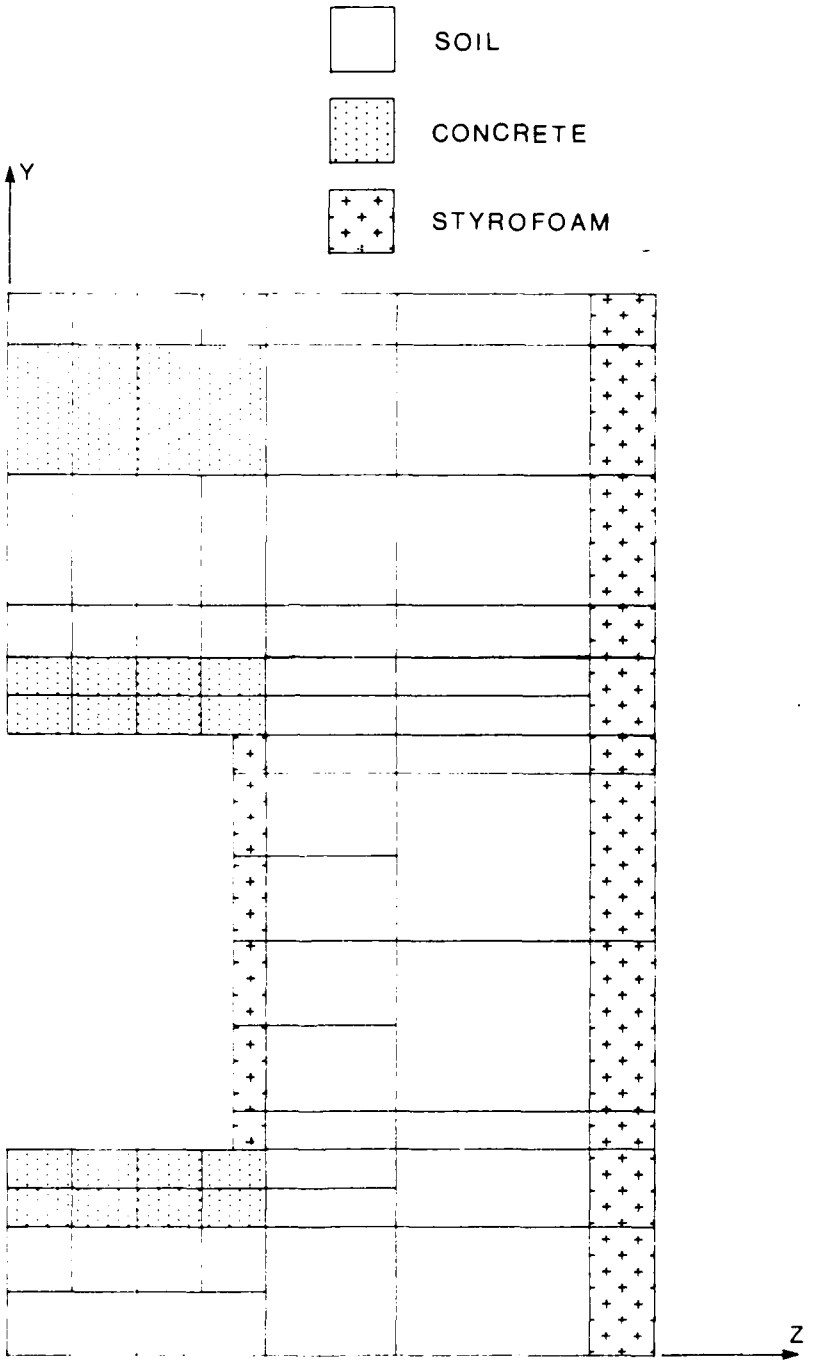

Figure 5.7. Discretization of the System in the z-y Plane for x=0.9

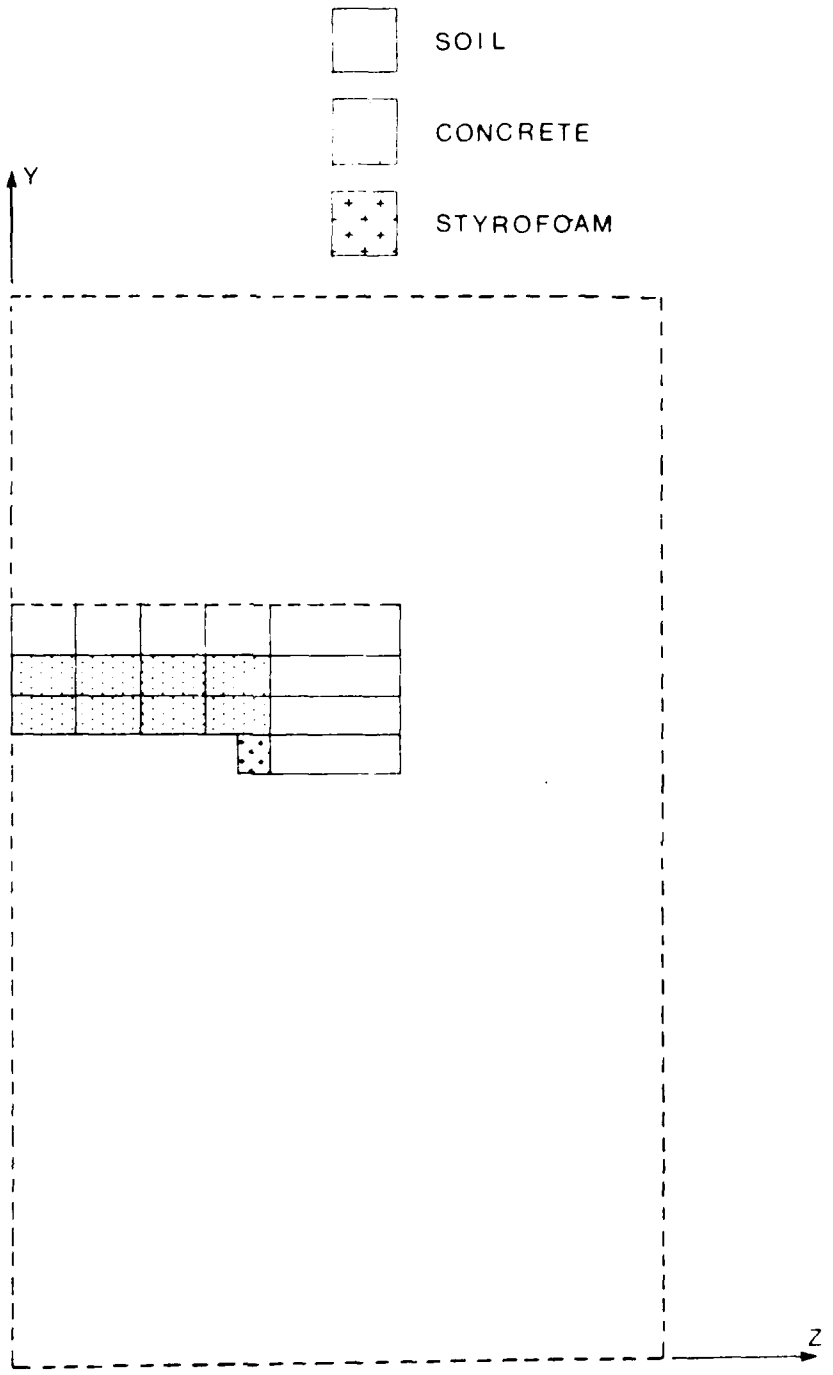

Figure 5.8. Discretization of the System in the z-y Plane for x=1.15

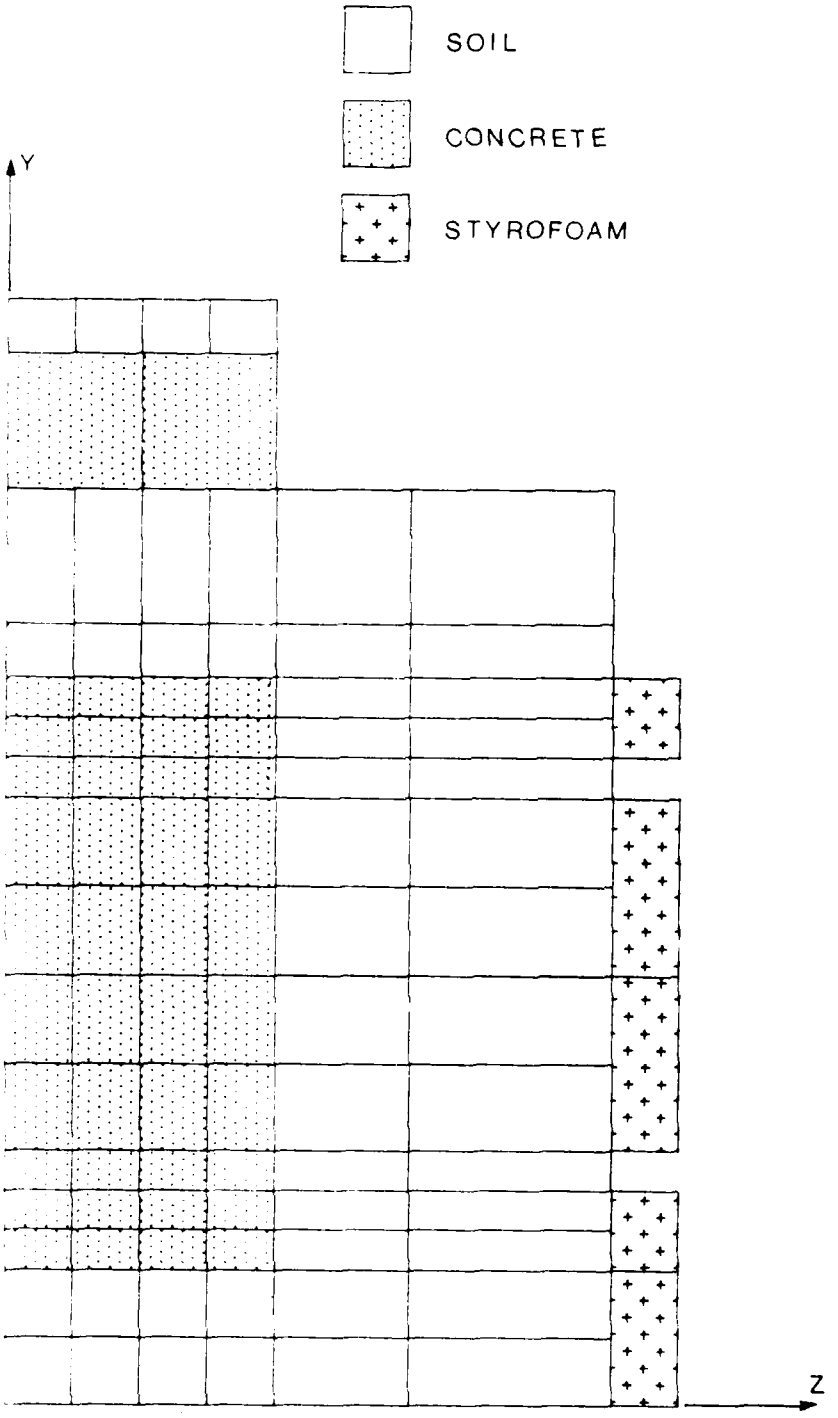

Figure 5.9. Discretization of the System in the z-y Plane for x=1.4

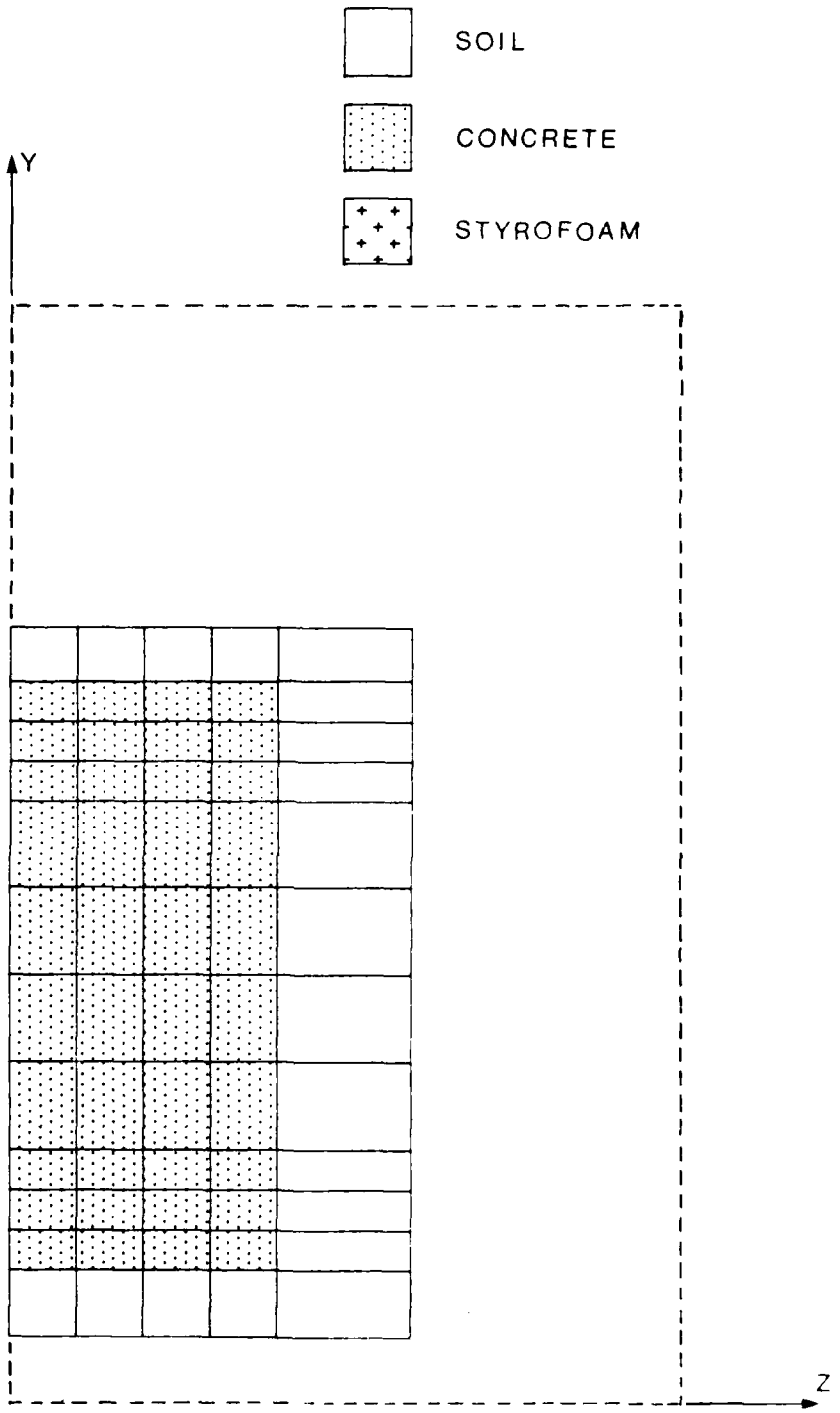

Figure 5.10. Discretization of the System in the z-y Plane for x=1.7

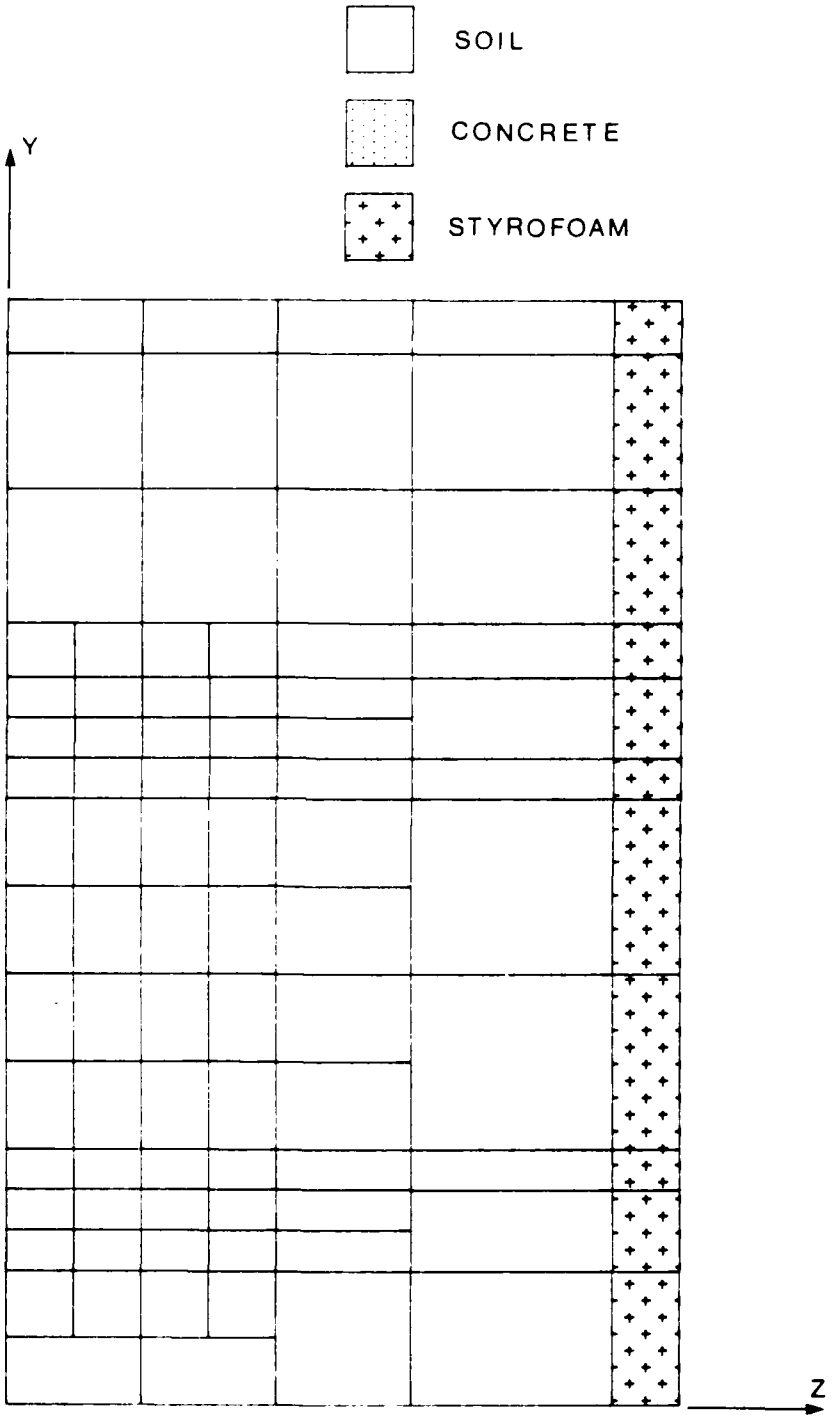

Figure 5.11. Discretization of the System in the z-y Plane for x=2.0

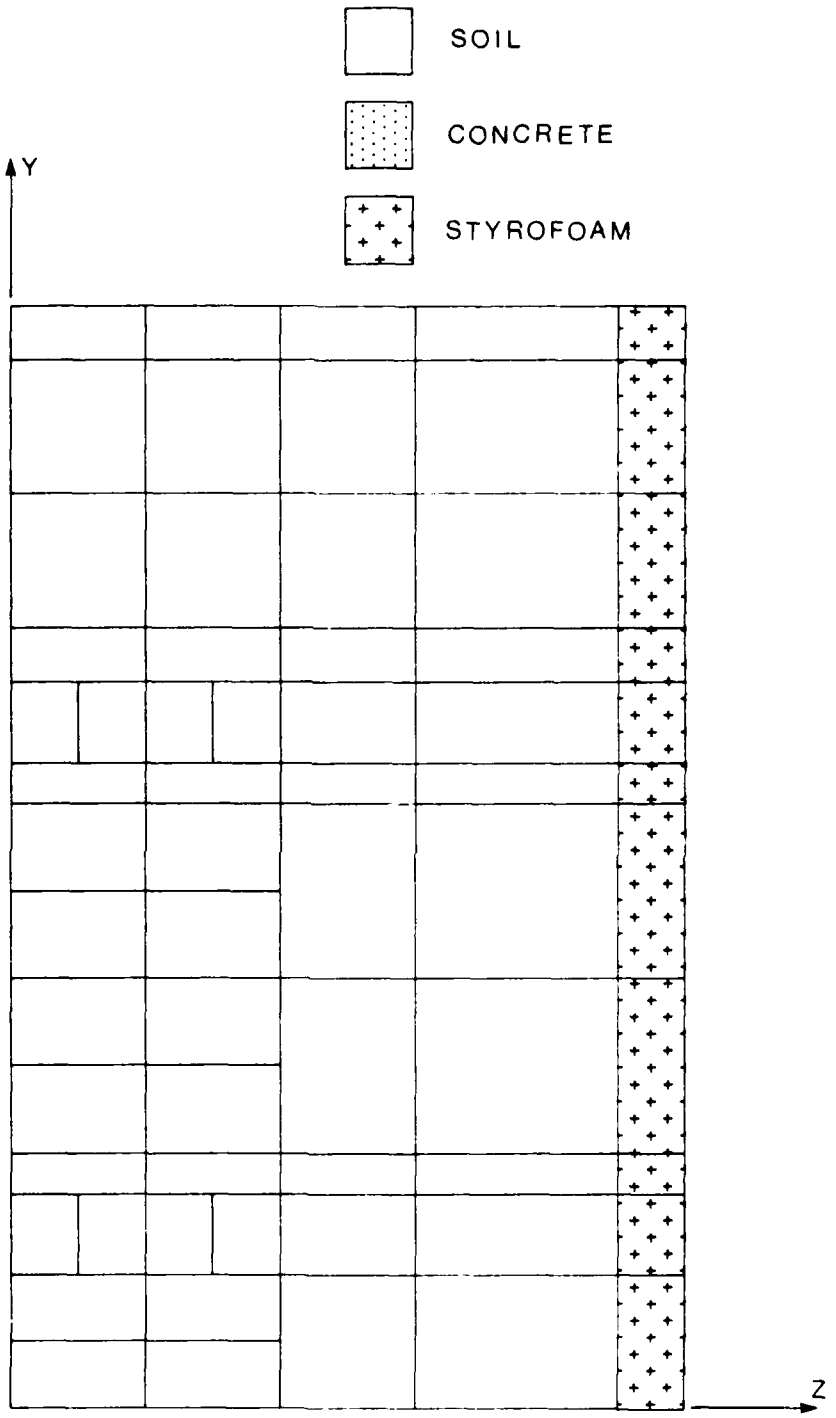

Figure 5.12. Discretization of the System in the z-y Plane for x=3.0

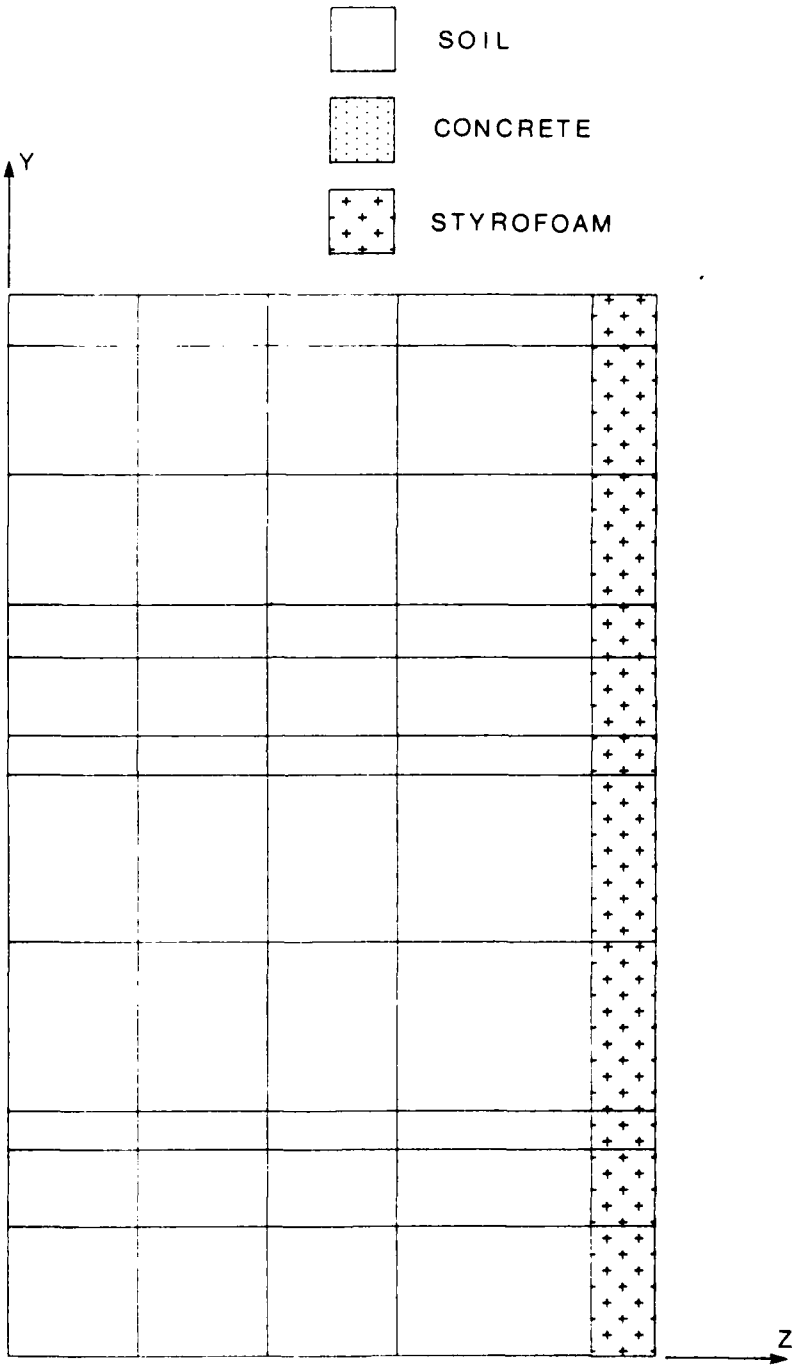

Figure 5.13. Discretization of the System in the z-y Plane for x=4.0

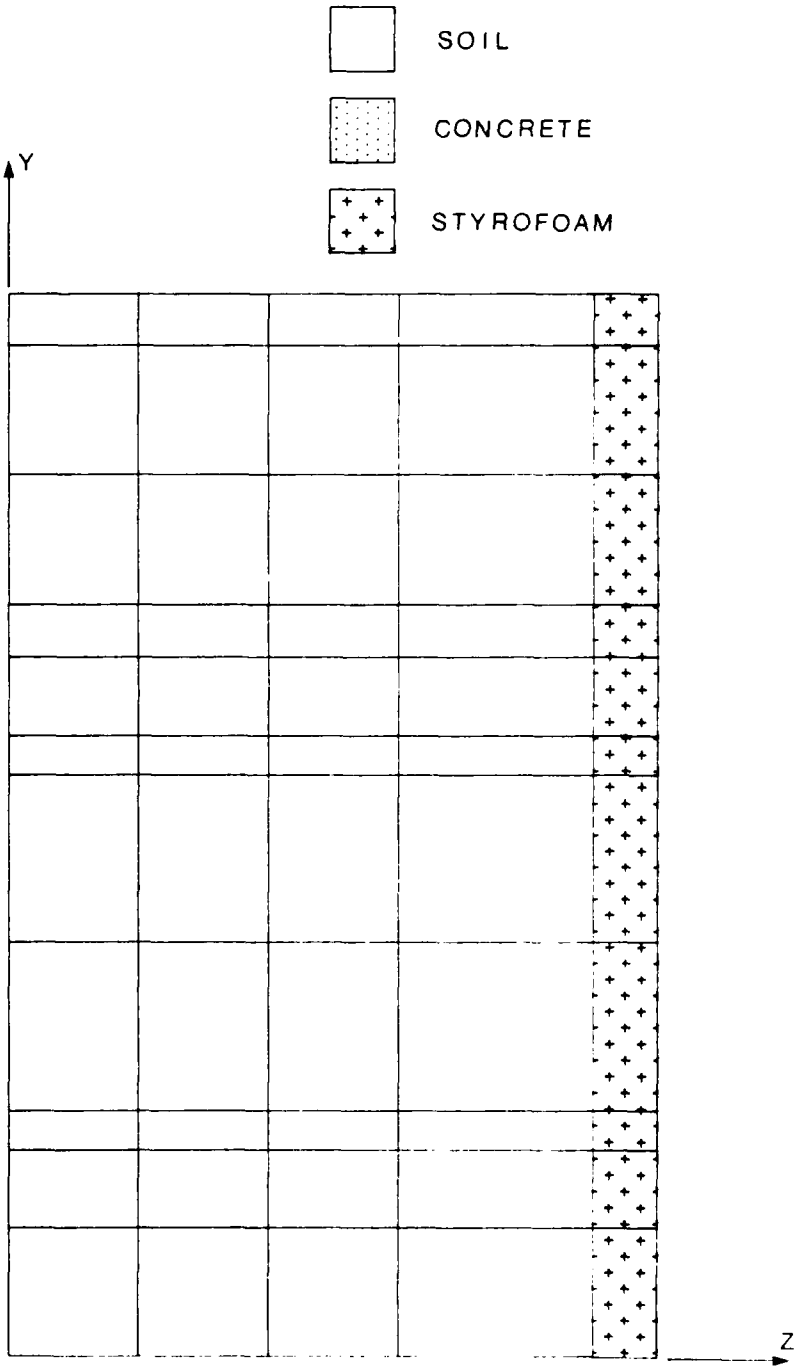

Figure 5.14. Discretization of the System in the z-y Plane for x=5.5

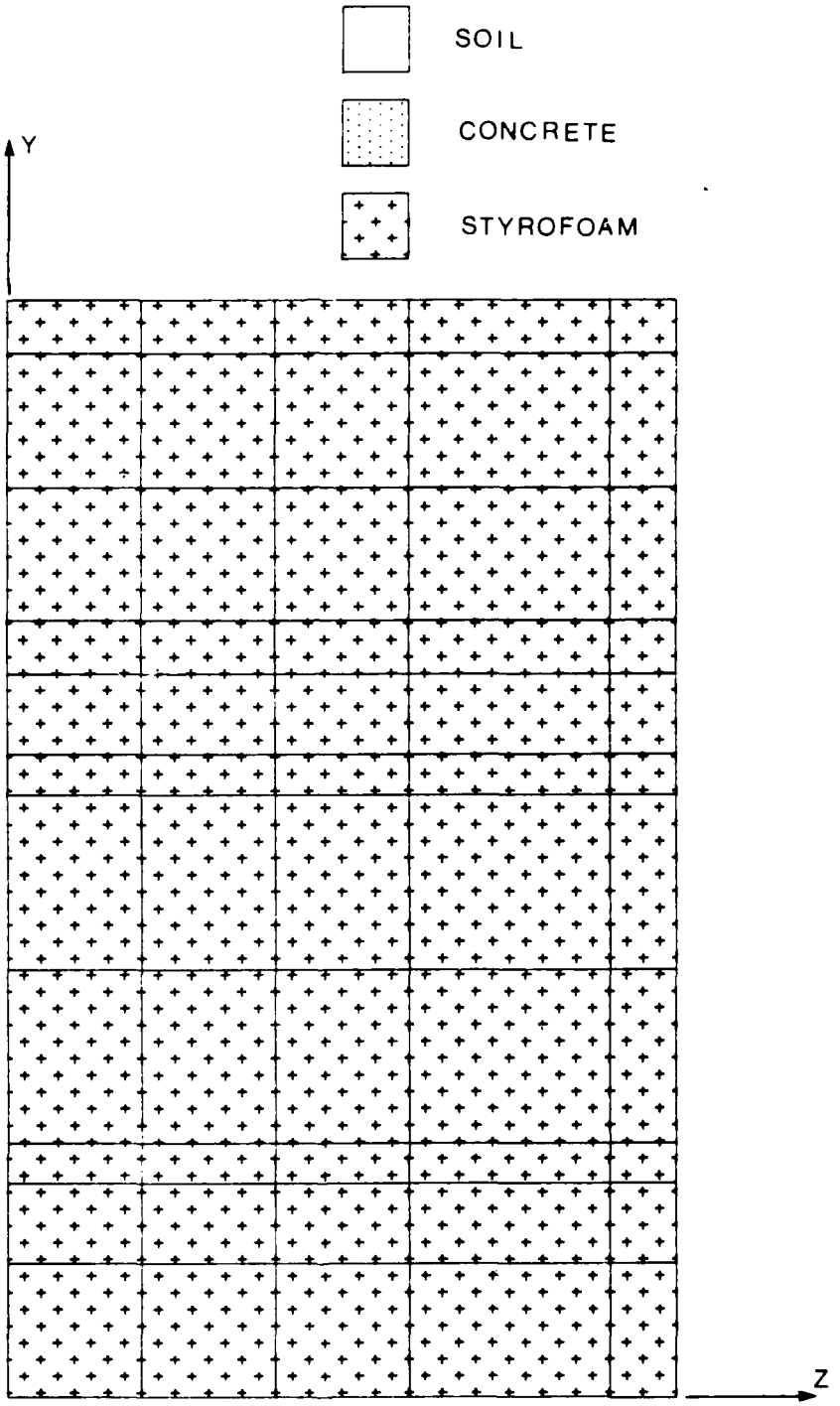

Figure 5.15. Discretization of the System in the z-y Plane for x=6.0

discretization of the structure. The spacing of the nodes and the size of the elements were increased as the distance from the detonation and from the structure became larger. The irregularity of the mesh did not allow the use of the generation schemes in NONSAP-C for the nodes and elements.

The total system was discretized using 1928 nodal points and 701 elements.

Calculation of Loading Functions

The explosive pressure to be modeled was the pressure generated by the detonation of a 500 lb bomb (equivalent to 267 lb of TNT) at a 2-foot standoff distance from the burster slab in the prototype structure. For the analysis of the scaled system, the weight of the load was reduced according to laws of similitude.

The procedure for determining the scaled charge for the 60-gravity environment is described below:

1. Determine the scaling relationships. The π-term for scaling explosive quantities is given by (Nielsen, 1983):

$$\pi = \frac{G\ (W)^{1/3}}{Q\ (\delta)^{1/3}}$$

where,

Q = heat of detonation/unit mass of explosive

δ = initial density of the explosive

W = mass of the explosive

G = gravity

2. Determine the equivalent weight of TNT in a 60-g environment for an explosive load of 267 lb of TNT in a 1-g environment.

$$\pi_{60\text{-g}} = \pi_{1\text{-g}}$$

$$\left(\frac{G\ (W)^{1/3}}{Q\ (\delta)^{1/3}}\right)_{60\text{-g}} = \left(\frac{G\ (W)^{1/3}}{Q\ (\delta)^{1/3}}\right)_{1\text{-g}}$$

$$(W)^{1/3}_{60\text{-g}} = \left(\frac{Q\ (\delta)^{1/3}}{G}\right)_{60\text{-g}} \left(\frac{G\ (W)^{1/3}}{Q\ (\delta)^{1/3}}\right)_{1\text{-g}}$$

The initial density of the explosive δ, and the heat of detonation/unit mass of explosive Q, have the same values at 1-g and at 60-g since the explosive is TNT in both cases and these parameters are independent of gravity. Therefore,

$$W_{60\text{-g}} = \frac{W_{1\text{-g}}}{(60)^3}$$

For $W_{1\text{-g}}$ = 267 lb, then:

$$W_{60\text{-g}} = 1.236 \times 10^{-3} \text{ lb}$$

The loading function was calculated based on a spherical charge of 1.236×10^{-3} lb of TNT detonated in the air 0.4 in above the center of the burster slab of the scaled system. The shock wave parametric representation in Figure 5.16 and the coefficient of the reflected pressure in Figure 5.17 were used to determine the pressure-time load history for the structure at selected points on the burster slab. These selected points coincide with the nodes at the corners of the element faces on the top of the burster slab (see Figure 5.18). The procedure for calculating the pressure time functions is described by Yovaish (1984). The values of the pressure-time functions used in the analysis are given in Table 5.1. Figure 5.18 shows the areas where each load function was applied.

Description of Element Groups

The soil structure system analyzed had four main components: 1) the single-bay structure, 2) the soil surrounding the structure, 3) the burster slab, and 4) the styrofoam. The styrofoam was used in the test to prevent reflection of the wave back into the structure, and was also used as a retaining wall to support the soil at the entrances. A total of 701 elements defined the system. The elements were divided into groups according to material size and their location in the system. The element groups were defined as follows:

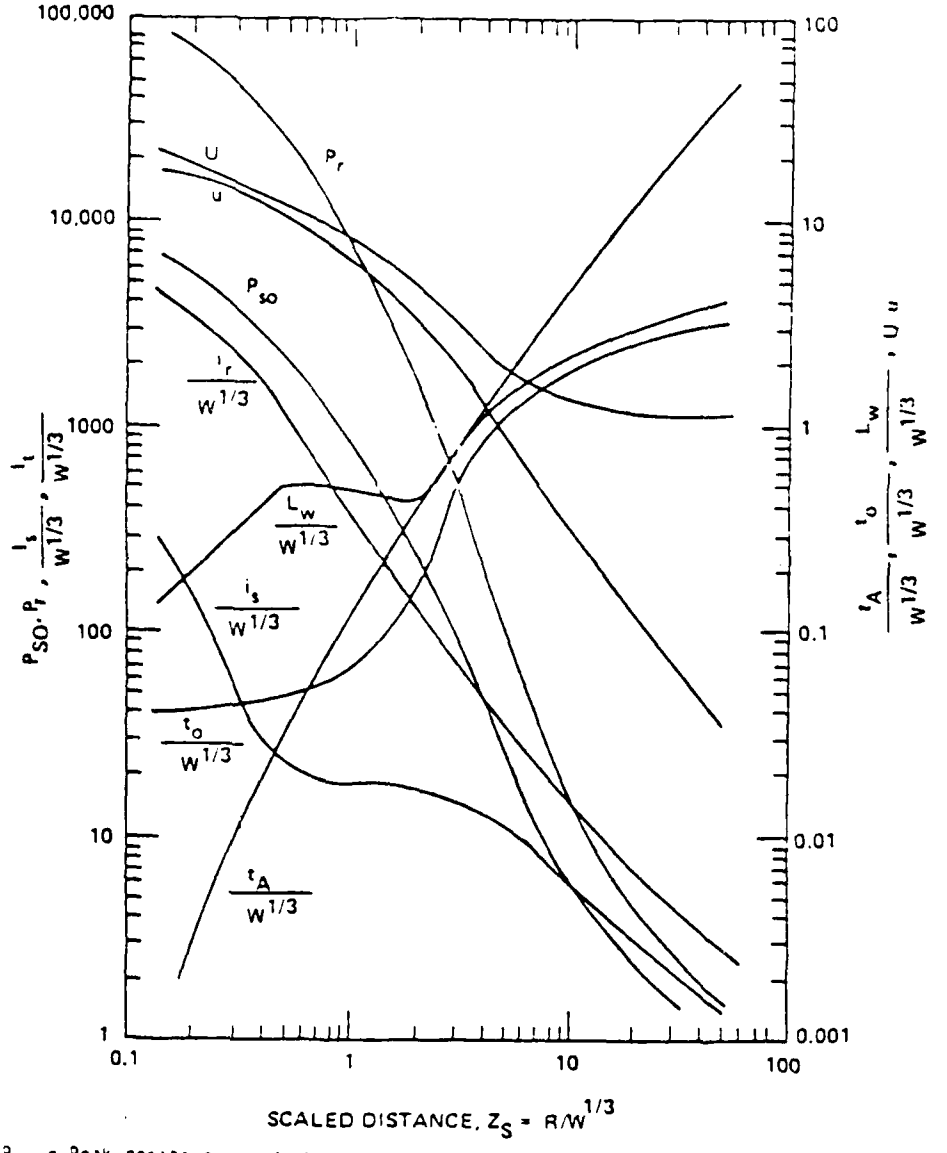

P_{so} = Peak positive incident pressure, psi

P_r = peak positive normal reflected pressure, psi

$i_s/W^{1/3}$ = Scaled unit positive incident impulse, psi-ms/lb$^{1/3}$

$i_r/W^{1/3}$ = Scaled unit positive normal reflected impulse, psi-ms-lb$^{1/3}$

$t_A/W^{1/3}$ = Scaled time of arrival of blast wave, ms/lb$^{1/3}$

$t_o/W^{1/3}$ = Scaled positive duration of positive phase, ms/lb$^{1/3}$

$L_w/W^{1/3}$ = Scaled wave length of positive phase, ft/lb$^{1/3}$

U = Shock front velocity, ft/ms

u = Partical Velocity, ft/ms

W = Charge weight, lbs

R = Radial distance from charge, ft

Z_S = Scaled Distance, ft/lb$^{1/3}$

Figure 5.16. Shock Wave Parameters for Spherical TNT Explosions in Free Air (after U.S. Army Engineer Waterways, 1982)

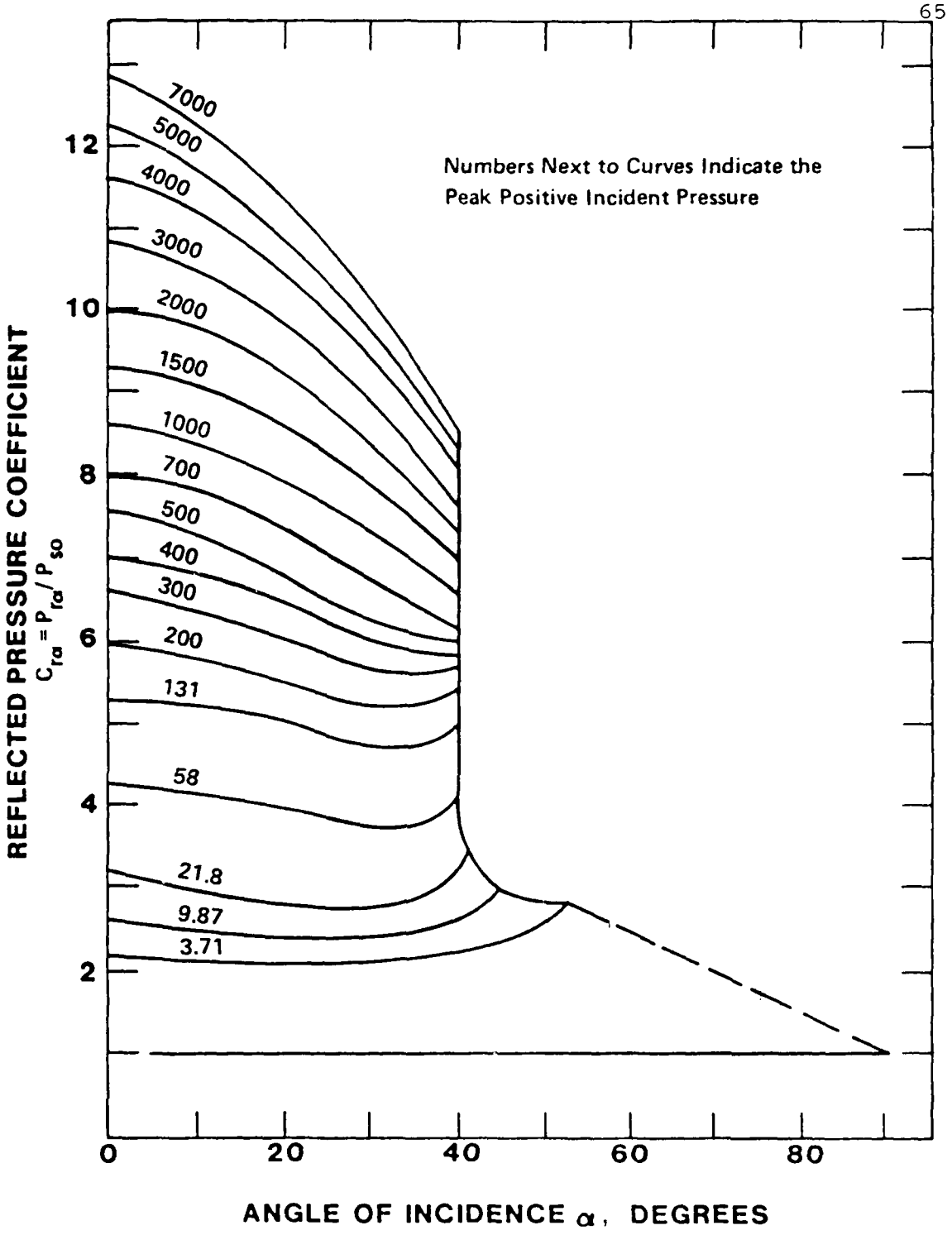

Figure 5.17. Reflected Pressure Coefficient versus Angle of Incidence (after U.S. Army Engineer Waterways, 1982)

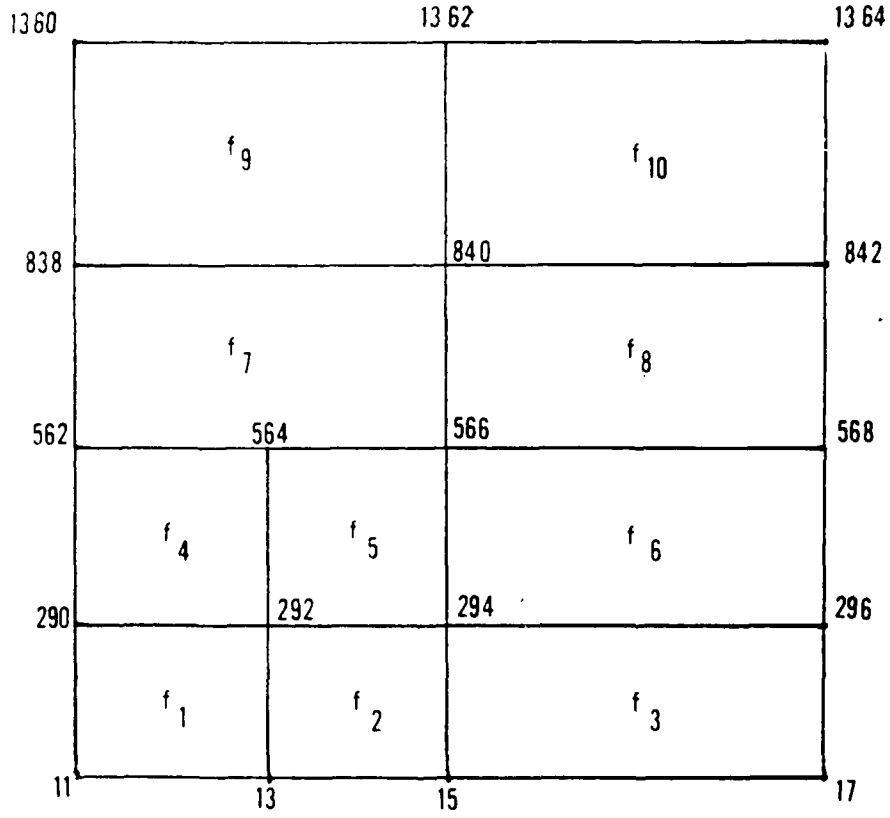

Figure 5.18. Global Nodes (represented by numbers) Used to Calculate the Pressure Time Functions (f_i) for Loading the Burster Slab

Table 5.1. Pressure Time Functions Used in NONSAP-C to Characterize the Shock Wave of the Blast

Load Function f_i	Peak Positive Reflected Pressure P_r (psi)	Start Time (ms)	End Time (ms)
1	15410.0	0.0	0.01062
2	3745.0	0.01457	0.02760
3	1371.0	0.04408	0.06231
4	3954.0	0.01390	0.02652
5	2324.0	0.02530	0.04066
6	983.0	0.05293	0.07424
7	1480.0	0.03469	0.05242
8	1123.0	0.04328	0.06314
9	638.0	0.06796	0.09406
10	645.0	0.06313	0.08902
11	413.0	0.09184	0.12356

- Styrofoam elements (three groups)

Retaining wall	21 elements
Wall (z-y plane)	55 elements
Wall (x-y plane)	61 elements

- Burster slab (one group) 11 elements

- Structure (three groups)

Top slab	64 elements
Wall	48 elements
Bottom slab	44 elements

- Soil (nine groups)

First group	30 elements
Second group	46 elements
Third group	98 elements
Fourth group	16 elements
Fifth group	12 elements
Sixth group	16 elements
Seventh group	48 elements
Eighth group	73 elements
Ninth group	62 elements

All elements in the structure were modeled using 20-node elements. The elements in the burster slab and soil elements next to the structure were modeled with 8- to 19-node elements. Most of the soil elements and the styrofoam elements were modeled with 8-node elements.

Details of the Analysis

Once the finite element mesh and the loading functions were determined, it was necessary to determine the material properties. It was decided from the beginning of the analysis to use a linear model to represent the behavior of all elements in the system. It was intended to use the

linear analysis to check whether any of the elements in the system showed nonlinear behavior, and if so, a nonlinear model would be included in a second analysis to represent the elements with expected nonlinear behavior. The linear model in NONSAP-C required as input parameters two elastic constants and the density of the material. The values of these parameters for each material type are listed in Table 5.2. The concrete was modeled without reinforcement.

The objective of this analysis was to simulate the blast load test performed in the centrifuge. Therefore, it was necessary to include in the analysis the effect of the gravity loads imposed by the 60-g environment. The program NONSAP-C has the capability of including the gravity loads. These loads are input in the data by specifying the number of g's in a given direction. In this case the number of g's was 60, and it was specified in the negative y-direction (Figure 5.3). The program uses this information to calculate the gravity loads and includes them in the load vector of the equation of motion. To the writer's knowledge, such an analysis of a centrifugal test of an underground structure subjected to a blast load has not been attempted before.

The blast analysis was performed without damping; and a consistent mass matrix was specified. The integration method used was the Wilson-Theta Method. The analysis was performed using an integration time step of 0.010 ms, and it was conducted through 100 steps.

Table 5.2. Material Properties Used in NONSAP-C for the Blast Load Analysis

Material Type	Modulus of Elasticity (psi)	Poisson's Ratio	Density ($lb \cdot s^2/in^4$)
Styrofoam	100.0	0.10	1.827E-06
Concrete	3300000.0	0.15	1.947E-04
Soil	50000.0	0.33	1.498E-04

CHAPTER SIX
PRESENTATION AND DISCUSSION OF THE RESULTS

Introduction

The results of each of the analyses are presented and discussed in the following order: static, dynamic, and blast load. The predicted results are compared to the respective observations from the static, dynamic, and blast load tests. A summary of the results is presented in Table 6.1.

Processing of the Results

Static Analysis

Observations from the static tests were compared to the respective predictions with respect to the strains induced by the static load at different points of the structure.

The strains in the static tests were measured by strain gages located in the structure as shown in Figure 6.1. These gages were oriented to measure bending strains.

The strains predicted in the numerical analyses were given at 8 integration points for each element. The strains at 4 of the 8 integration points were averaged for comparison with the strains measured in the static tests.

The elements in the finite element mesh of the strip that correspond to the location of each strain gage are

Table 6.1. Summary of Results

Type of Analysis	Model	Figures
Static	Nonreinforced	6.3 - 6.9
	Reinforced	6.10 - 6.17
Dynamic	Nonreinforced	6.18 - 6.22
	Reinforced	6.23 - 6.32
Blast	Nonreinforced	6.33 - 6.40

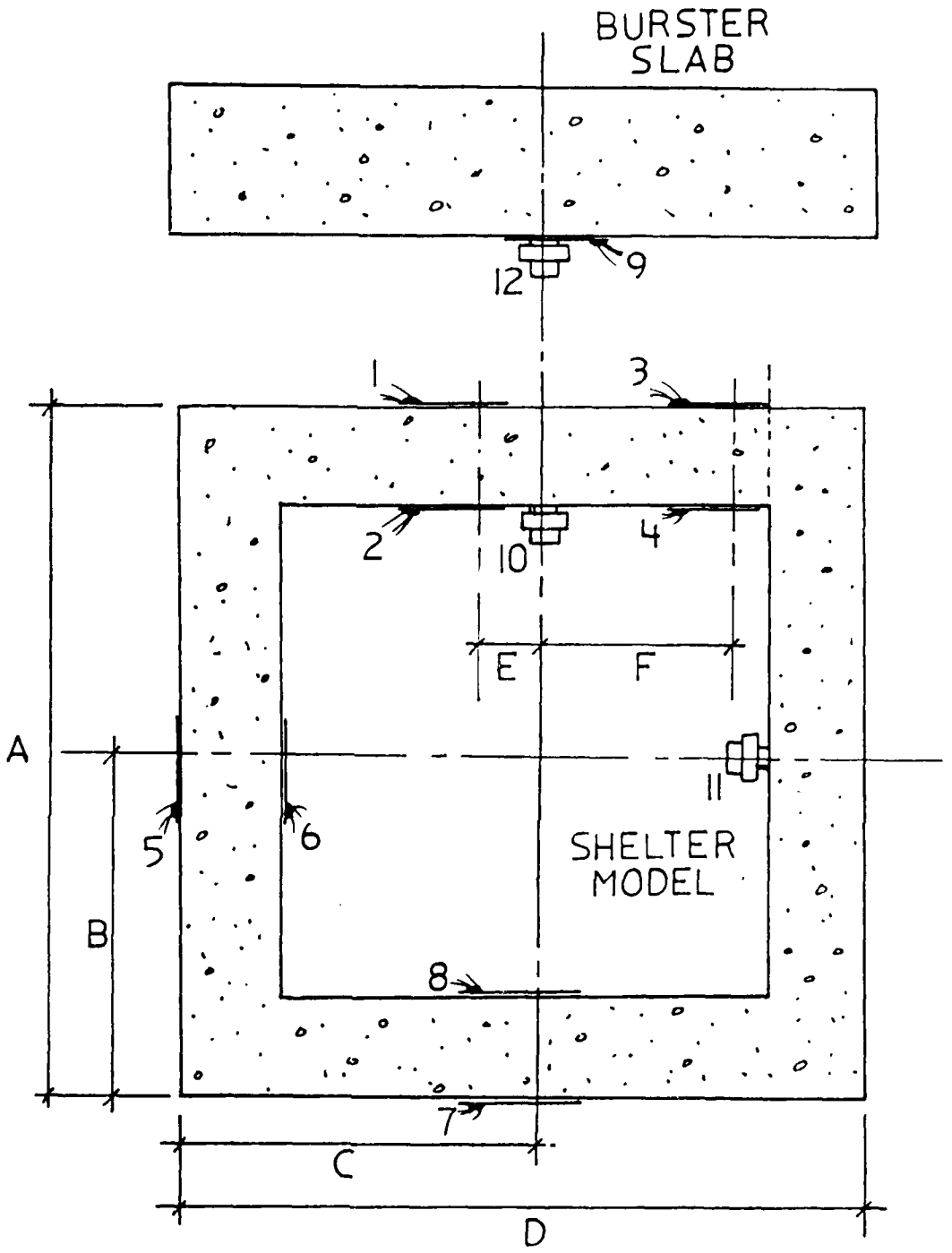

A = 111.8 mm. D = 101.6 mm.
B = 55.9 mm. E = 12.1 mm.
C = 50.8 mm. F = 31.1 mm.

Figure 6.1. Location of Accelerometers and Strain Gages (numbers designate accelerometers and gage numbers)

given in Table 6.2 (refer to Figures 6.1 and 6.2 for the strain gage numbers and the element numbers, respectively). Also listed in Table 6.2 are the 4 integration point numbers used to calculate the average strain in the corresponding element. The integration point numbers were shown in Figure 4.1.

Dynamic Analysis

Observations from the dynamic tests included the measurement of dynamic strains and accelerations. The strains were measured at the same points on the structure as in the static tests. The accelerations were measured at the center of the bottom of the top slab and at the center of the inside wall.

The strains predicted by the dynamic analyses were given at 27 integration points for each element. The strains at either 6 or 9 of the 27 integration points were averaged for comparison with the measured strains. The elements and the corresponding integration point numbers used to calculate the average strains in the elements are given in Table 6.2 (refer to Figures 4.2 and 6.2 for the integration point numbers and the element numbers, respectively).

The accelerations predicted by the numerical analyses were given at nodal points. The accelerations at the top slab were measured in the y-direction, and the accelerations at the wall were measured in the z-direction (Figure 6.2). The predicted accelerations at two nodal points were

Table 6.2. Finite Element Numbers and Integration Point Numbers Used for Comparison of Strains With Static and Dynamic Tests

Gage Number	Element Number	Integration Point Numbers	
		Static Analysis	Dynamic Analysis
1	2,3	2,4,6,8	3,6,9,12,15,18,21,24,27
2	22,23	1,3,5,7	1,4,7,10,13,16,19,22,25
3	6	2,4,6,8	3,6,9,12,15,18,21,24,27
4	26	1,3,5,7	1,4,7,10,13,16,19,22,25
5	55,56	1,5,2,6	1,10,19,3,12,21
6	35,36	3,7,4,8	7,16,25,9,18,27
7	90	1,3,5,7	1,4,7,10,13,16,19,22,25
8	70	2,4,6,8	3,6,9,12,15,18,21,24,27

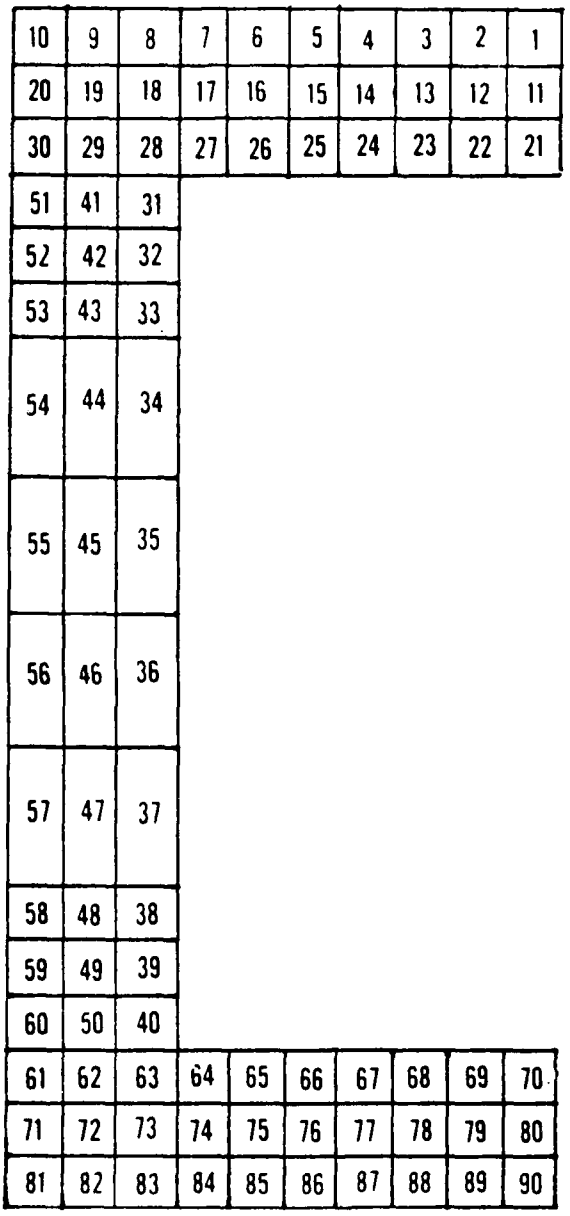

Figure 6.2. Element Numbers in the Coarse Discretization of the Strip

averaged to obtain the accelerations at the middle of the strip.

Blast Analysis

Observations from the blast tests in the centrifuge included the measurement of dynamic strains, accelerations, and pressures on the structure. The location of all gages used in these tests were shown in Figure 5.1.

The numerical analysis predicted the stresses at the center of each element. Assuming a linear stress distribution across the top and bottom slabs and across the wall, the appropriate stresses were calculated at the surface of the appropriate elements where the strains were measured. Once the appropriate stress was obtained, the strain was calculated by dividing the stress by the Young's Modulus of the concrete.

The accelerations predicted by the numerical analysis were given at nodal points. These accelerations were averaged at the appropriate points for comparison with the centrifuge tests.

The observed pressures were measured at the soil-structure interface, and their direction was perpendicular to the surface of the structure. However, the numerical analysis predicted these pressures (stresses) at the center of each element. The stresses at the surface of the element where the observed pressures were measured could not be calculated because the stress distribution across the soil-

structure interface is not known. Therefore, the predicted pressures could not be compared to those observed.

Presentation and Discussion

Static Analysis

The predicted strains from the static analyses are presented with the observed strains for the non-reinforced and the reinforced models.

Nonreinforced Model. Figures 6.3 through 6.9 present the predicted and observed strains in the nonreinforced model. Each figure corresponds to the results of a different strain gage. Negative strains indicate compression.

In general, the predicted behavior was similar to the observed; the magnitude of the strains increased as the load was increased. The predicted strains were larger than the observed, except for those predicted at the location of gages 3 and 4.

The differences between predicted and observed values can be explained by the errors associated with the assumptions made in the numerical model or with the experimental conditions or both.

Gill (1985) reported that the Doric transducer recording the data during the static tests produced unstable readings. These readings tend to decrease after the load increment had been applied. He concluded that this behavior was due to the elastic deformation of the structure during

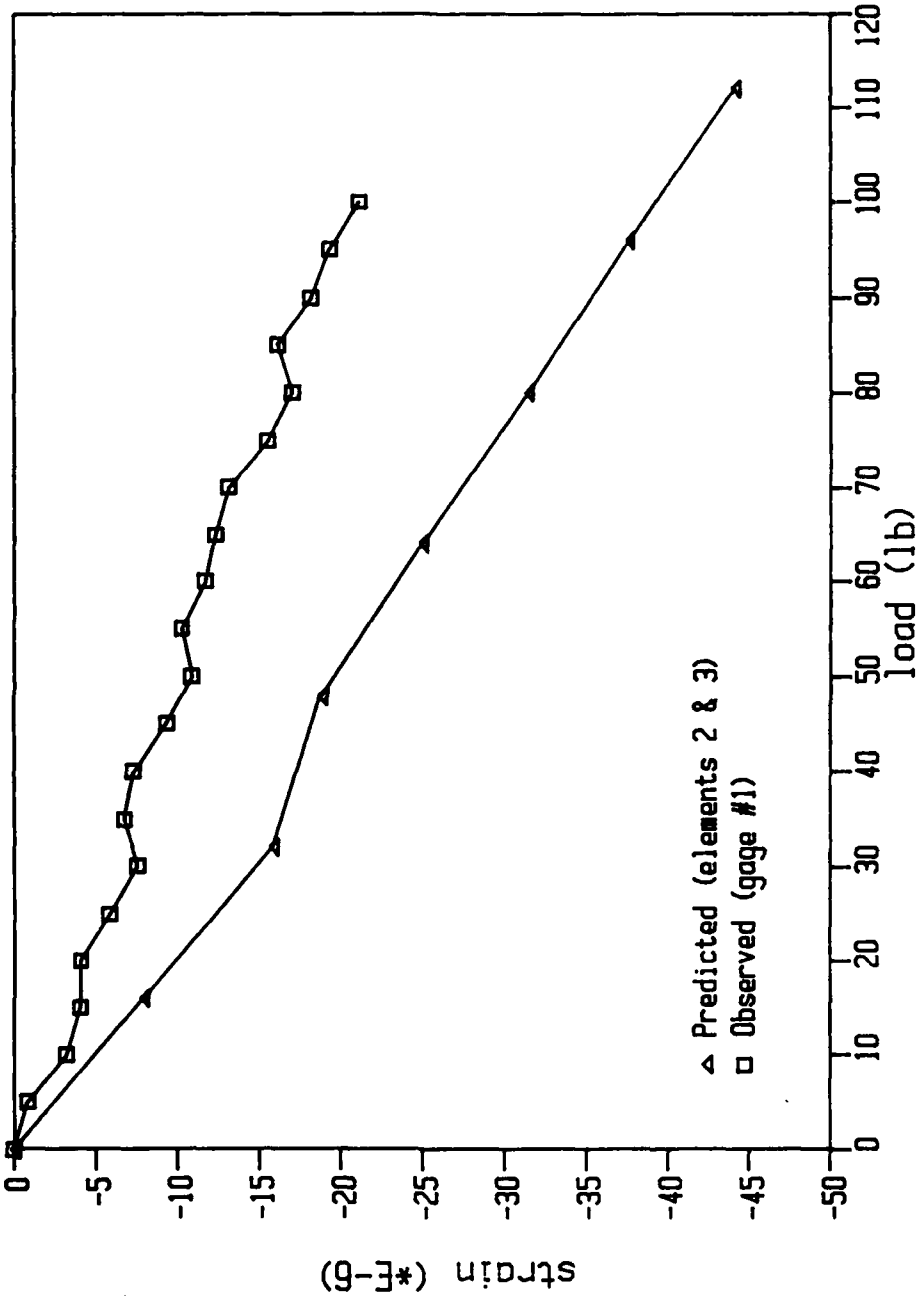

Figure 6.3. Comparison of Predicted and Observed Strains in the Static Analysis of the Non-Reinforced Structure (gage # 1)

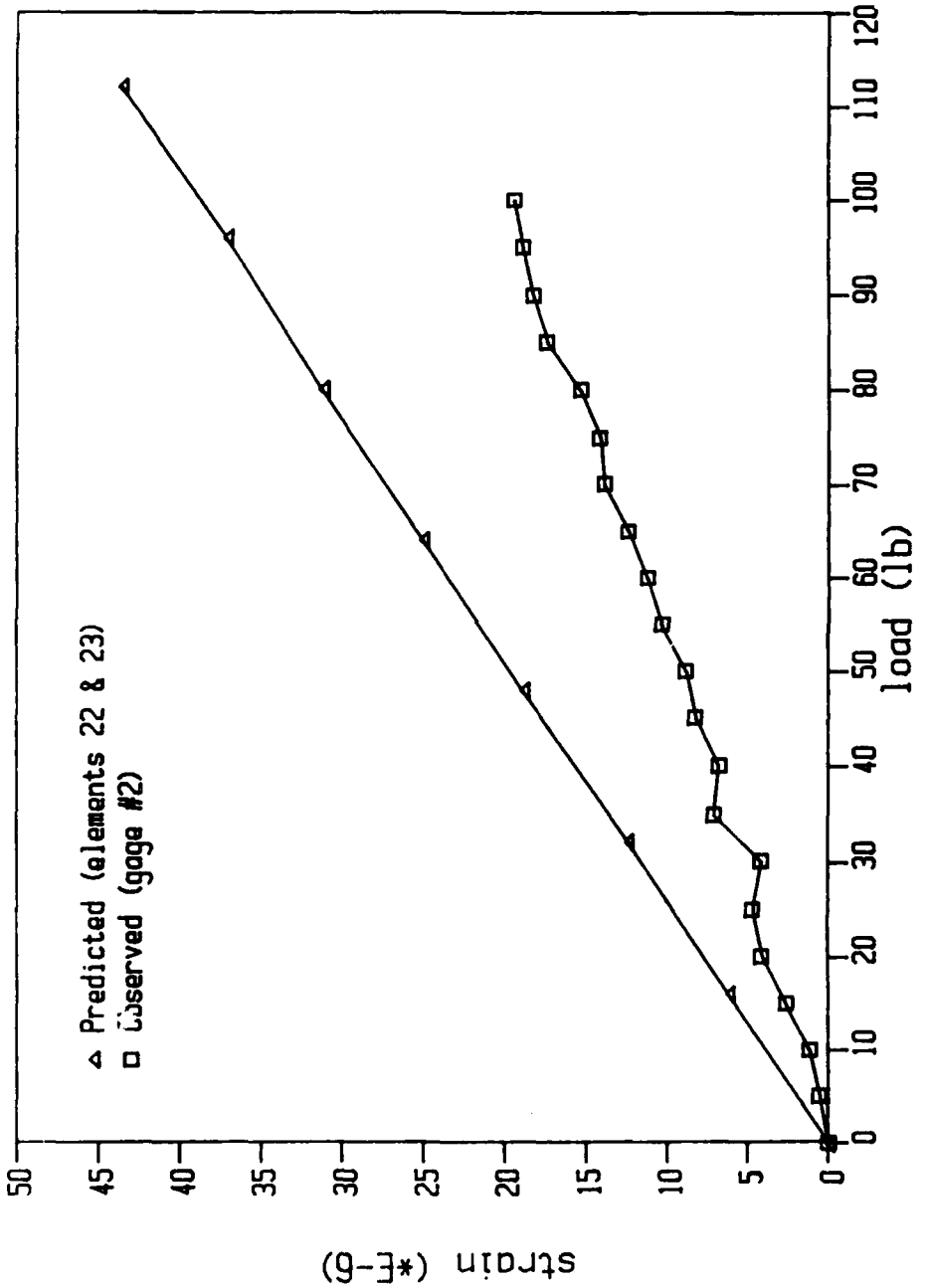

Figure 6.4. Comparison of Predicted and Observed Strains in the Static Analysis of the Non-Reinforced Structure (gage # 2)

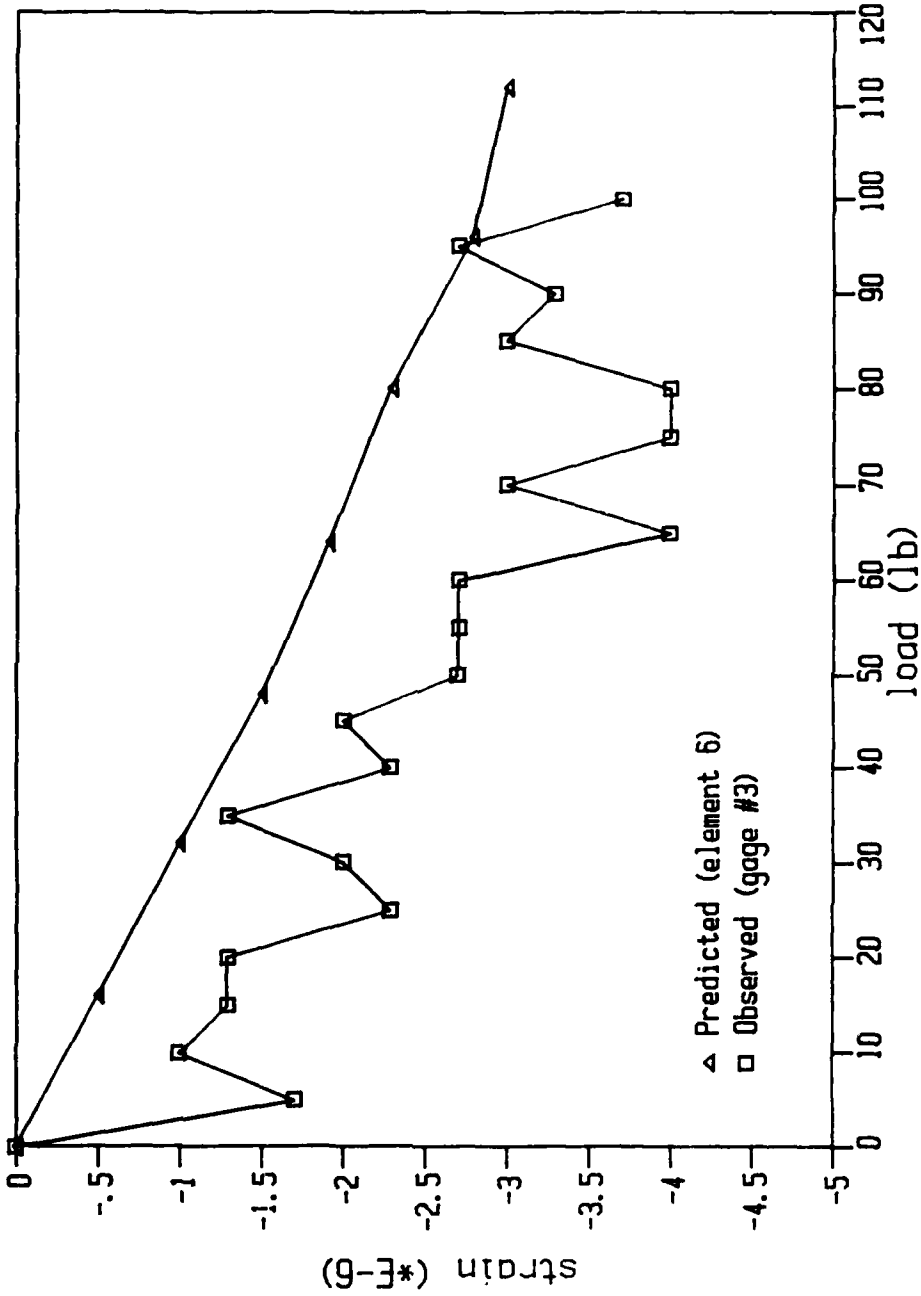

Figure 6.5. Comparison of Predicted and Observed Strains in the Static Analysis of the Non-Reinforced Structure (gage # 3)

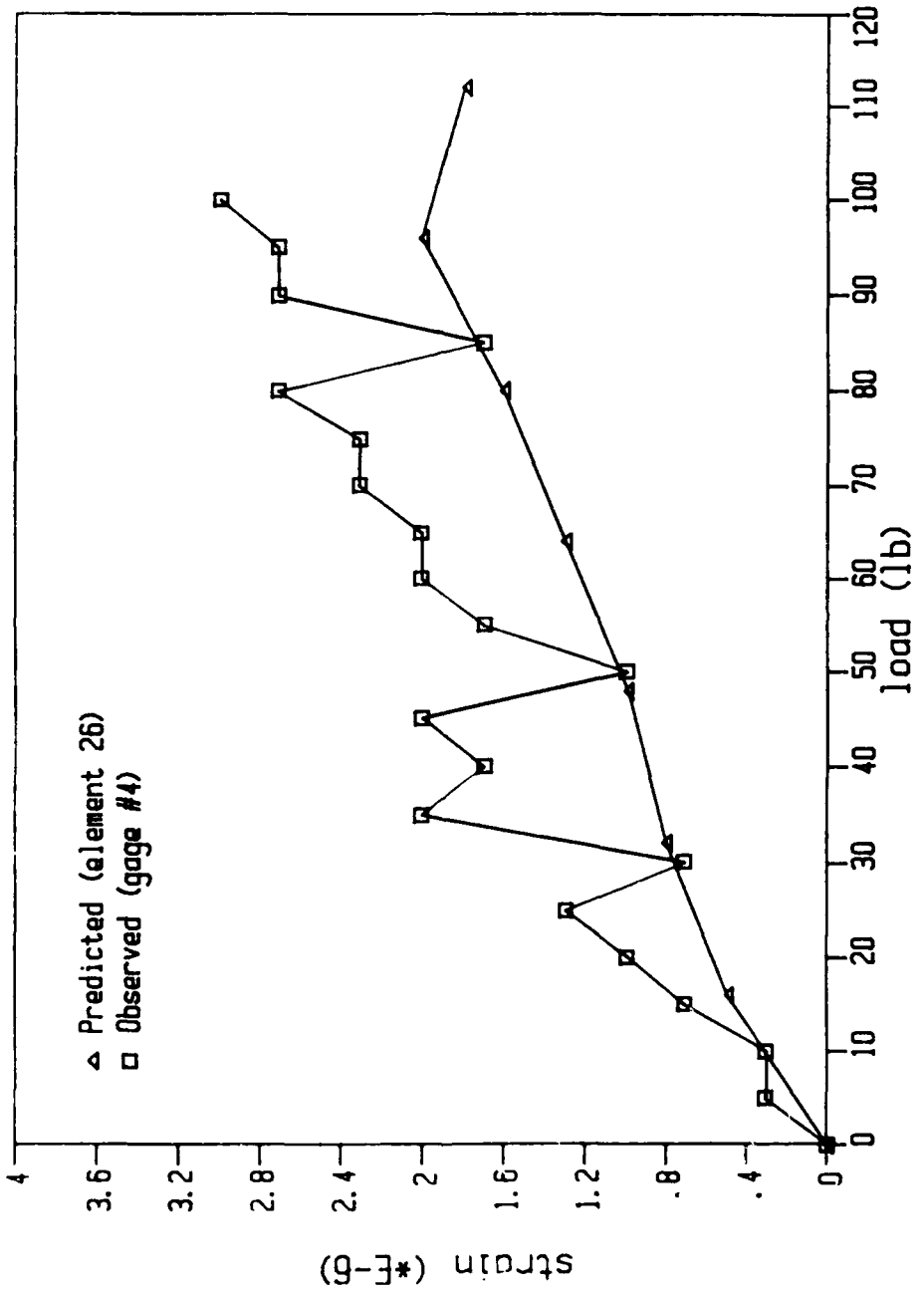

Figure 6.6. Comparison of Predicted and Observed Strains in the Static Analysis of the Non-Reinforced Structure (gage # 4)

AD-A191 747 FINITE ELEMENT ANALYSIS OF AN UNDERGROUND STRUCTURE(U) 2/2
FLORIDAUUNIV GAINESVILLE DEPT OF CIVIL ENGINEERING
N C MCVAY ET AL JAN 88 AFESC/ESL-TR-87-05
UNCLASSIFIED F08635-83-C-0136 F/G 13/13 NL

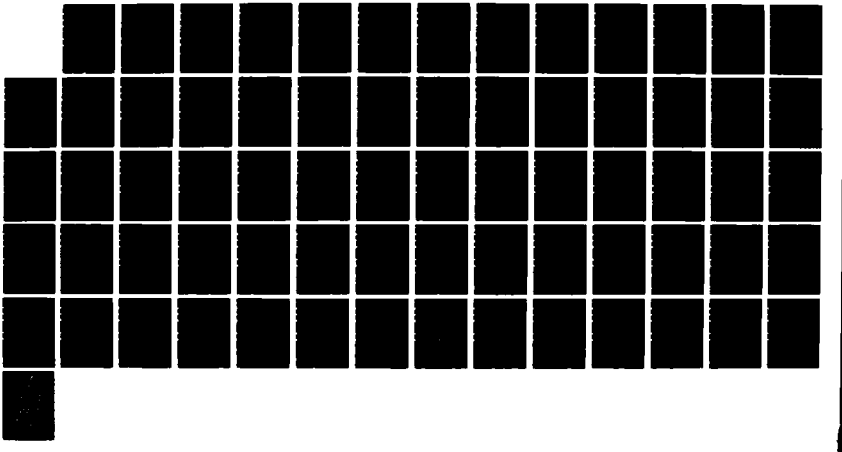

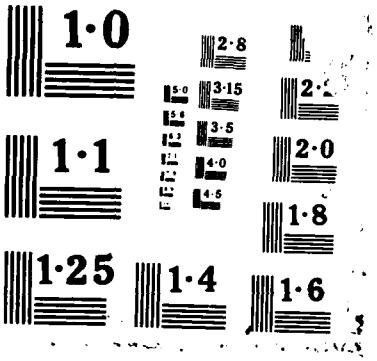
1·0
1·1
1·25
1·4
1·6
2·8
3·15
3·5
4·0
4·5
2·0
1·8

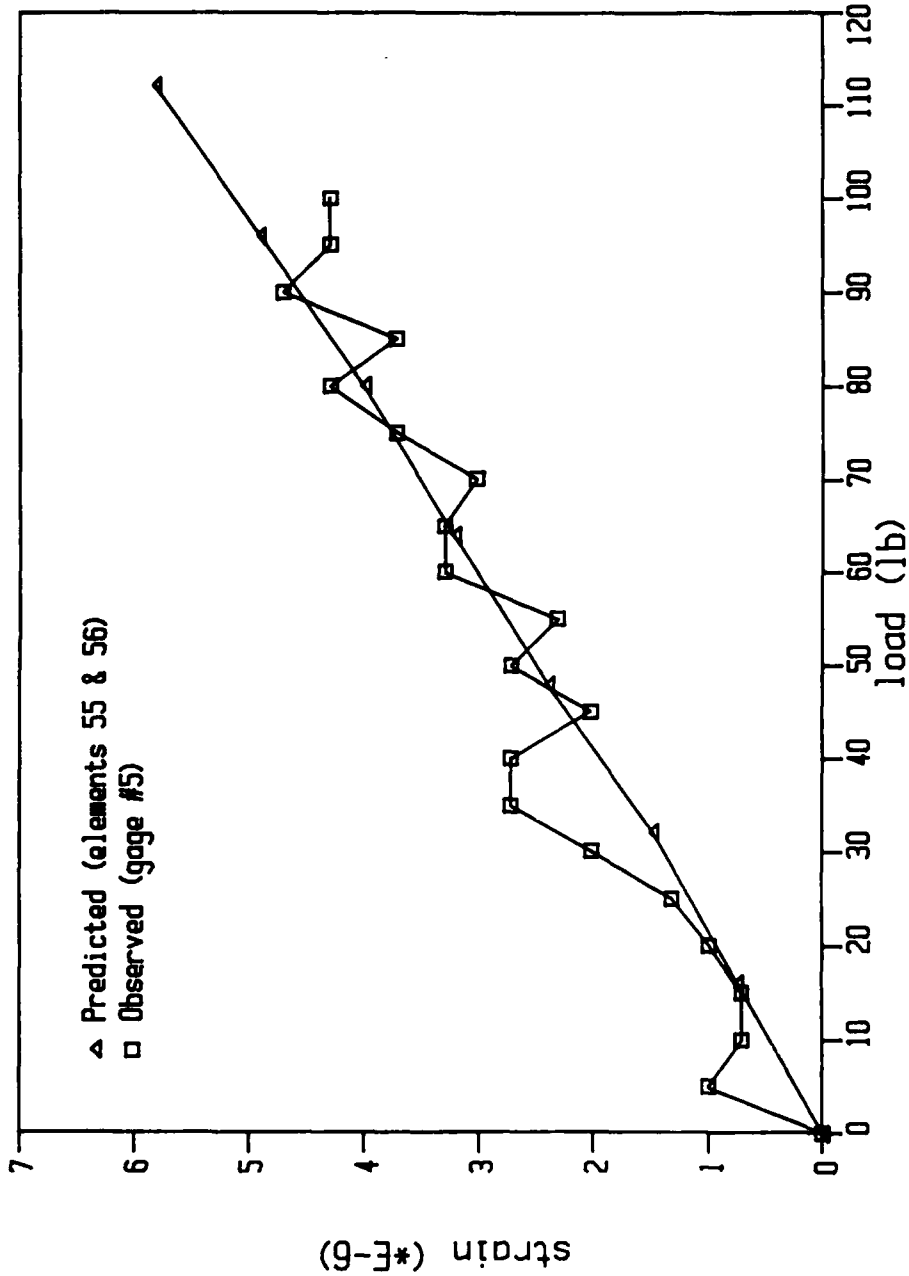

Figure 6.7. Comparison of Predicted and Observed Strains in the Static Analysis of the Non-Reinforced Structure (gage # 5)

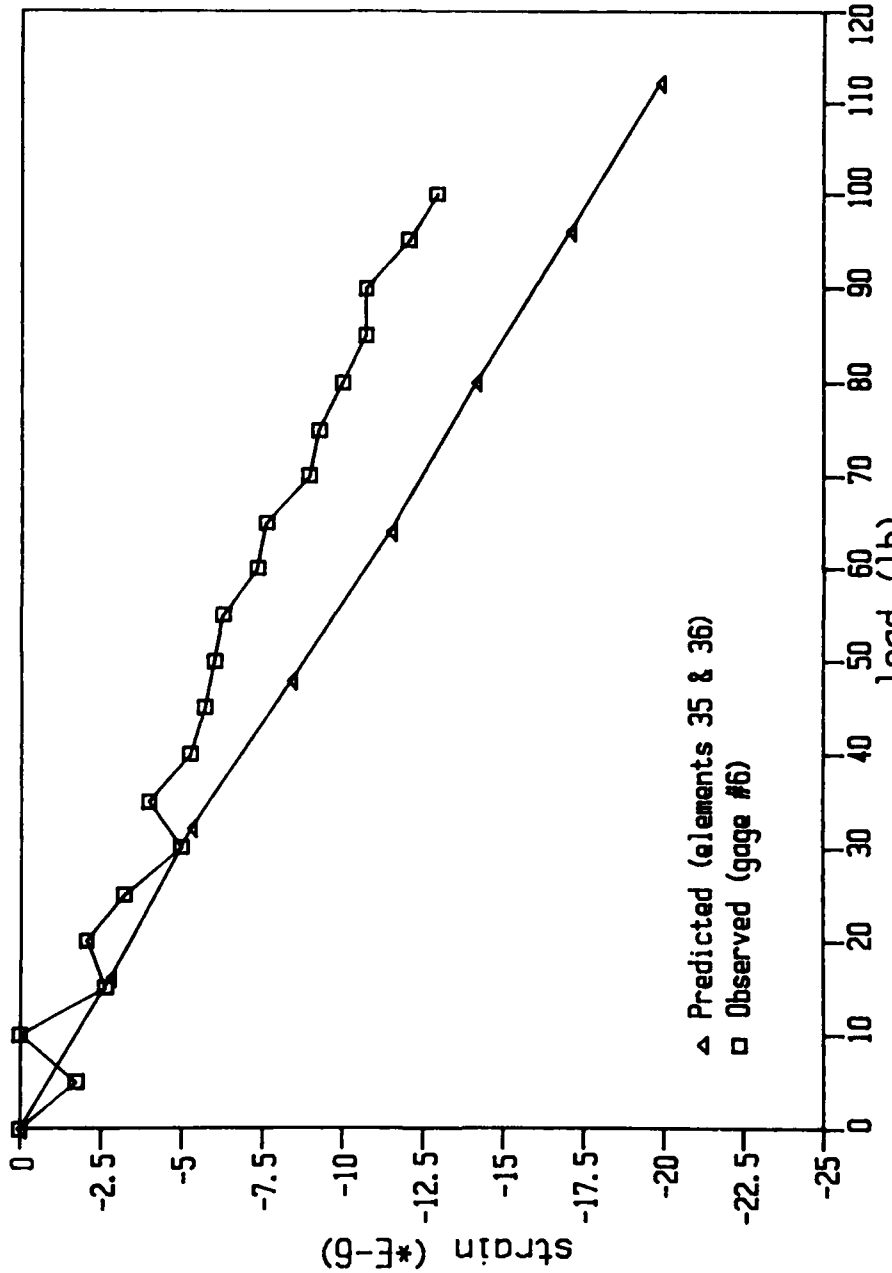

Figure 6.8. Comparison of Predicted and Observed Strains in the Static Analysis of the Non-Reinforced Structure (gage # 6)

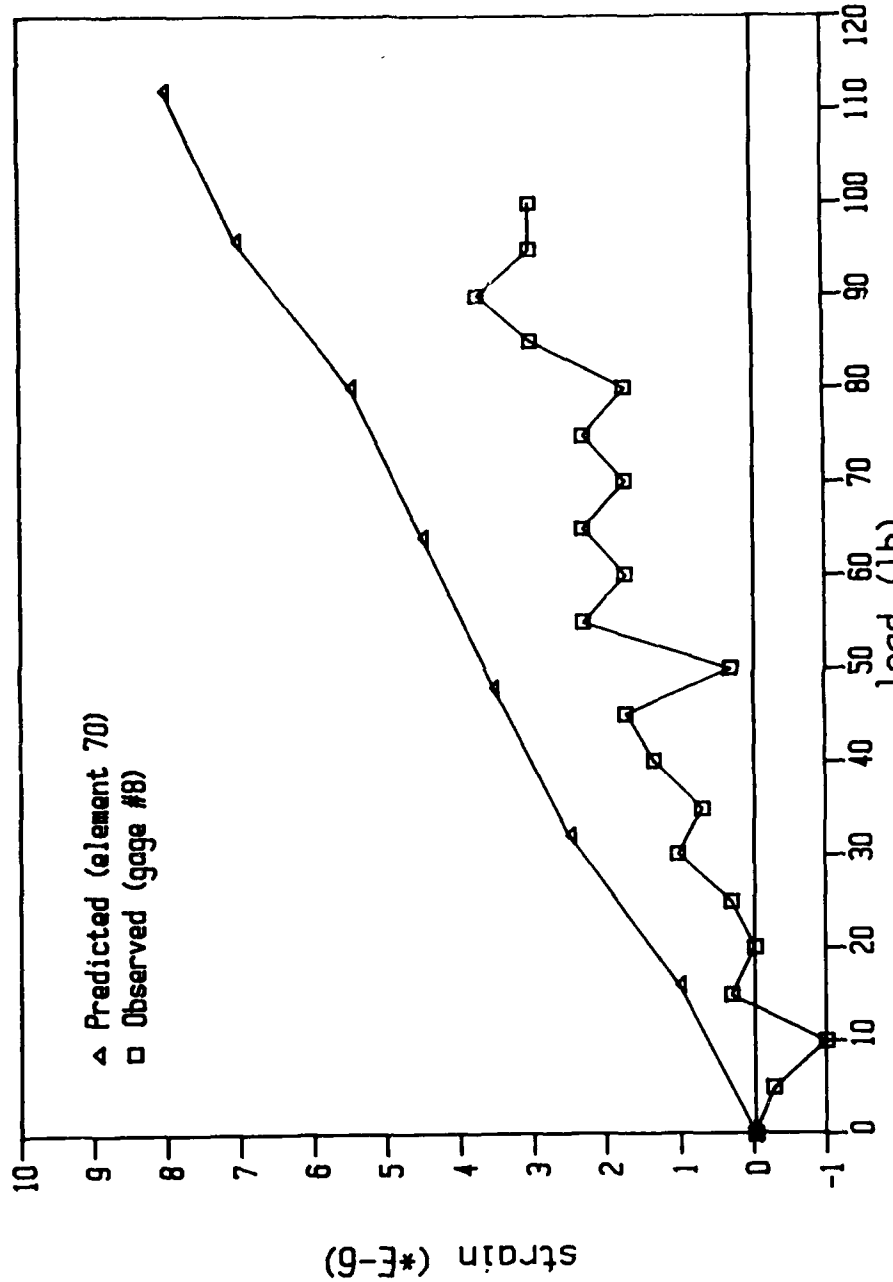

Figure 6.9. Comparison of Predicted and Observed Strains in the Static Analysis of the Non-Reinforced Structure (gage # 8)

the test. Gill also reported that the light load applied to the structure produced strains that were affected by creep, which is not accounted for in the analysis. Gill suggested that further loading of the structure was required to eliminate this effect and to better define the static loading response of the model.

In the numerical analyses it was assumed that the behavior of the structure would be plain strain under the applied load. However, this assumption was based on a dynamic analysis of the structure which led to the discretization of only a portion of the structure (strip). Although the load was reduced accordingly to the strip size, this load was distributed through the small thickness of the strip, thus, inducing high stresses throughout the structure. Also, the plain strain condition was not satisfied in the analyses because the translations of some of the nodes were released (see Chapter 4).

A different behavior was observed in gages 3 and 4, where the magnitudes of the observed strains were larger than those predicted. Gages 3 and 4 were located in an area of transition. The analysis predicted a change of stresses from compression to tension in element 6 (gage 3) and from tension to compression in element 26 (gage 4). This transition lowered the calculated average strains in the elements.

Reinforced model. Figures 6.10 through 6.17 present the predicted and observed strains in the reinforced model. Each

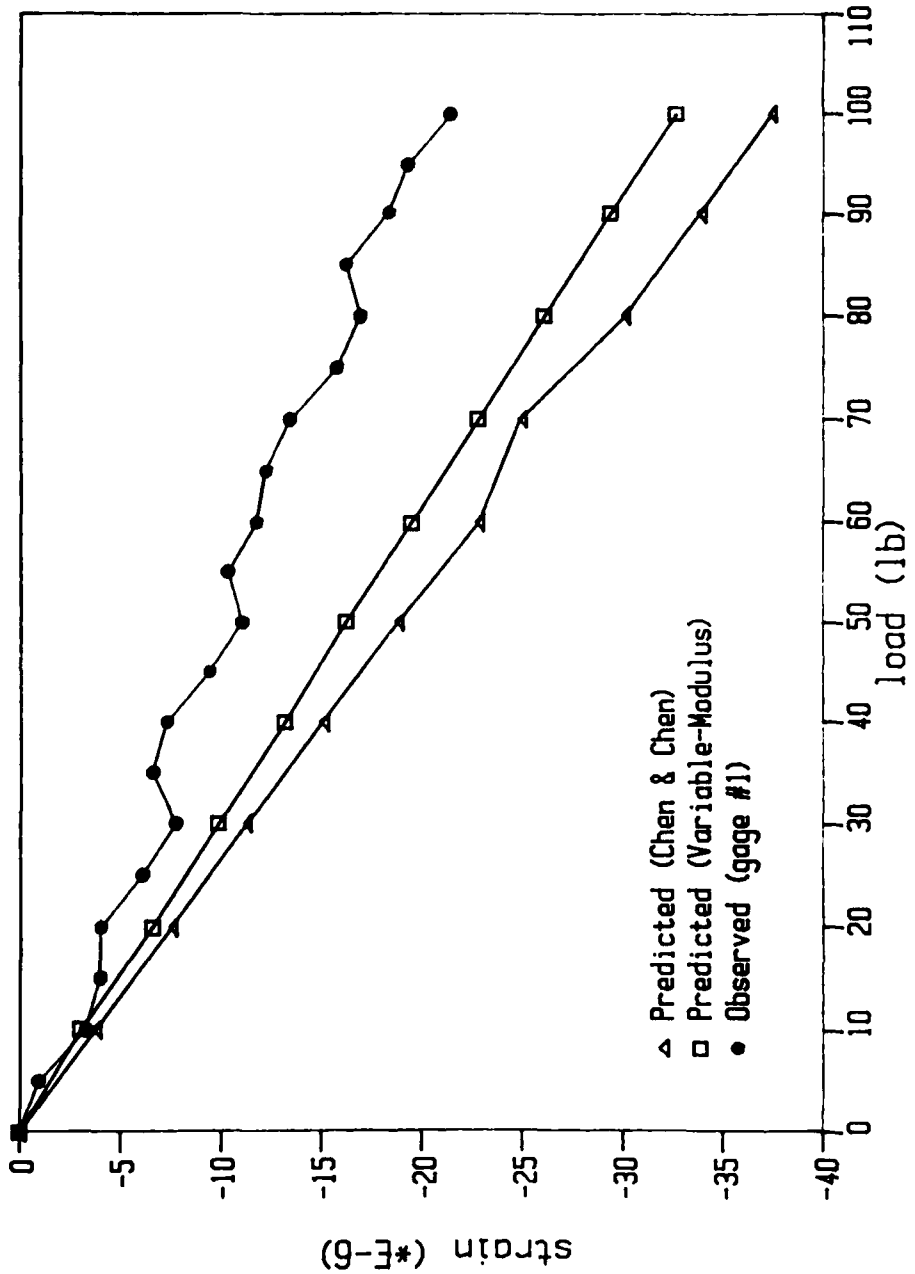

Figure 6.10. Comparison of Predicted and Observed Strains in the Static Analysis of the Reinforced Structure (gage # 1)

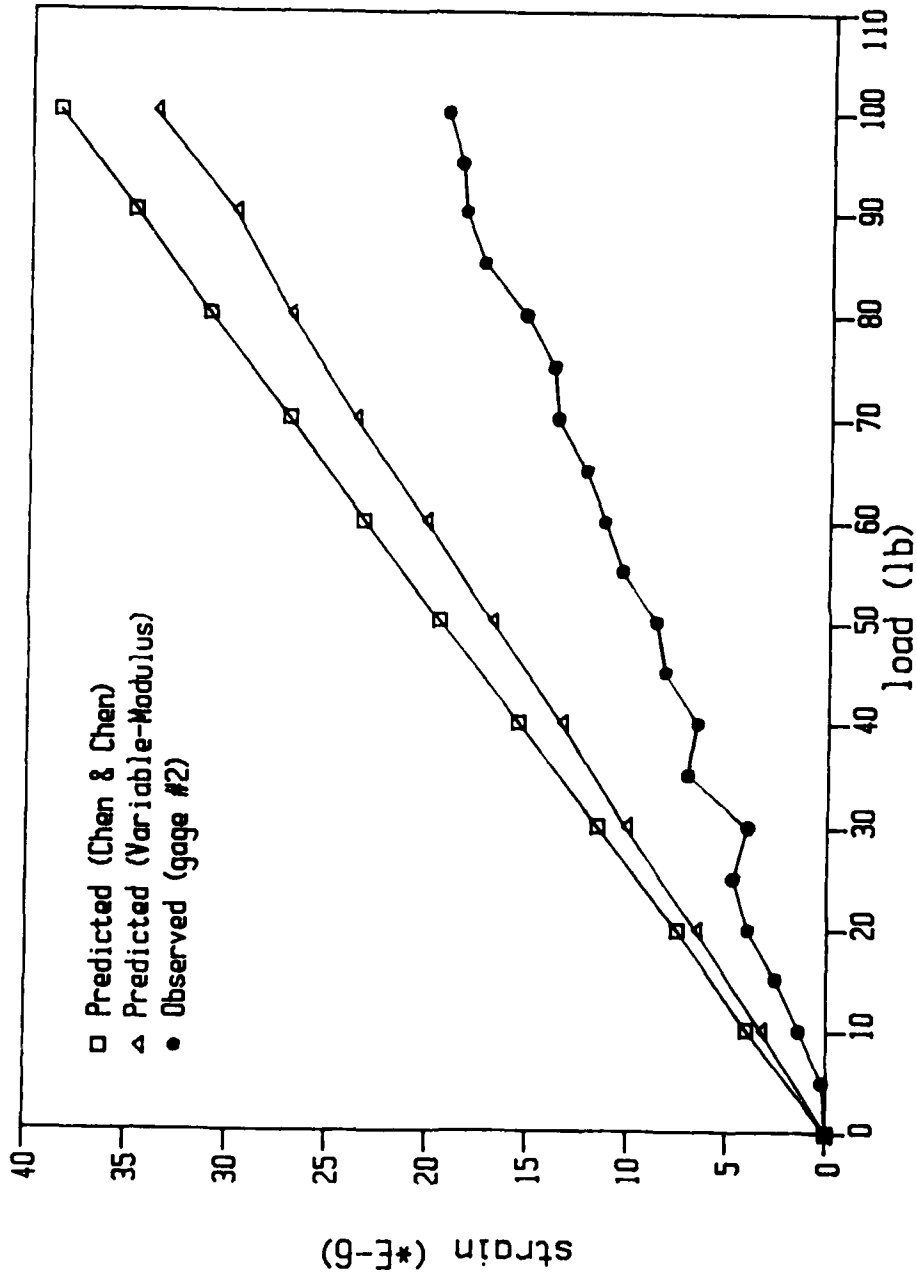

Figure 6.11. Comparison of Predicted and Observed Strains in the Static Analysis of the Reinforced Structure (gage # 2)

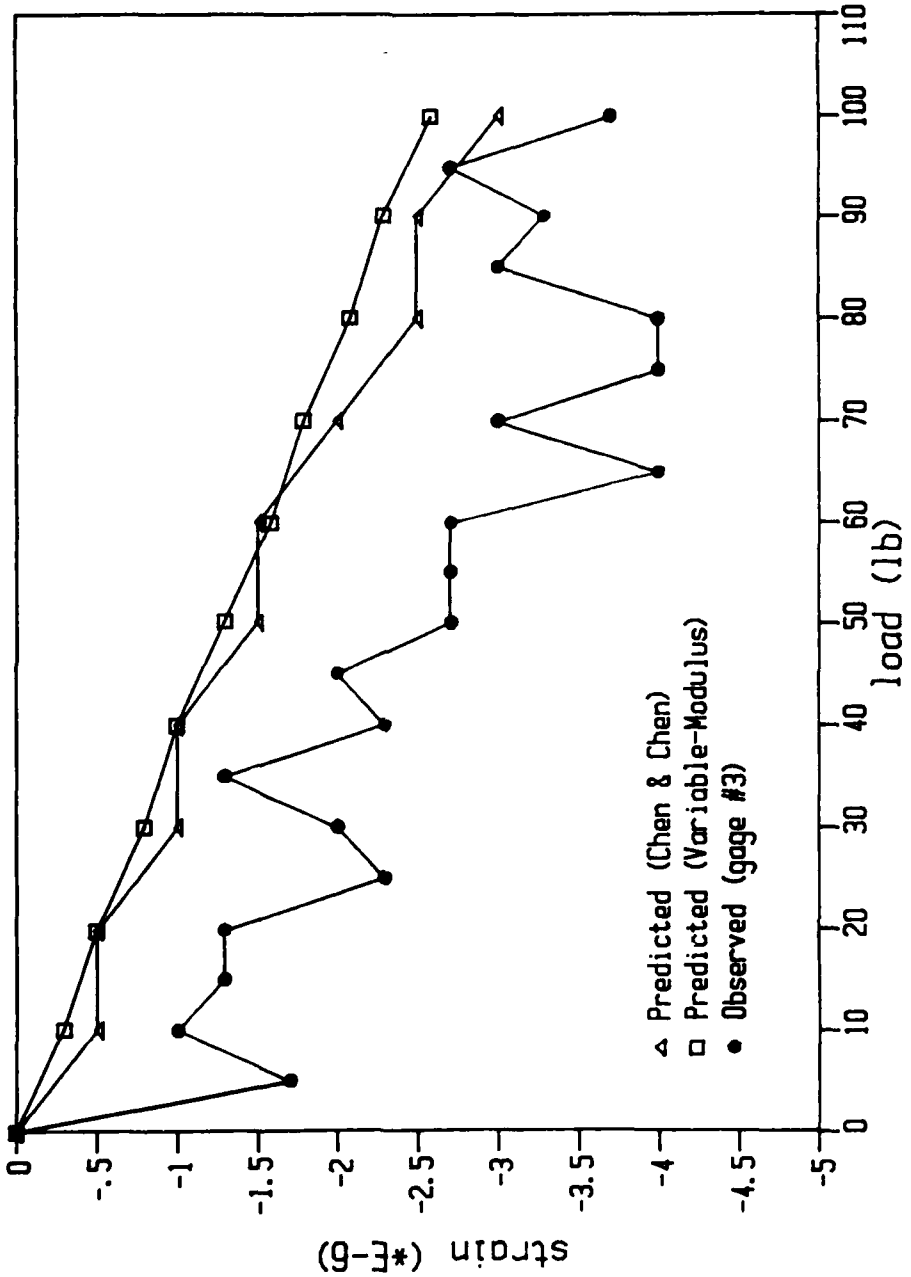

Figure 6.12. Comparison of Predicted and Observed Strains in the Static Analysis of the Reinforced Structure (gage # 3)

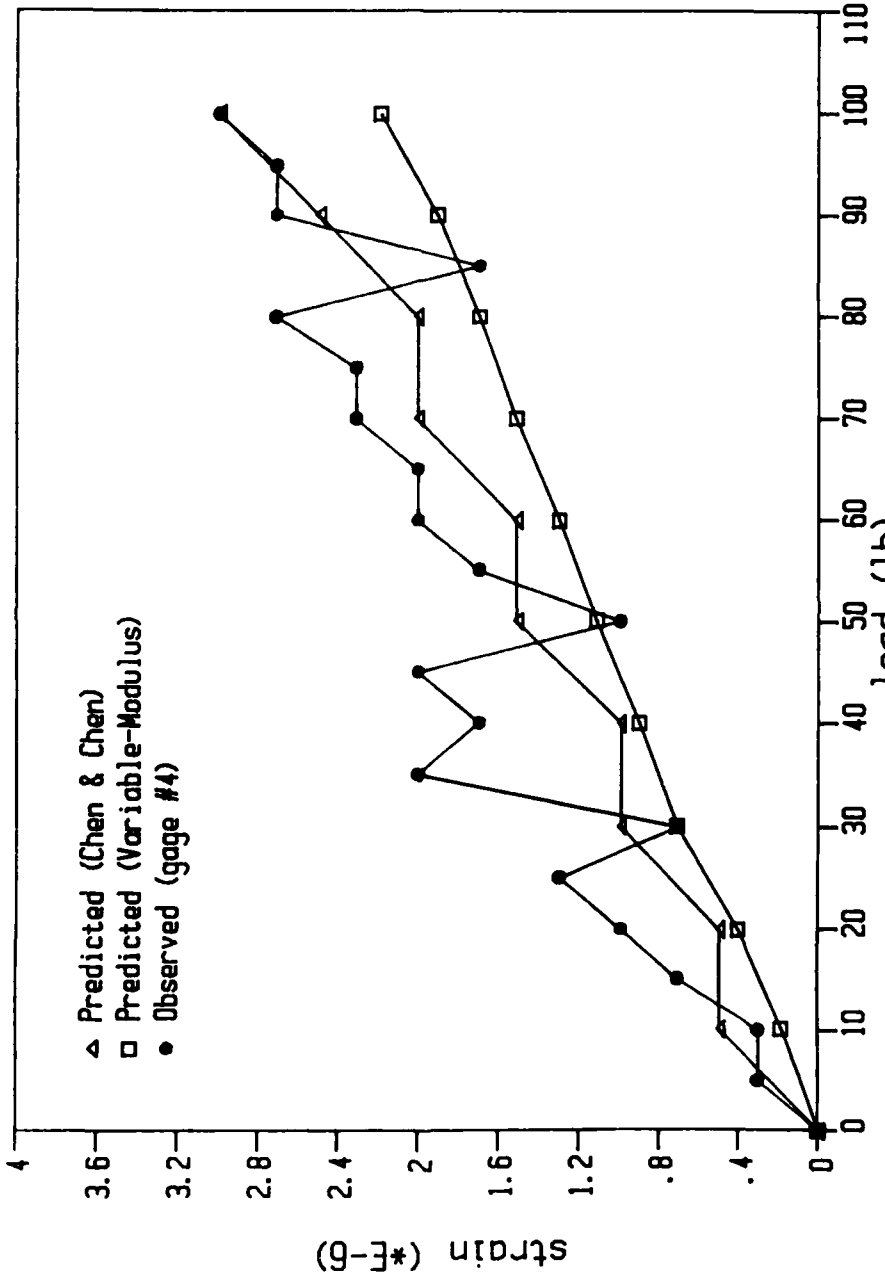

Figure 6.13. Comparison of Predicted and Observed Strains in the Static Analysis of the Reinforced Structure (gage # 4)

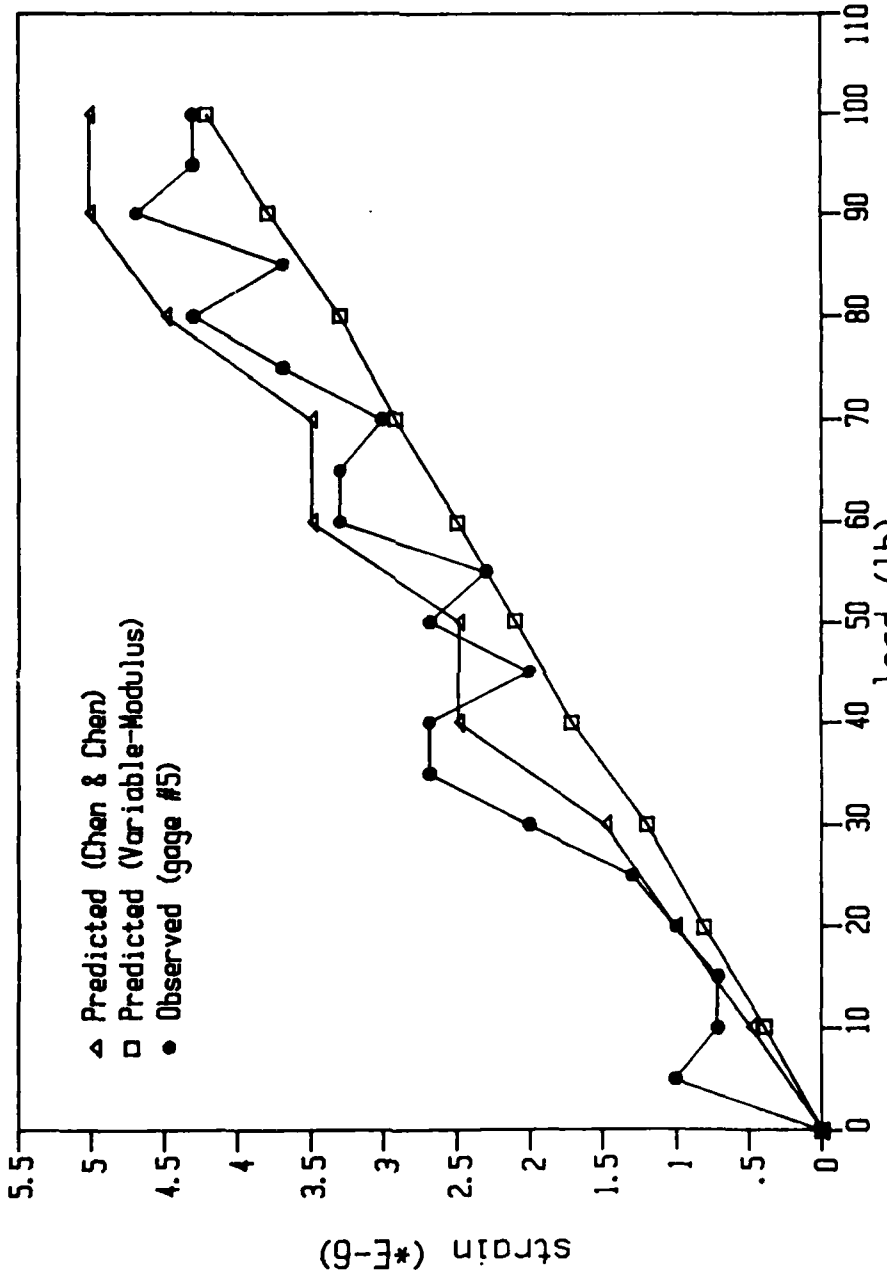

Figure 6.14. Comparison of Predicted and Observed Strains in the Static Analysis of the Reinforced Structure (gage # 5)

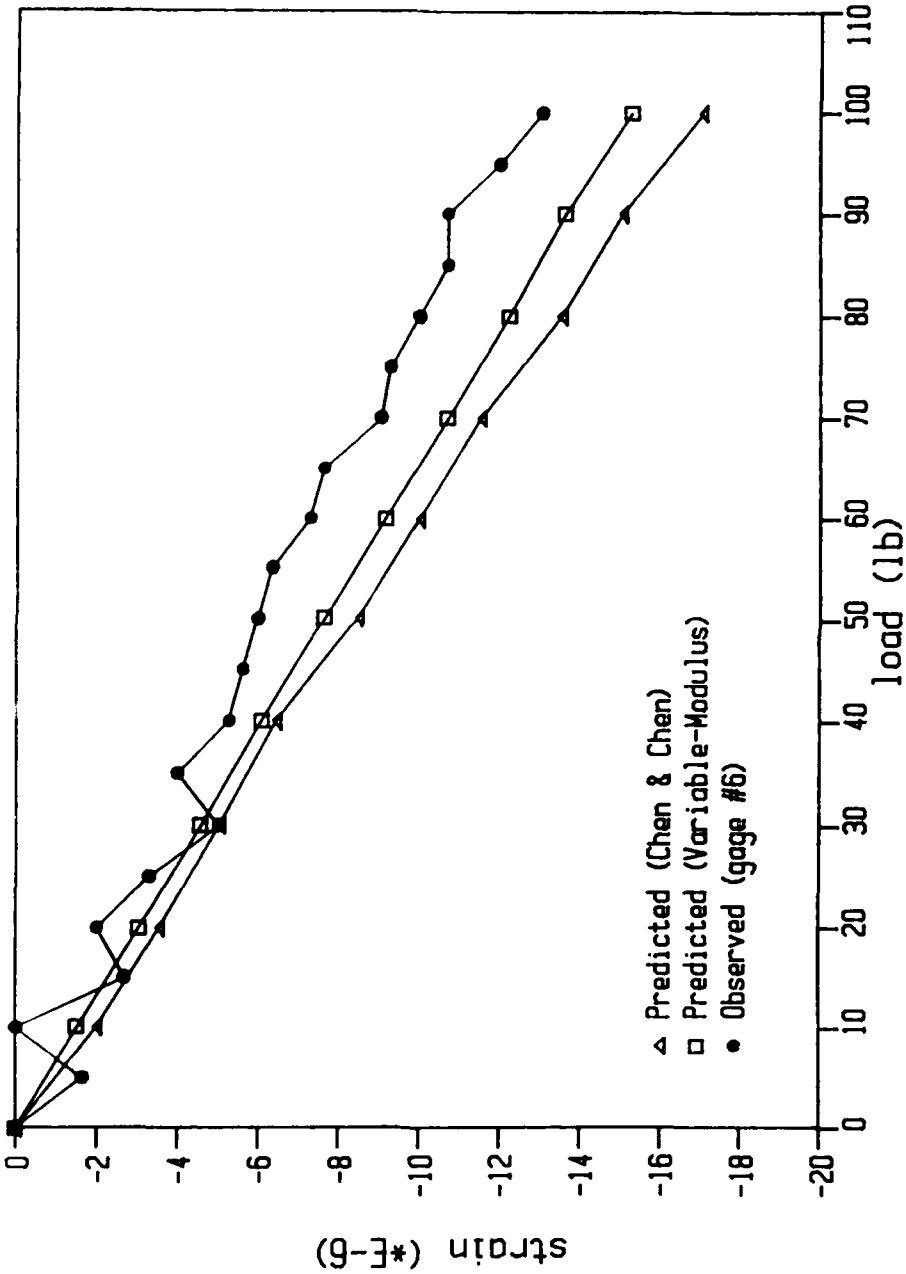

Figure 6.15. Comparison of Predicted and Observed Strains in the Static Analysis of the Reinforced Structure (gage # 6)

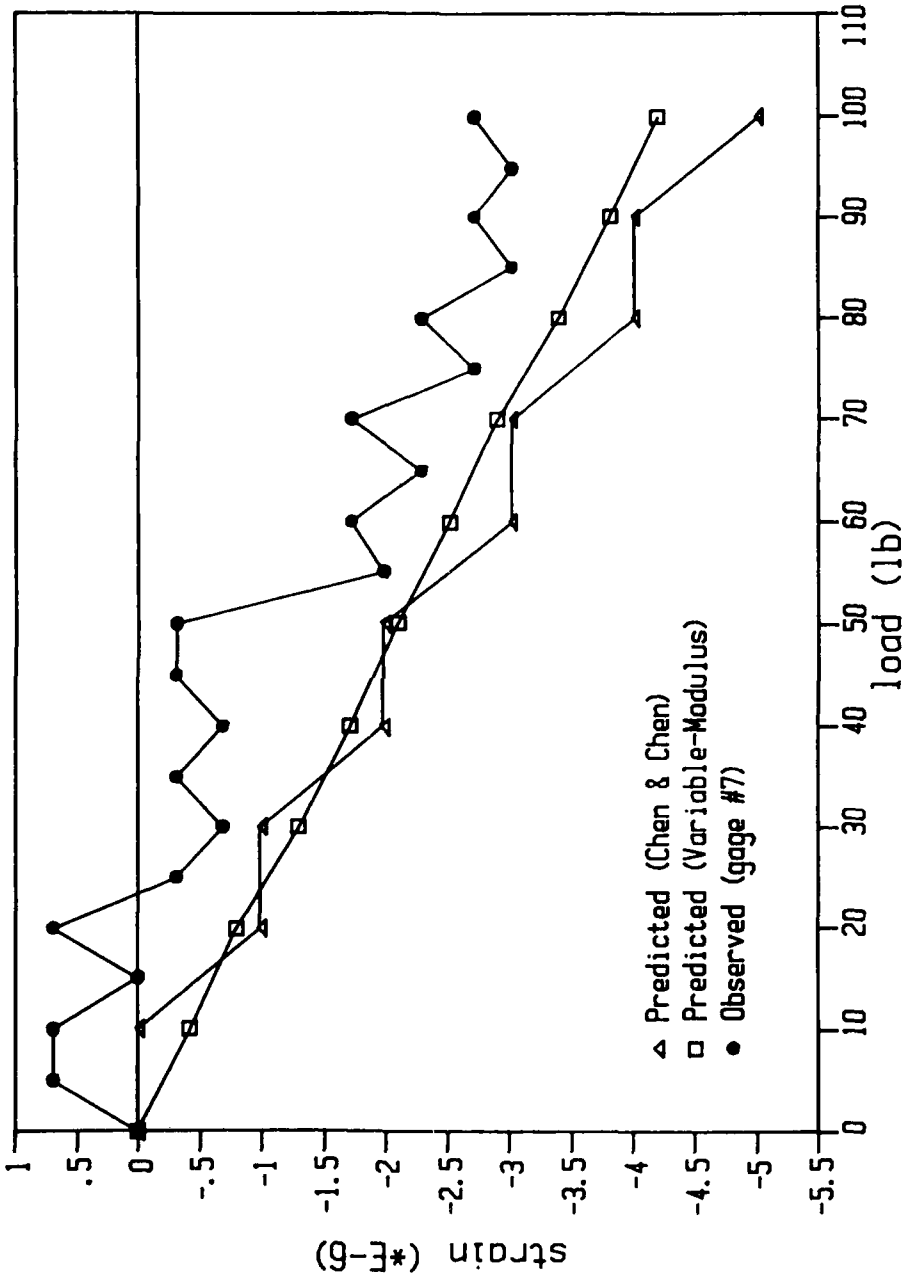

Figure 6.16. Comparison of Predicted and Observed Strains in the Static Analysis of the Reinforced Structure (gage # 7)

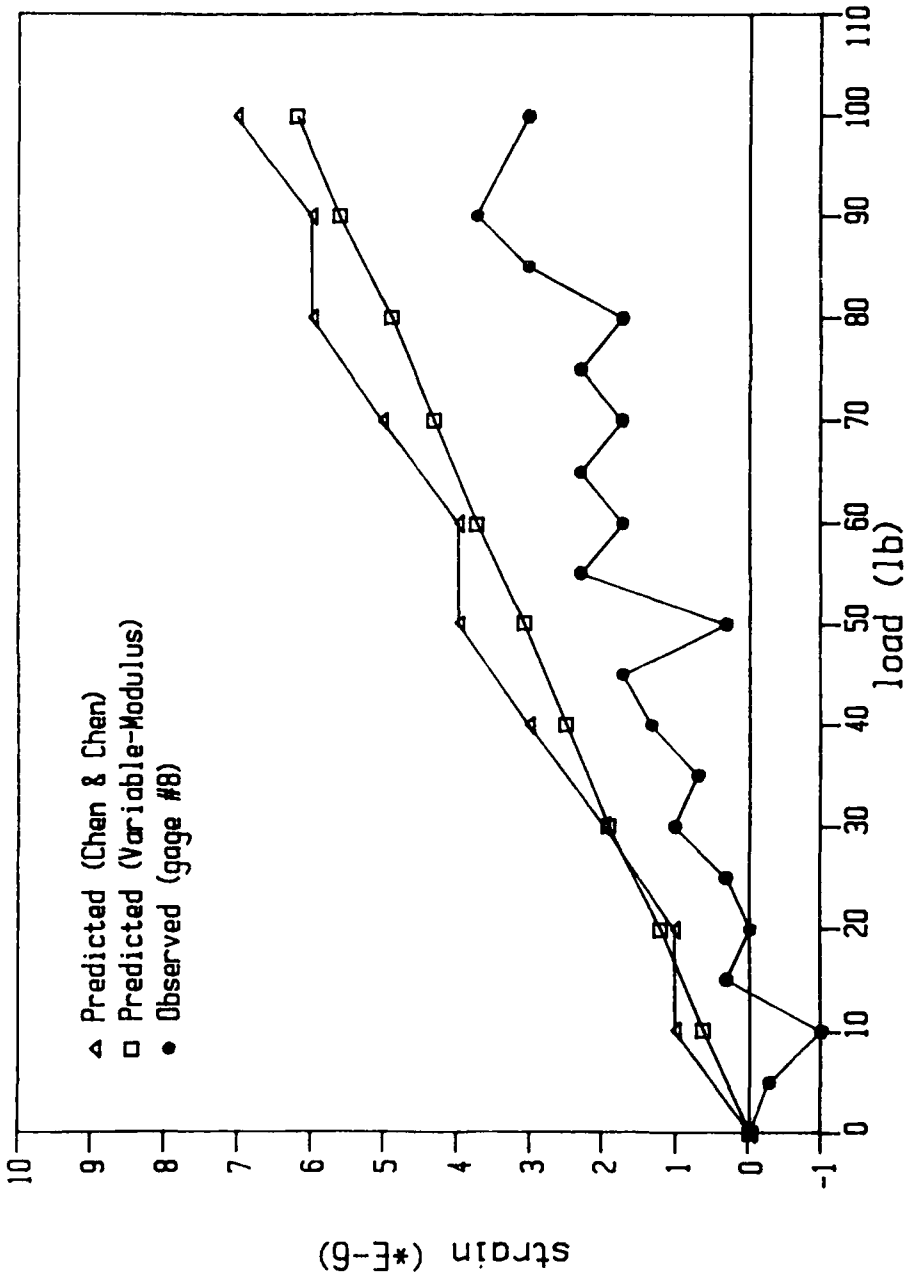

Figure 6.17. Comparison of Predicted and Observed Strains in the Static Analysis of the Reinforced Structure (gage # 8)

figure corresponds to the results of a different strain gage. The strains predicted by the two reinforced model representations are presented in each figure.

The predicted and observed responses of the reinforced model compared similarly to the predicted and observed responses of the nonreinforced model, and the same explanation for the differences applies to both models.

The two nonlinear models used to represent the reinforced structure produced similar results. However, the Chen and Chen model seemed to produce a better response than the Variable-Modulus model. The Chen and Chen model predicted a redistribution of strains similar to the one observed, although the magnitudes were not the same.

Dynamic Analysis

As mentioned before, dynamic strains and accelerations were recorded from the dynamic tests. However, these data were recorded on paper, and it were difficult to read, especially the strain data. Furthermore, the time scale used to record the strains was too large, and a valuable part of the response was not recorded (Gill, 1985). Also, the strain data were distorted due to noise recorded in the oscilloscope channels in which the strains were recorded. For these reasons, the comparisons between predicted and observed dynamic strains are not presented except for the response of gages 1 and 3 in the dynamic test of the non-reinforced model.

Non-Reinforced Model. Figures 6.18 and 6.19 present the comparisons between predicted and observed accelerations at the top slab and at the wall, respectively. The nonlinear (Chen and Chen) and linear predictions are presented in both figures.

The predicted accelerations at the center of the bottom of the top slab did not agree with the observed accelerations (Figure 6.18) except for the first 0.25 ms of the analyses. The bottom of the top slab was in tension during the time of load application, and as shown in Figure 6.20, the tensional stresses went into the plastic range at the beginning of the nonlinear analysis. In the plastic range the stiffness of the material decreases and this reduction may account for the increase in the acceleration. After the load is applied, the material becomes stiffer very rapidly, and the accelerations and the frequencies of the structural response become smaller. It is noted that the Chen and Chen model introduces the biaxial strength and the initial yield strength of concrete. These values were assumed based on previous investigations of concrete (Chen and Chen, 1975). However, these values were not verified for the microconcrete used in the laboratory models. This assumption seemed to introduce a softer material in the analyses.

The high stresses predicted in the center of the top slab were expected because this portion of the structure is

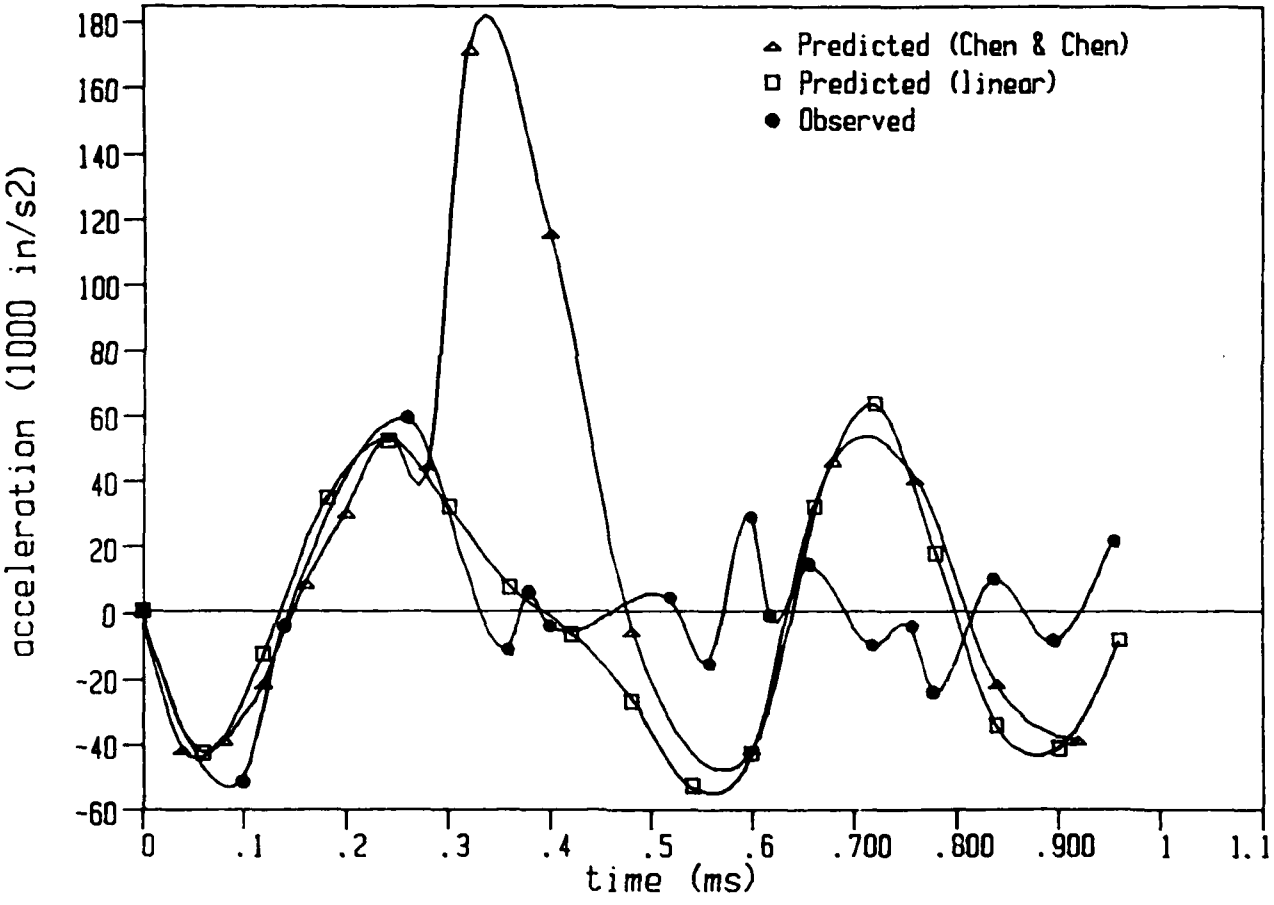

Figure 6.18. Comparison of Predicted and Observed Accelerations at the Center of the Top Slab of the Non-Reinforced Structure

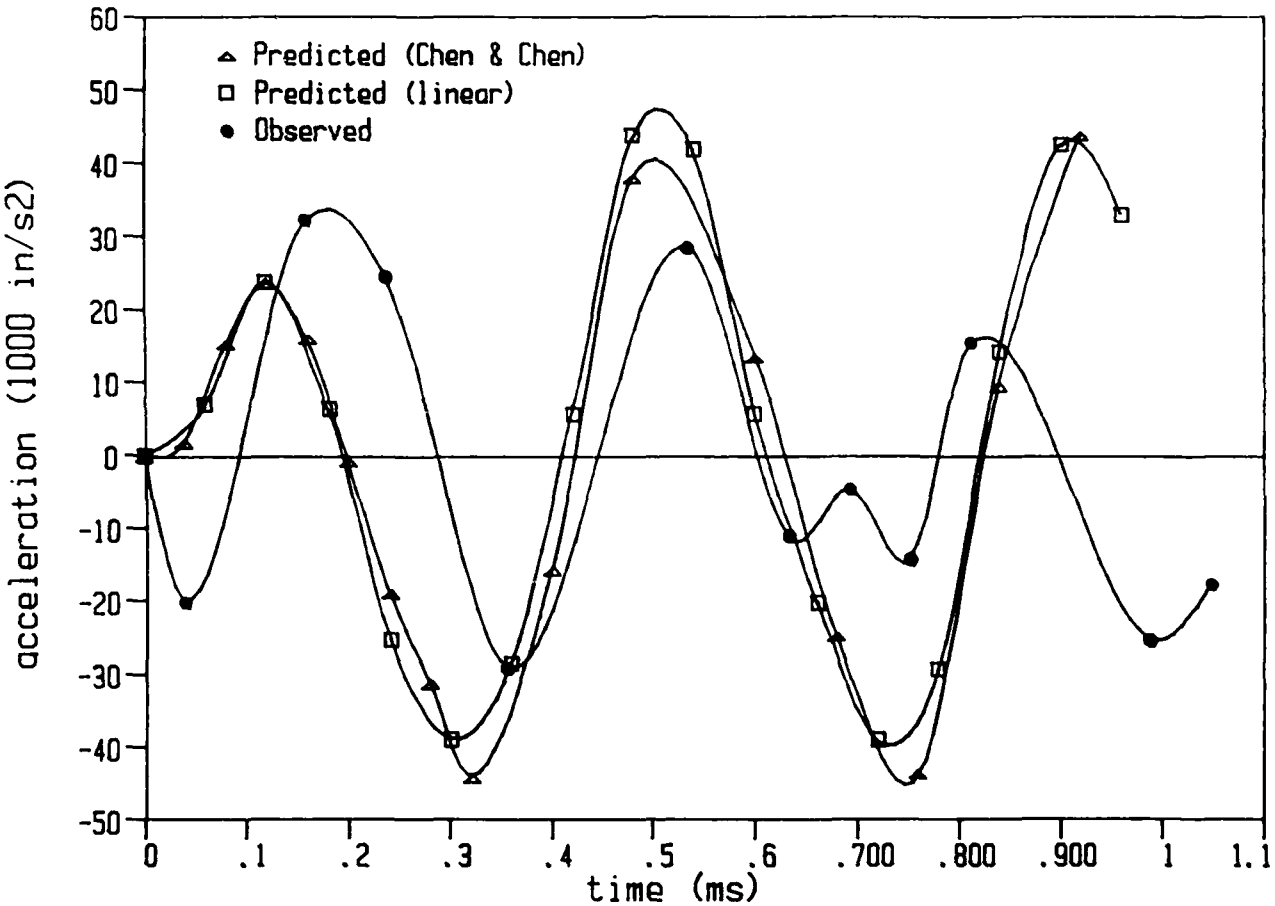

Figure 6.19. Comparison of Predicted and Observed Accelerations at the Center of the Inside Wall of the Non-Reinforced Structure

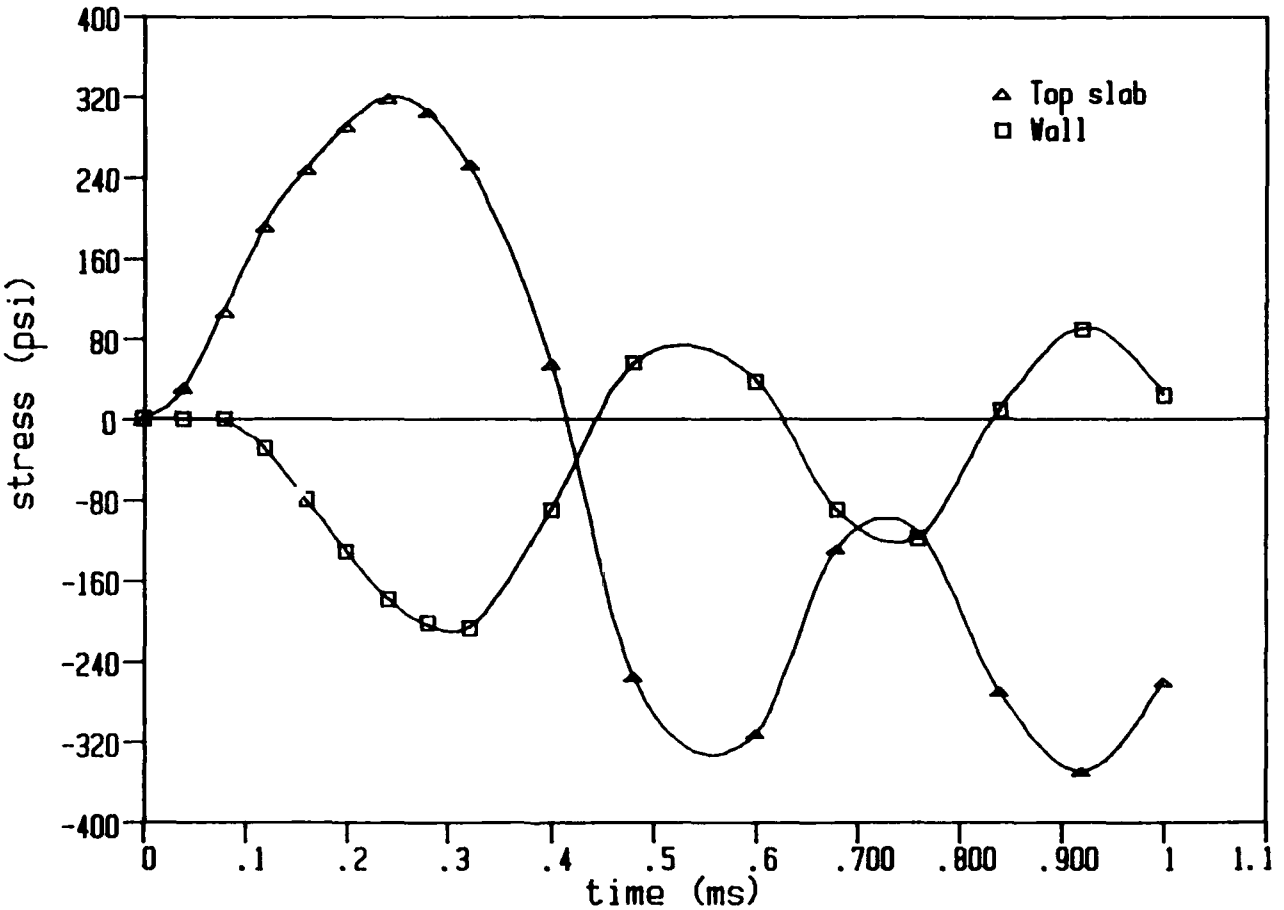

Figure 6.20. Predicted Average Bending Stresses at the Center of the Inside Top Slab and at the Center of the Inside Wall (non-reinforced model)

near the point of load application. A finer discretization of this area would better accomodate the high stresses in the concrete associated with the load.

The time integration step is also an important factor in the solution. Although the time step used in the analyses (0.020 ms) seemed adequate, the difference in the linear and nonlinear predictions may be an indication that solution convergence was not obtained for this time step. The use of a smaller time step may be appropriate for accurate integration of the structural response near the point of load application.

The predicted accelerations at the center of the inside wall (Figure 6.19) showed reasonably good agreement with the observed accelerations. The linear and nonlinear analyses predicted similar values indicating that the discretization in this area was adequate and that solution convergence was obtained. The predicted accelerations were slightly higher than the observed; however, there was good agreement in the frequencies of the response.

Figures 6.21 and 6.22 present the predicted (nonlinear) and observed strains from gages 1 and 3, respectively. Both figures showed good agreement between predicted and observed values. However, the observed strain curves were fit through only a few points which may not show the true response of the structure.

Reinforced Model. A complete solution for the analysis of the reinforced model was more difficult to obtain than

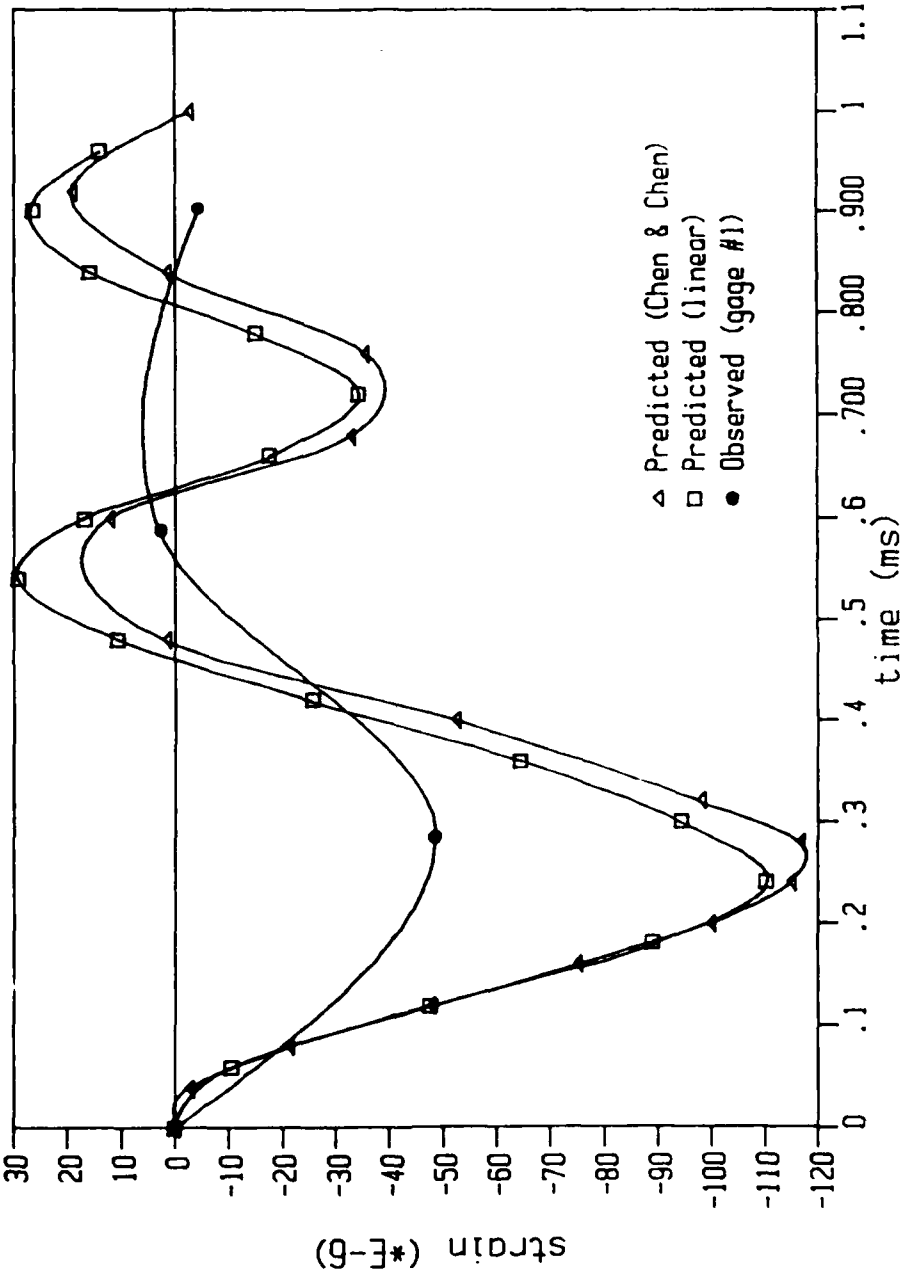

Figure 6.21. Comparison of Predicted and Observed Strains in the Dynamic Analysis of the Non-Reinforced Structure (gage # 1)

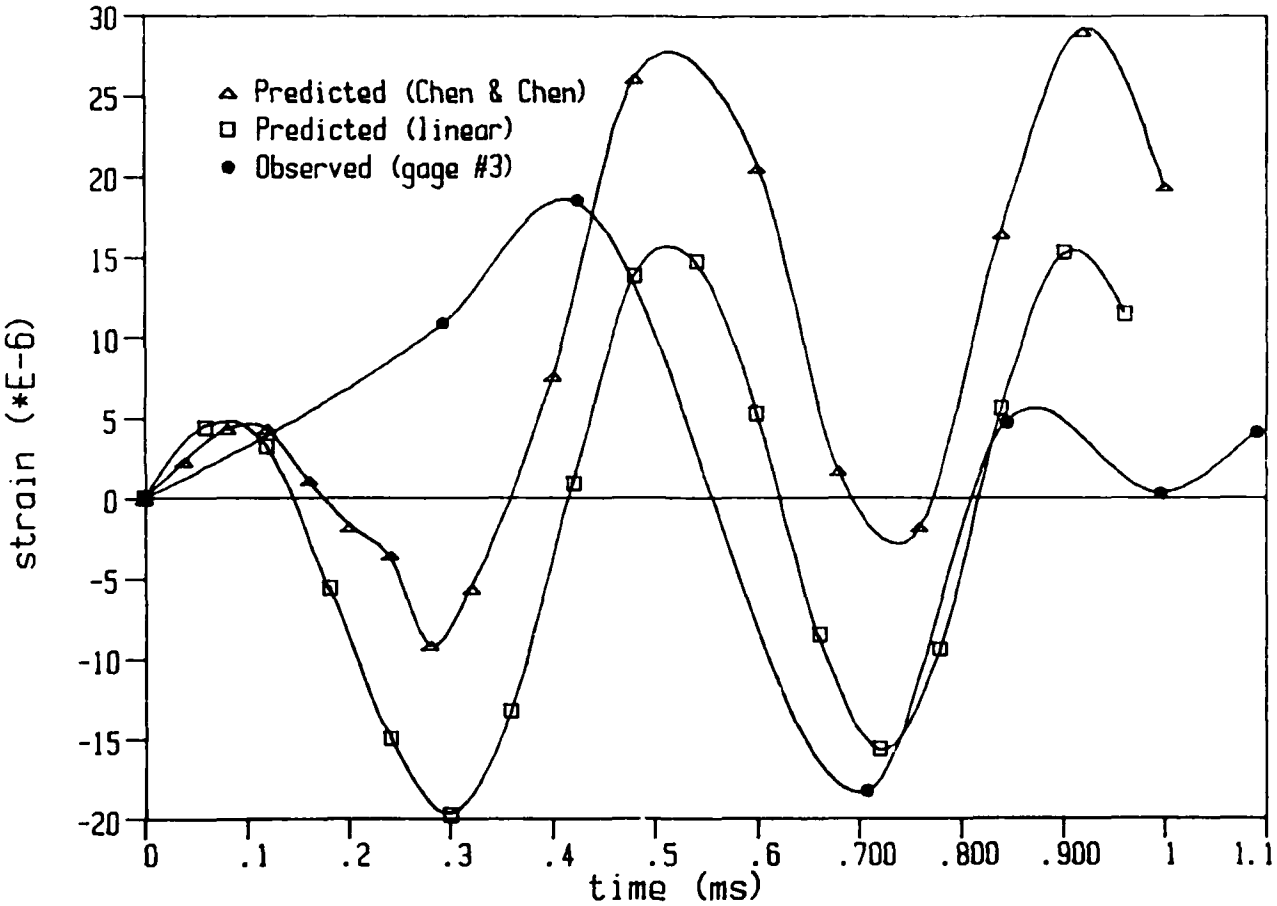

Figure 6.22. Comparison of Predicted and Observed Strains in the Dynamic Analysis of the Non-Reinforced Structure (gage # 3)

for the nonreinforced model. The magnitude of the load applied to the reinforced model was larger than the applied to the nonreinforced model although they had approximately the same duration. Therefore, it was necessary to reduce the time step for accurate integration of the load and for the reduction of the errors introduced in the step-by-step linear approximation. From the three nonlinear analyses performed on the reinforced model, only one solution converged. This solution was obtained with the Orthotropic Variable-Modulus using a time step of 0.010 ms. The analyses with the Chen and Chen model were performed with time steps of 0.010 ms and 0.015 ms, and neither produced a converged solution. Another analysis with a smaller time step would required a large cpu time and it was not justifiable. However, the results predicted by the Chen and Chen model are presented for comparison and to show some of the problems involved with the assumptions made in the numerical analysis.

The nonlinear (Chen and Chen) and linear accelerations predicted at the top slab with a time step of 0.015 ms are presented in Figure 6.23. This figure is presented to show how the errors introduced in the solution by the step-by-step integration method result in an uncontrolled growth in energy (instability). The sources of error associated with this growth are the secant approximation to the material nonlinearity and the unbalanced forces that can occur in the step-by-step integration (Yovaish, 1984). In this case, the

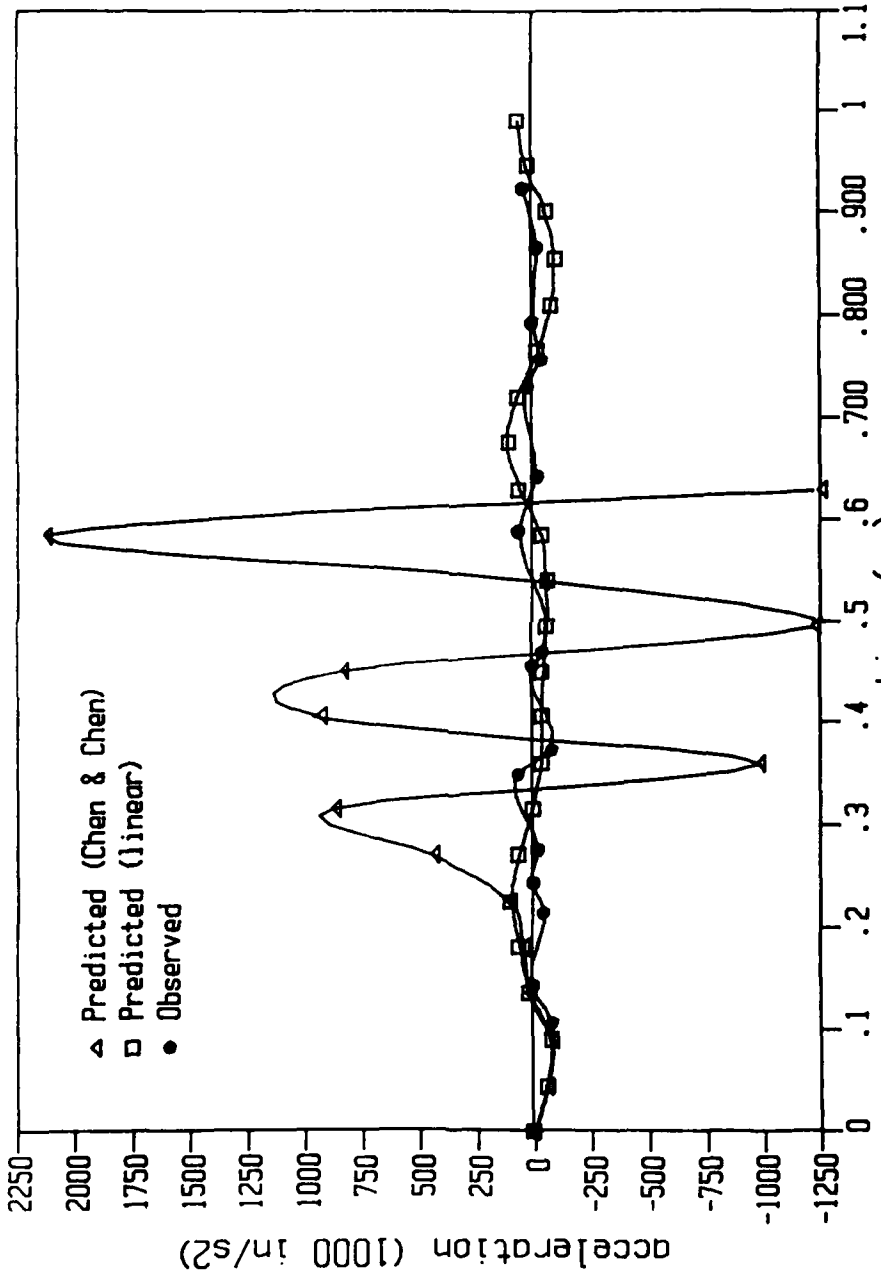

Figure 6.23. Comparison of Predicted (time step of 0.015 ms) and Observed Accelerations at the Center of the Top Slab of the Reinforced Structure

energy growth is associated with the first source of error, the secant approximation to the material nonlinearity. The program NONSAP-C stops the analysis when the second error occurs, that is, when the unbalanced forces go uncorrected. This second error occured in the Chen and Chen analysis when a time step of 0.010 ms was used. This response is illustrated in Figures 6.24 and 6.25. Figure 6.24 shows the predicted accelerations at the center of the top slab, and Figure 6.25 shows the predicted accelerations at the center of the inside wall. Also shown in these figures are the predictions with the Orthotropic Variable-Modulus model. As shown in the figures, the solution with the Chen and Chen model stopped at approximately 0.3 ms due to the growth of the unbalanced forces.

Figure 6.26 presents the predicted (linear and nonlinear) and the observed accelerations at the center of the top slab. The linear and nonlinear (Variable-Modulus) analyses were performed with a time step of 0.010 ms. Both predictions show good agreement with the observations through the first 0.15 ms of the analyses. A similar result was obtained with the nonreinforced model. Figure 6.26 is repeated in Figure 6.27 except for the linear predictions. Reasonably good agreement is observed between the predicted and observed frequencies, except between times 0.15 ms and 0.30 ms of the analysis. During this time, the predicted frequencies were higher than the observed. This behavior is due primarily to the high stress gradient in this area (near

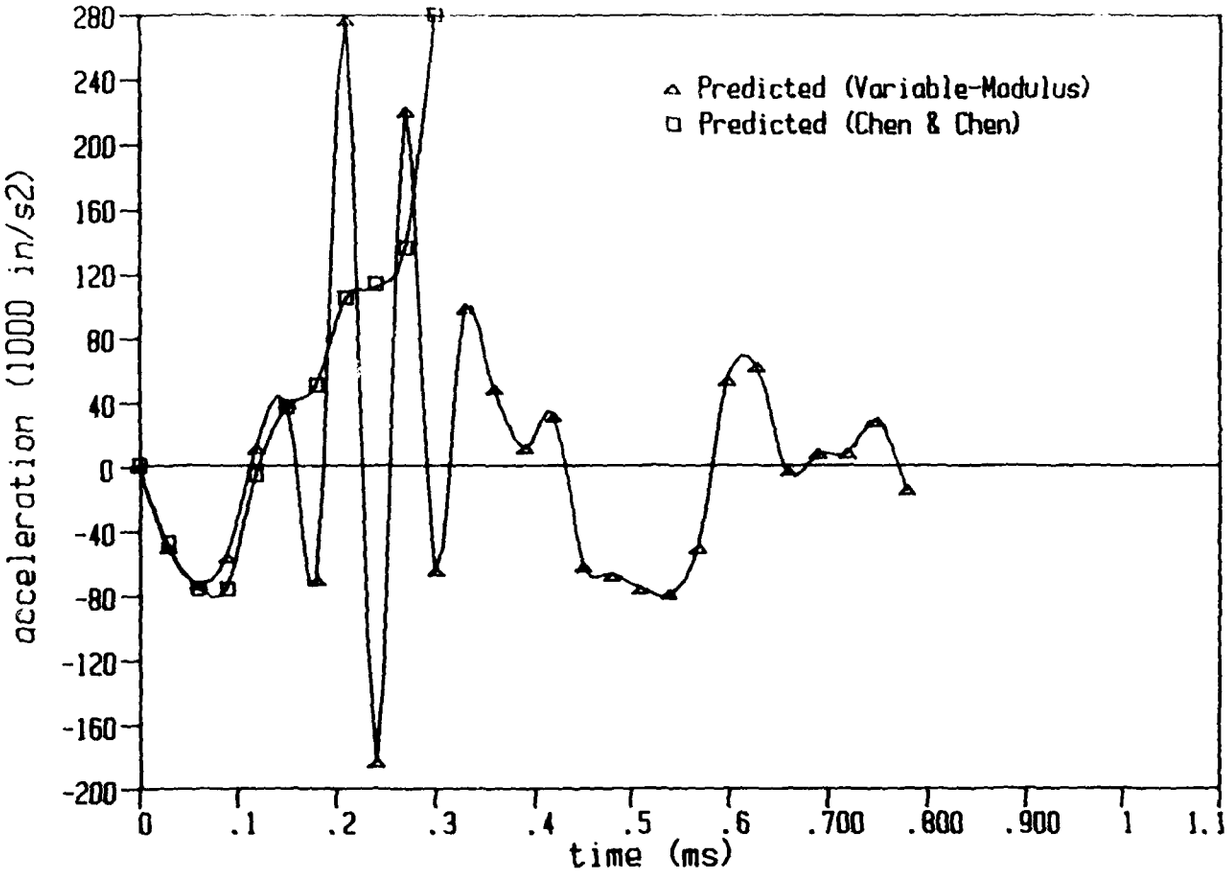

Figure 6.24. Comparison of Predicted (time step of 0.010 ms) Accelerations at the Center of the Top Slab of the Reinforced Structure

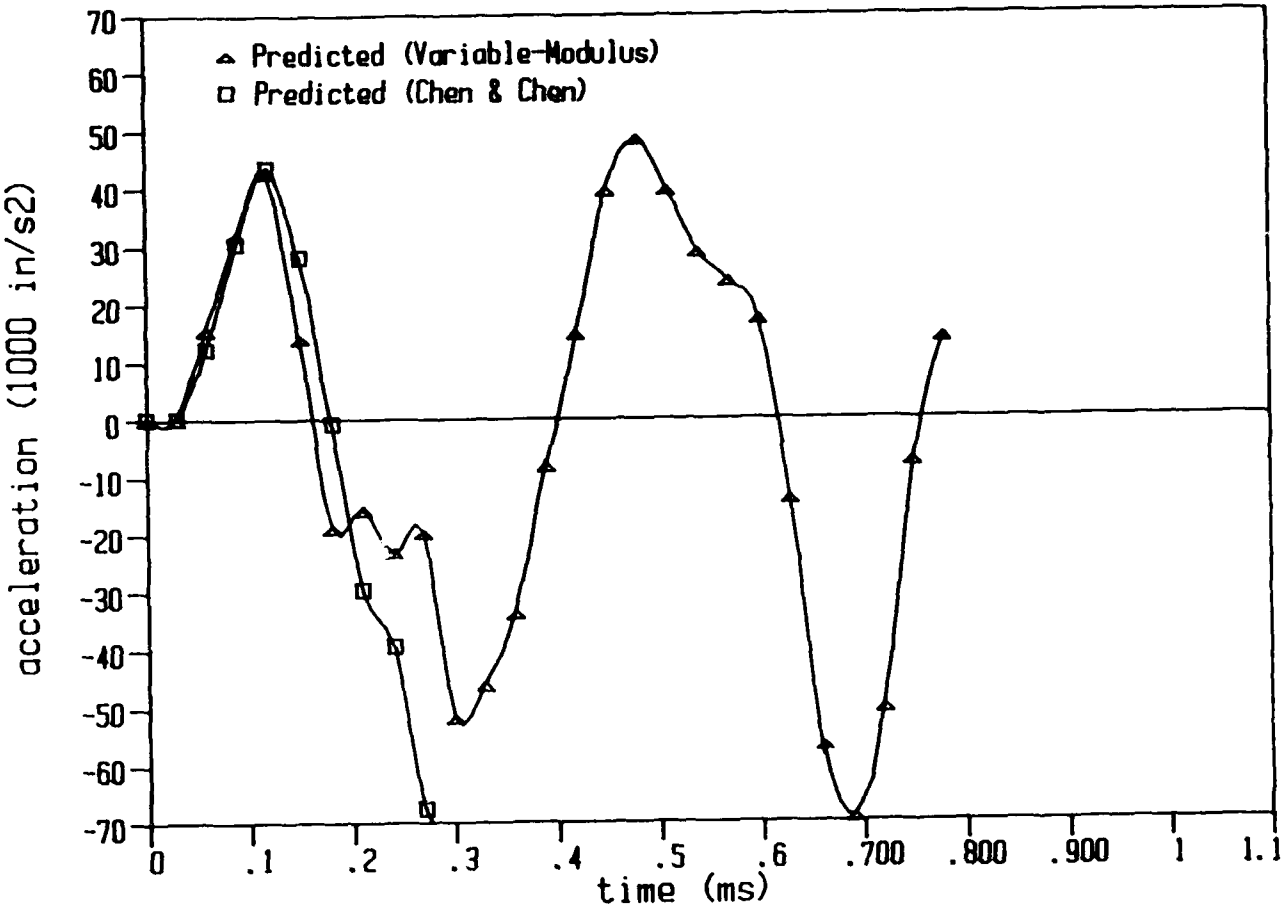

Figure 6.25. Comparison of Predicted (time step of 0.010 ms) Accelerations at the Center of the Inside Wall of the Reinforced Structure

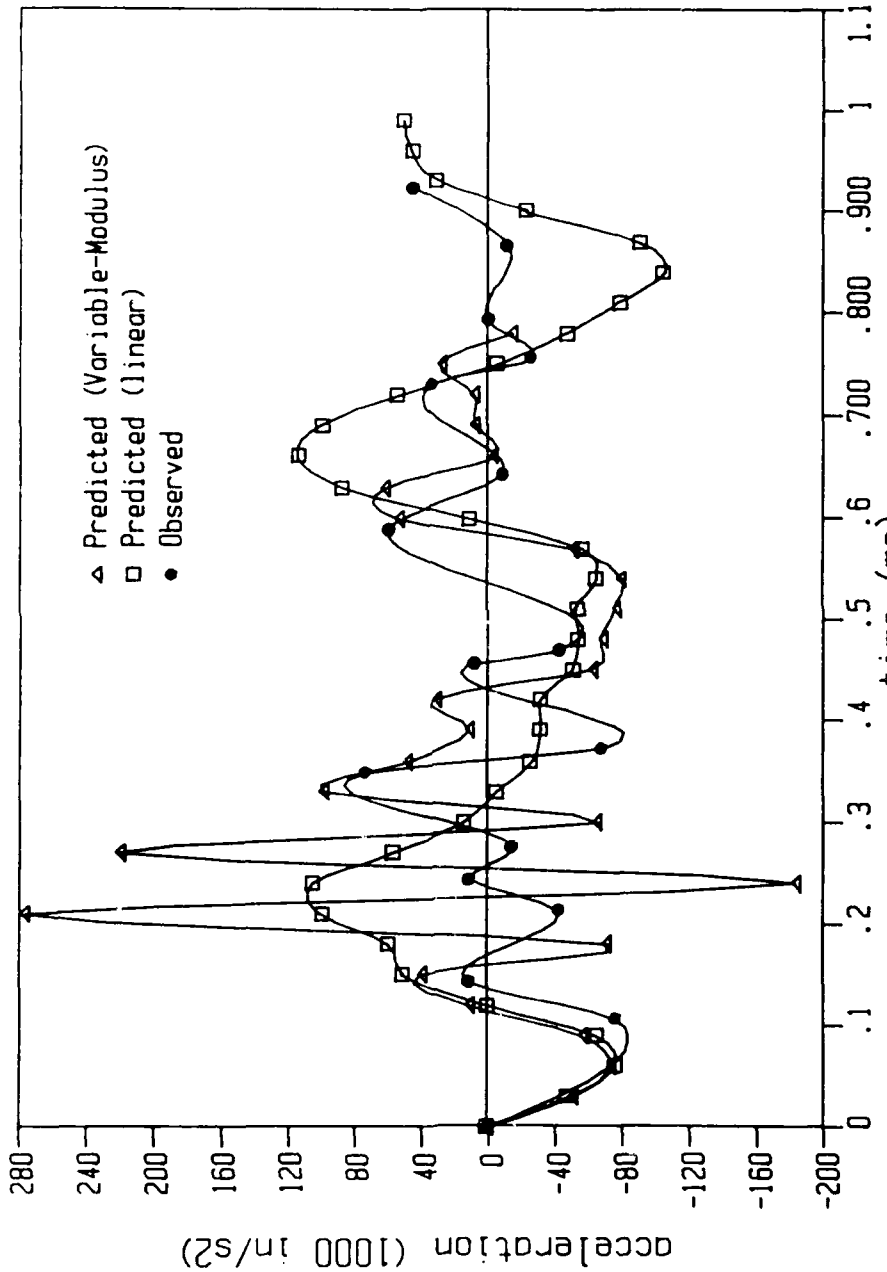

Figure 6.26. Comparison of Predicted (time step of 0.010 ms) and Observed Accelerations at the Center of the Top Slab of the Reinforced Structure

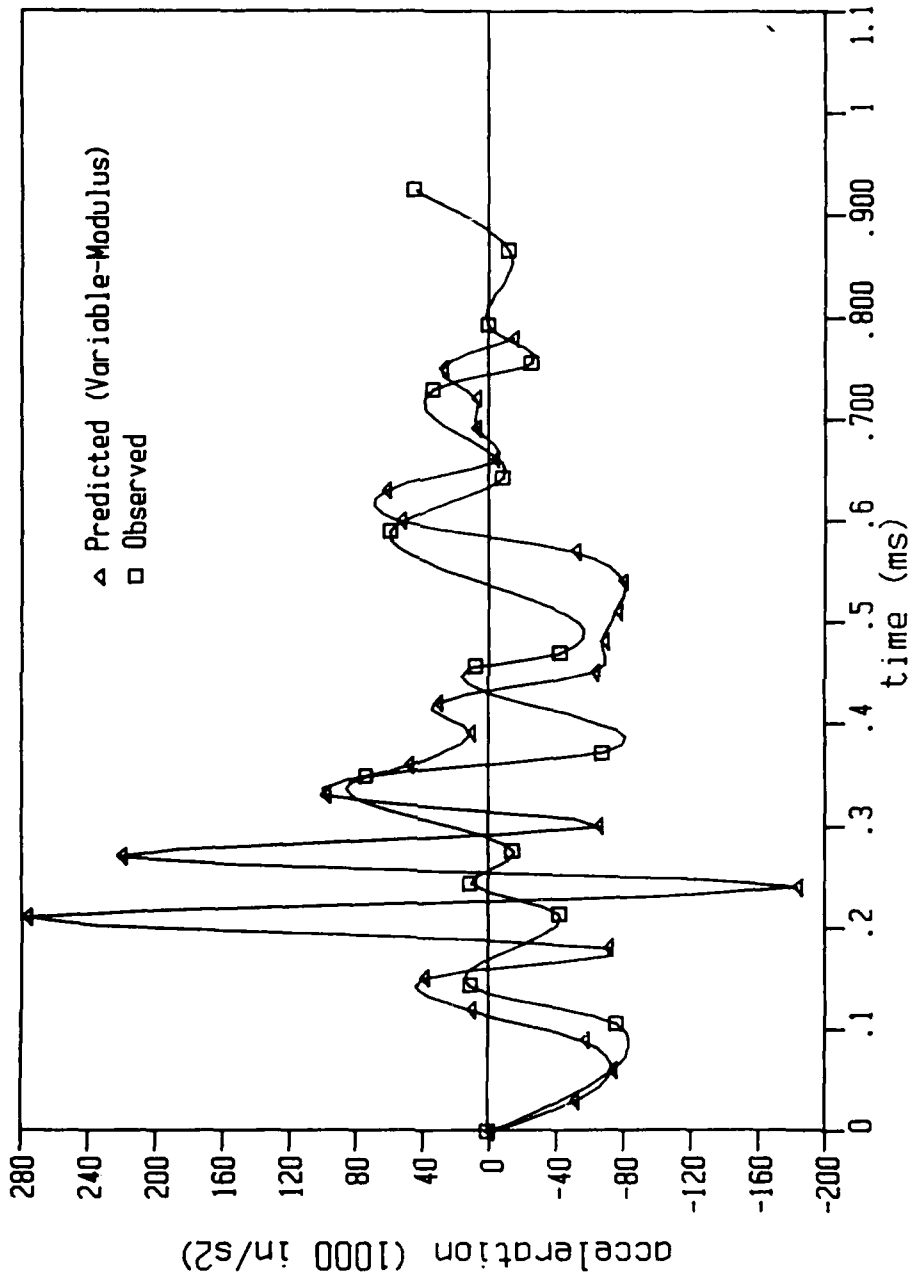

Figure 6.27. Comparison of Predicted (Variable-Modulus) and Observed Accelerations at the Center of the Top Slab of the Reinforced Structure

the point of load application). The nonlinear analysis predicted cracks in the bottom of the slab thus reducing the stiffness of the material and producing higher frequencies and higher accelerations. The predicted stresses in this area are presented in Figure 6.28 and this figure shows how the stresses are redistributed when the crack forms.

Figure 6.29 presents the predicted (linear and nonlinear) and observed accelerations at the center of the inside wall. Both solutions show reasonably good agreement between the predicted and observed frequencies. Figure 6.29 is repeated in Figure 6.30 without the linear solution. The Variable-Modulus analysis showed good agreement with the test both in the frequencies and in the magnitudes. Failure was not predicted in this area.

Figures 6.31 and 6.32 present the comparison between the observed and predicted (linear) accelerations at the center of the top slab and at the center of the inside wall, respectively. The linear predictions are given for the two different time steps of 0.010 ms and 0.015 ms. The use of different type steps has little effect in the linear analyses because the concrete material is defined with the same properties in tension and in compression. During the time of load application, the bottom of the top slab is in tension and the analyses predict tensional stresses that are in the nonlinear range. However, the material definition does not change in the linear analysis and the true behavior of the concrete is not predicted.

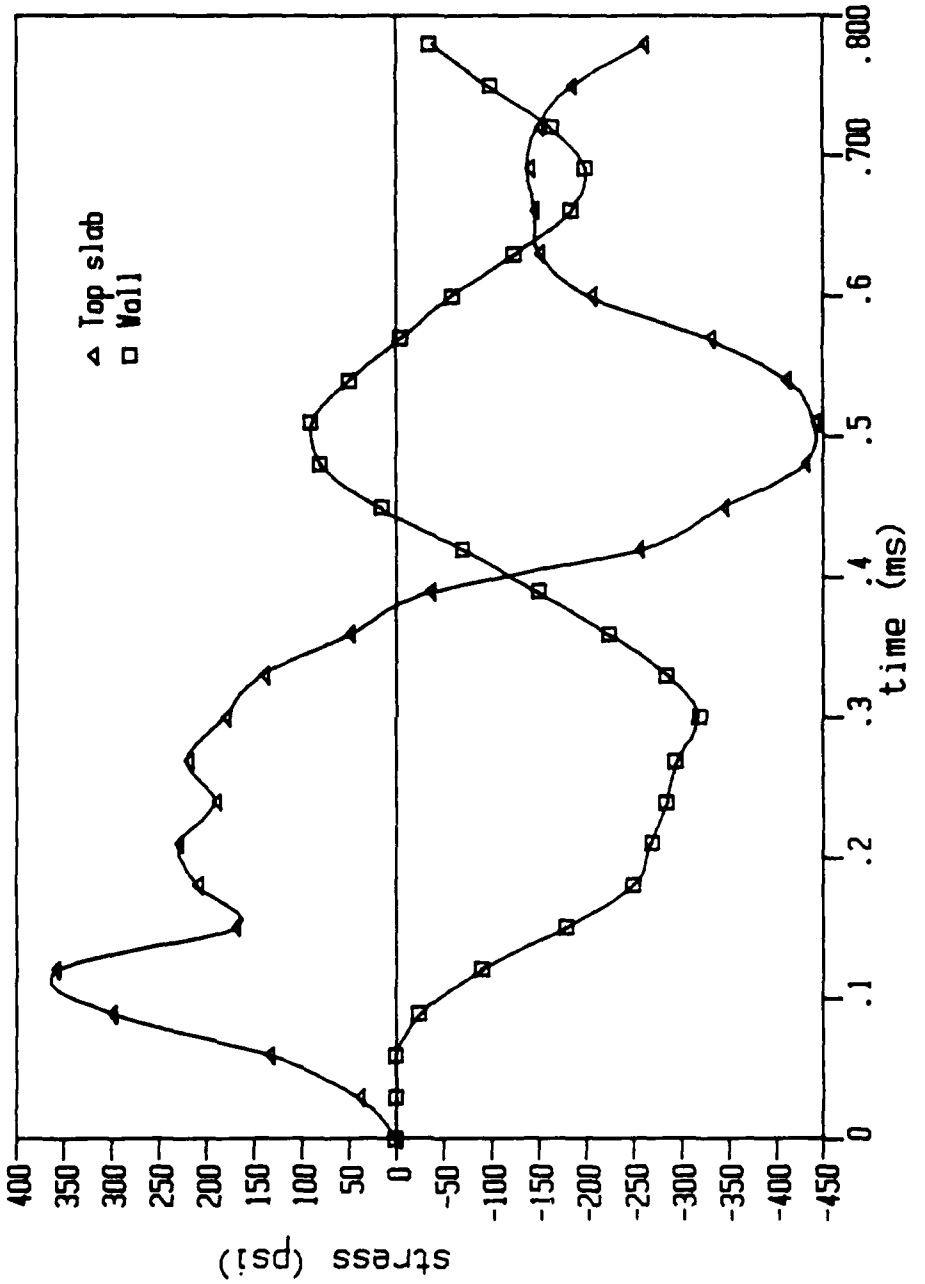

Figure 6.28. Predicted Average Bending Stresses at the Center of the Inside Top Slab and at the Center of the Inside Wall (reinforced model)

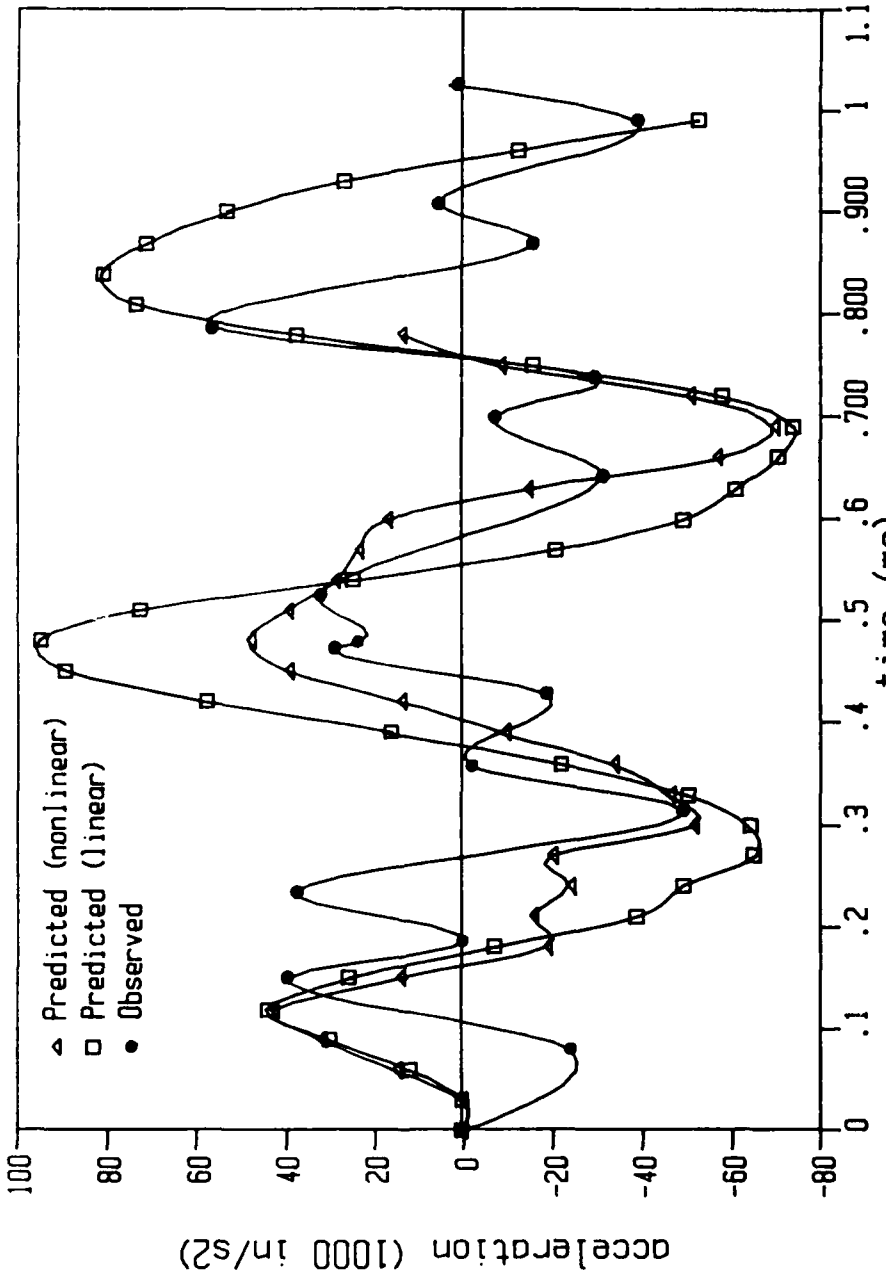

Figure 6.29. Comparison of Predicted (time step of 0.010 ms) and Observed Accelerations at the Center of the Inside Wall of the Reinforced Structure

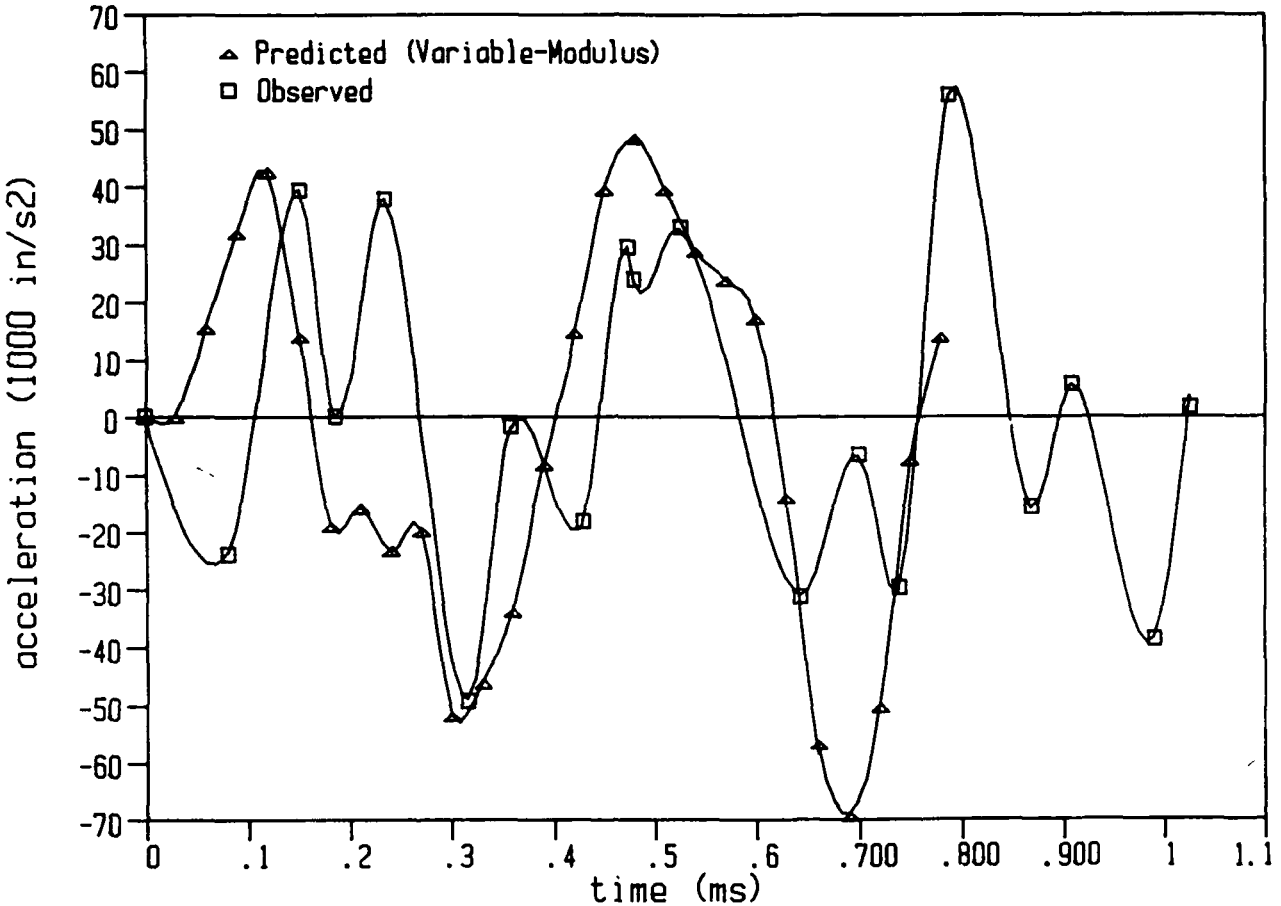

Figure 6.30. Comparison of Predicted (Variable-Modulus) and Observed Accelerations at the Center of the Inside Wall of the Reinforced Structure

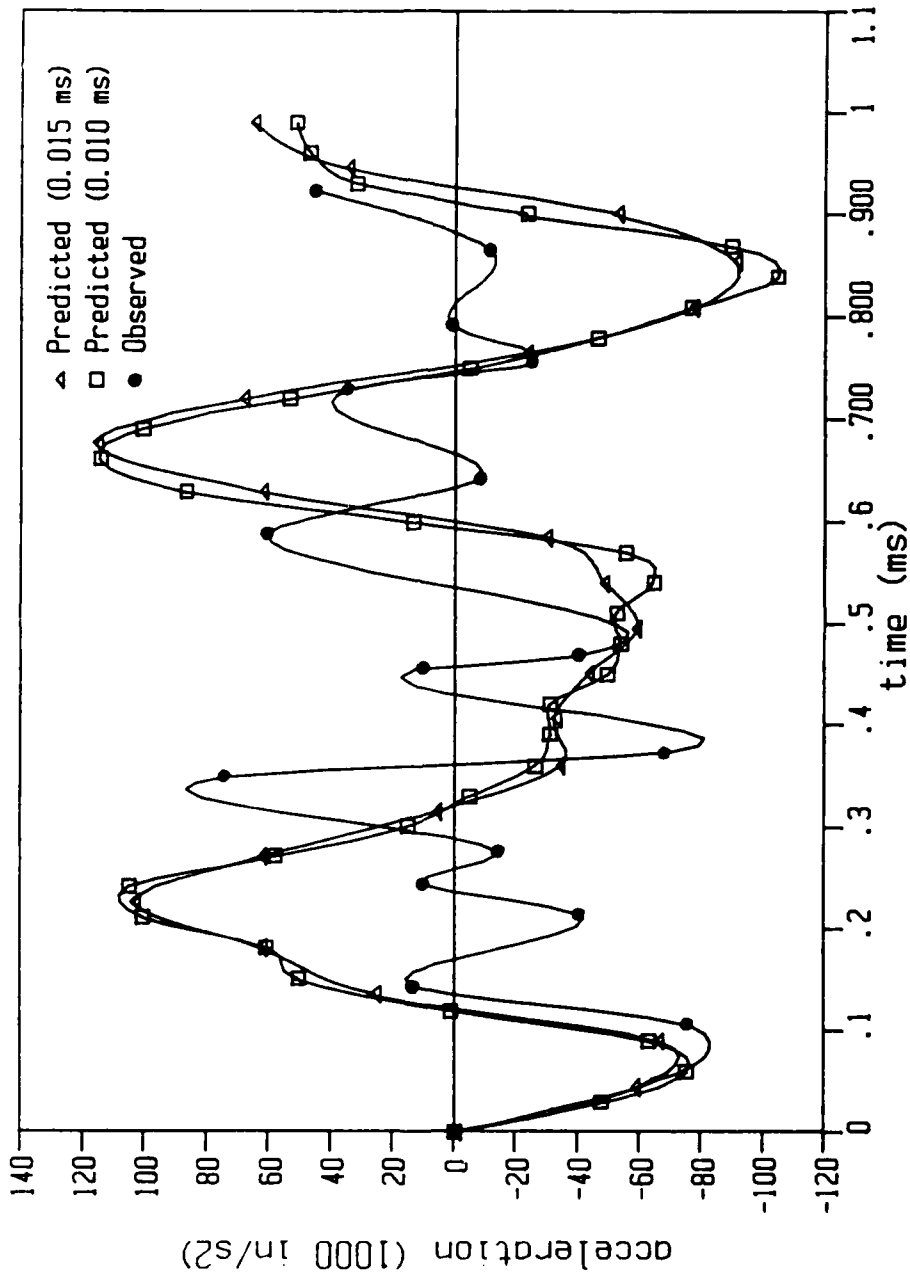

Figure 6.31. Comparison of Predicted (linear) and Observed Accelerations at the Center of the Top Slab of the Reinforced Structure

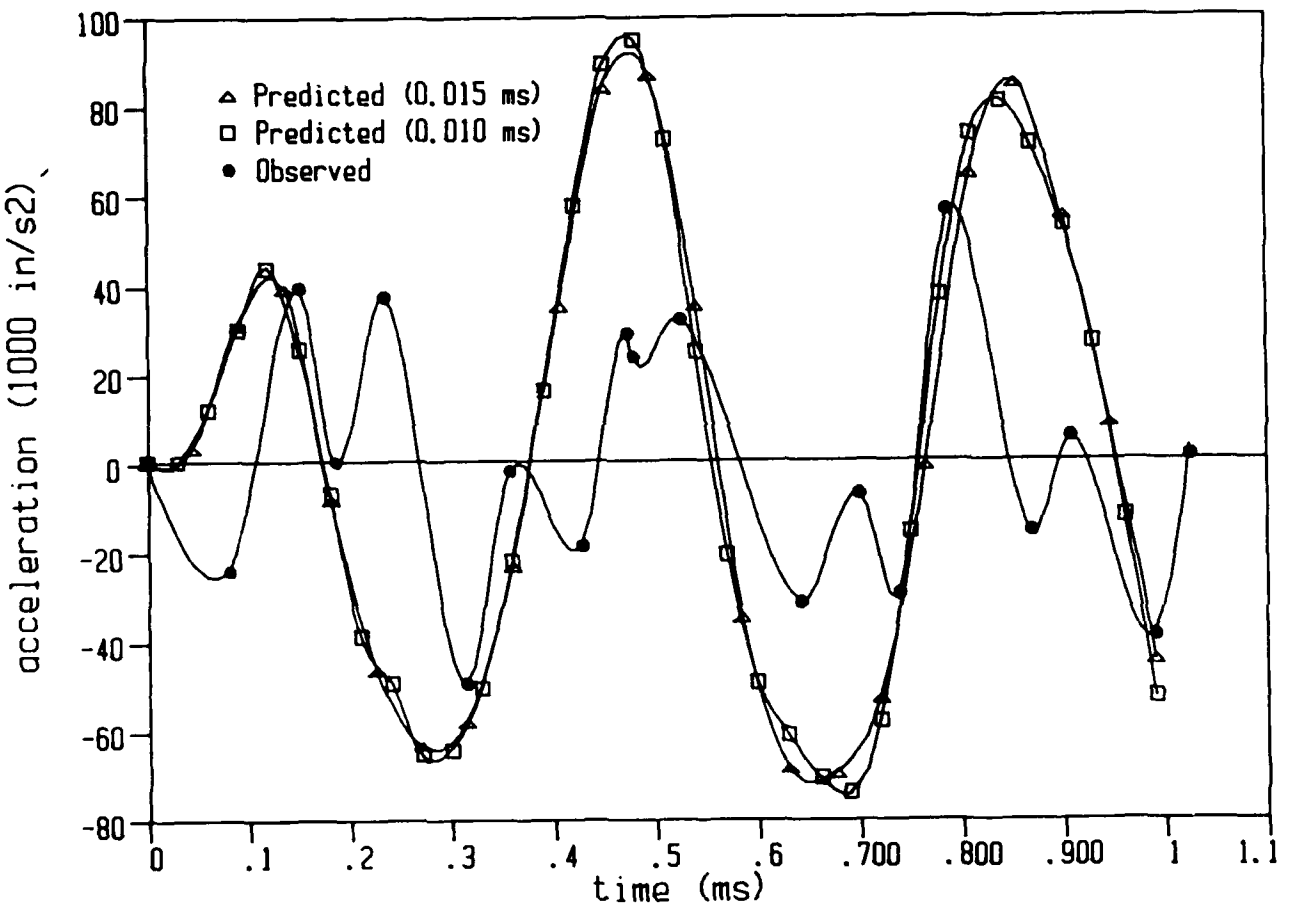

Figure 6.32. Comparison of Predicted (linear) and Observed Accelerations at the Center of the Inside Wall of the Reinforced Structure

Blast Analysis

The predicted responses of the blast load analysis were not compared to the observed responses of the tests performed by Gill (1985). The tests performed by Gill were affected by experimental problems associated with the data recording equipment. However, the blast analysis predictions were compared to observations from similar tests performed by Habibollah Tabatabai whose data are more reliable. The observations by Tabatabai have not yet been reported and will be part of his dissertation for his doctoral degree.

Figure 6.33 presents the comparison of predicted and observed accelerations at the center of the bottom of the top slab of the structure. The predicted peak acceleration occurred at approximately 0.12 ms, and the observed peak acceleration occurred at approximately 0.27 ms. After the peaks occurred, both the frequencies of the response and the magnitudes of the accelerations were about the same. After 0.55 ms, the predicted values became positive, and the observed values became negative; however, there was some agreement in the frequencies of the response.

Figure 6.34 presents the predicted and observed accelerations at the center of the inside wall of the structure. The magnitudes of the observed values are larger than the predicted values. The observed peak positive acceleration occurred at approximately 0.5 ms and the predicted peak positive acceleration at 0.18 ms. The peak

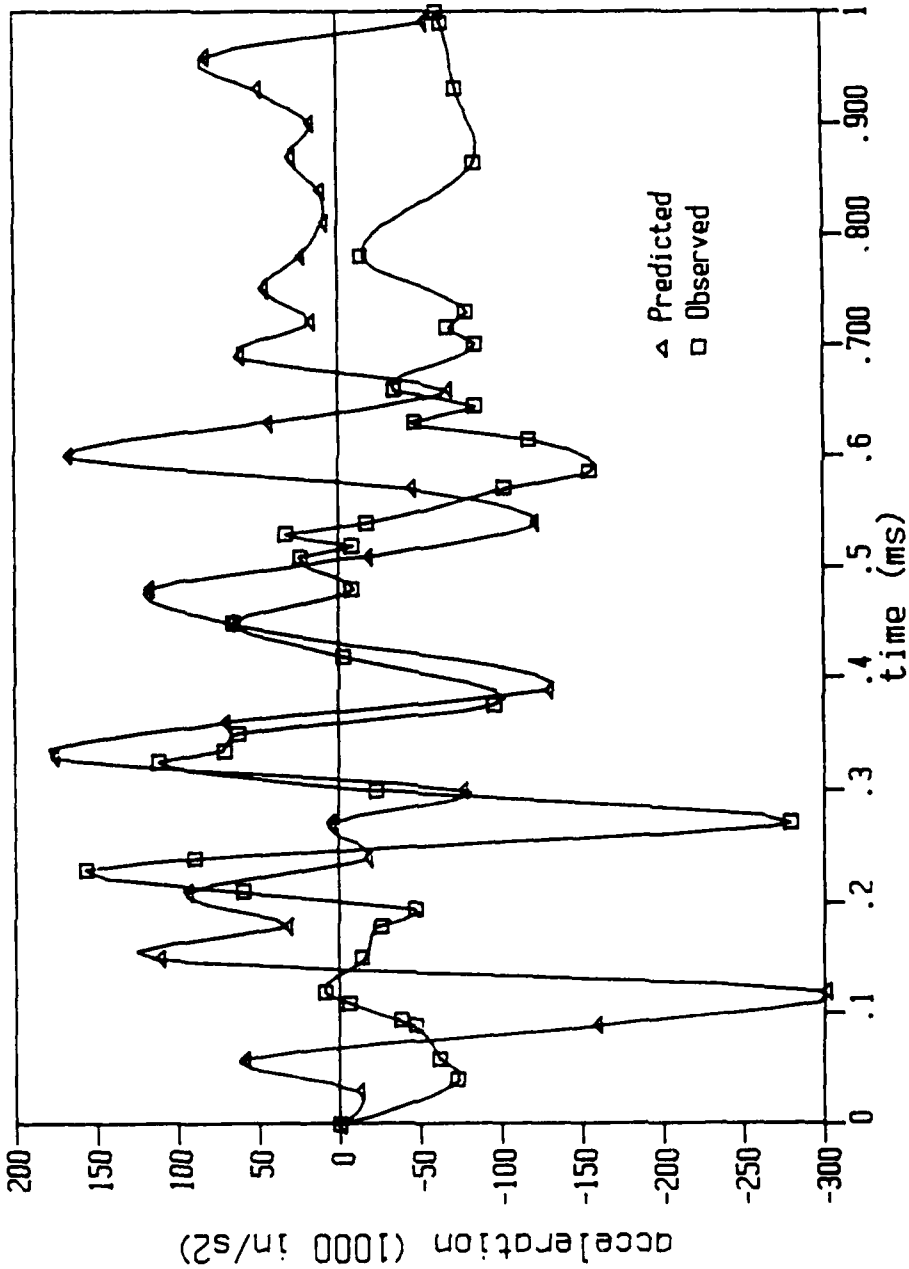

Figure 6.33. Comparison of Predicted and Observed Accelerations at the Center of the Top Slab (blast analysis)

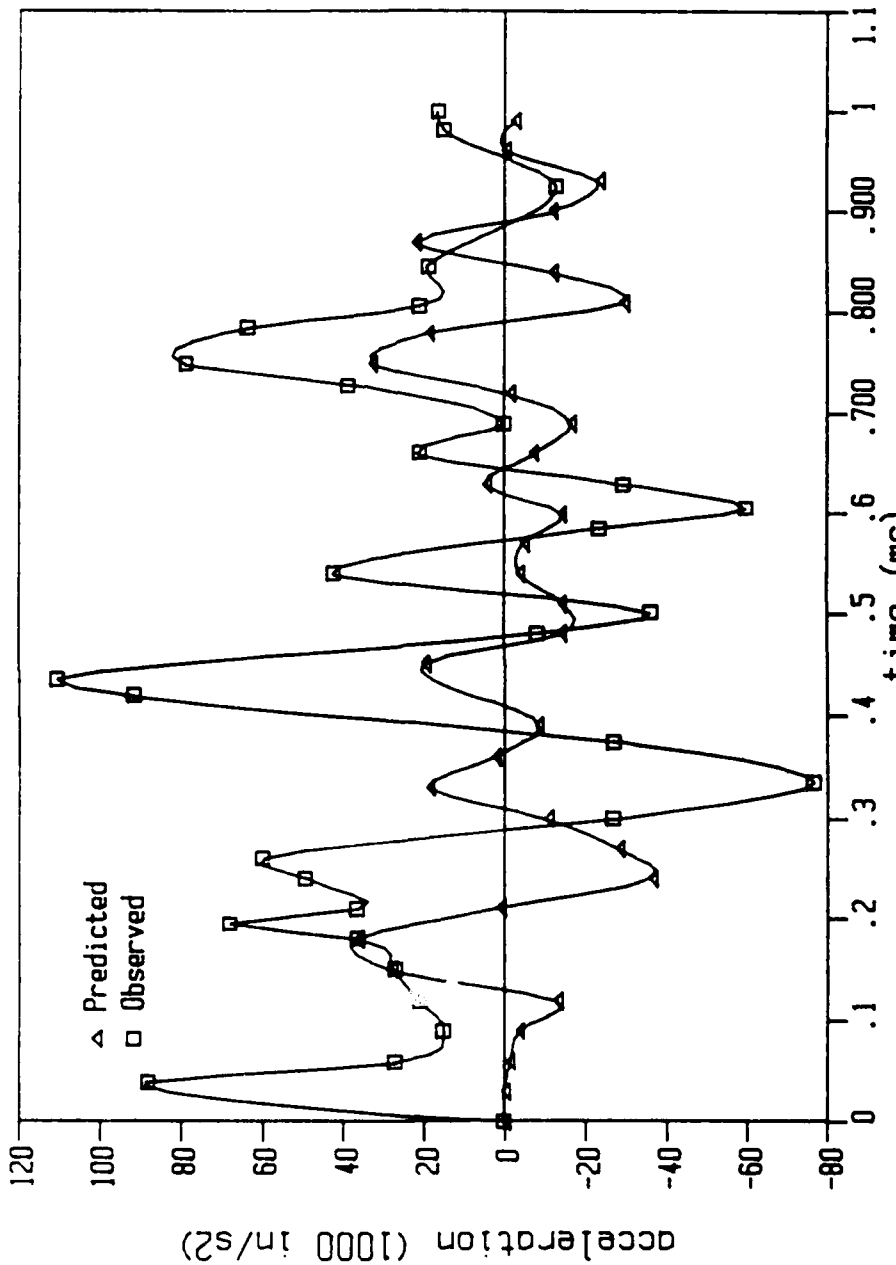

Figure 6.34. Comparison of Predicted and Observed Accelerations at the Center of the Inside Wall (blast analysis)

negative accelerations occurred at 0.33 ms and 0.24 ms for the observed and predicted, respectively. After 0.55 ms, the frequencies of the predicted and observed responses agreed to some extent.

Figures 6.35 through 6.40 present the comparison of predicted and observed strains at different points on the structure. Each figure corresponds to a different strain gage. In all figures, the observed response during the first 0.15 ms of the test was omitted because it was clearly affected by the shock of the blast. Negative strains indicate compression. In general, the observed strains were larger than the predicted strains, and the observed peak variations were more pronounced than those predicted. Also, in the numerical analysis the predicted predominant behavior of the structure was flexural, while in the test the observed behavior included large in plane or axial stresses.

In all strain gages where compression was measured (gages 1, 5, 6, and 8) the peak strain occurred at approximately the same time (0.30 ms). After the peak occurred, the observed strains gradually became less negative. Although the analysis also predicted compressive strains where these gages were located (Figures 6.35, 6.37, 6.38, 6.40), the predicted response did not show a definite peak but rather a gradual increase of the strain magnitudes.

Figure 6.36 presents the predicted and observed strains at the bottom and center of the top slab and Figure 6.39 at the top and center of the bottom slab. In both figures, the

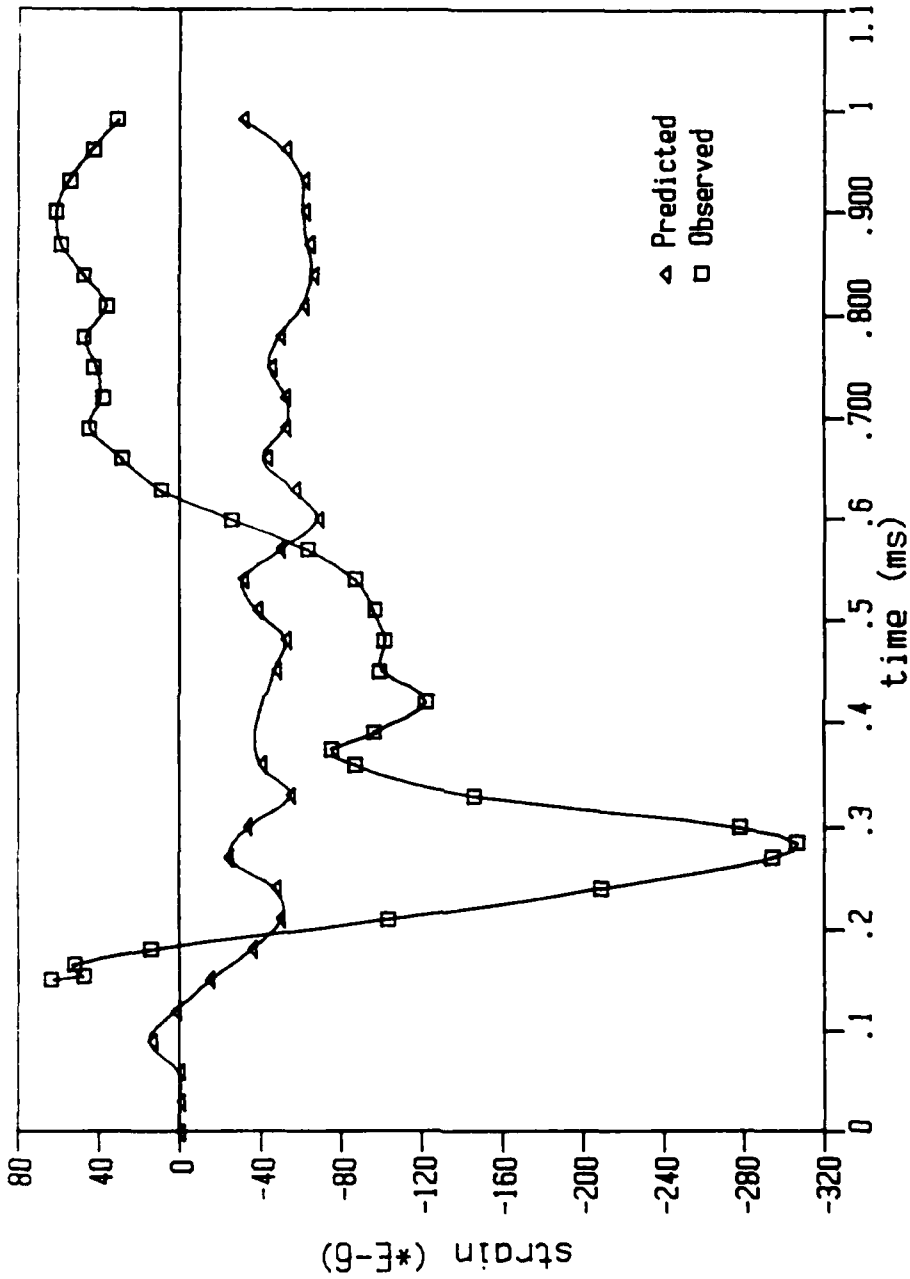

Figure 6.35. Comparison of Predicted and Observed Strains in the Blast Analysis of the Soil-Structure System (gage # 1)

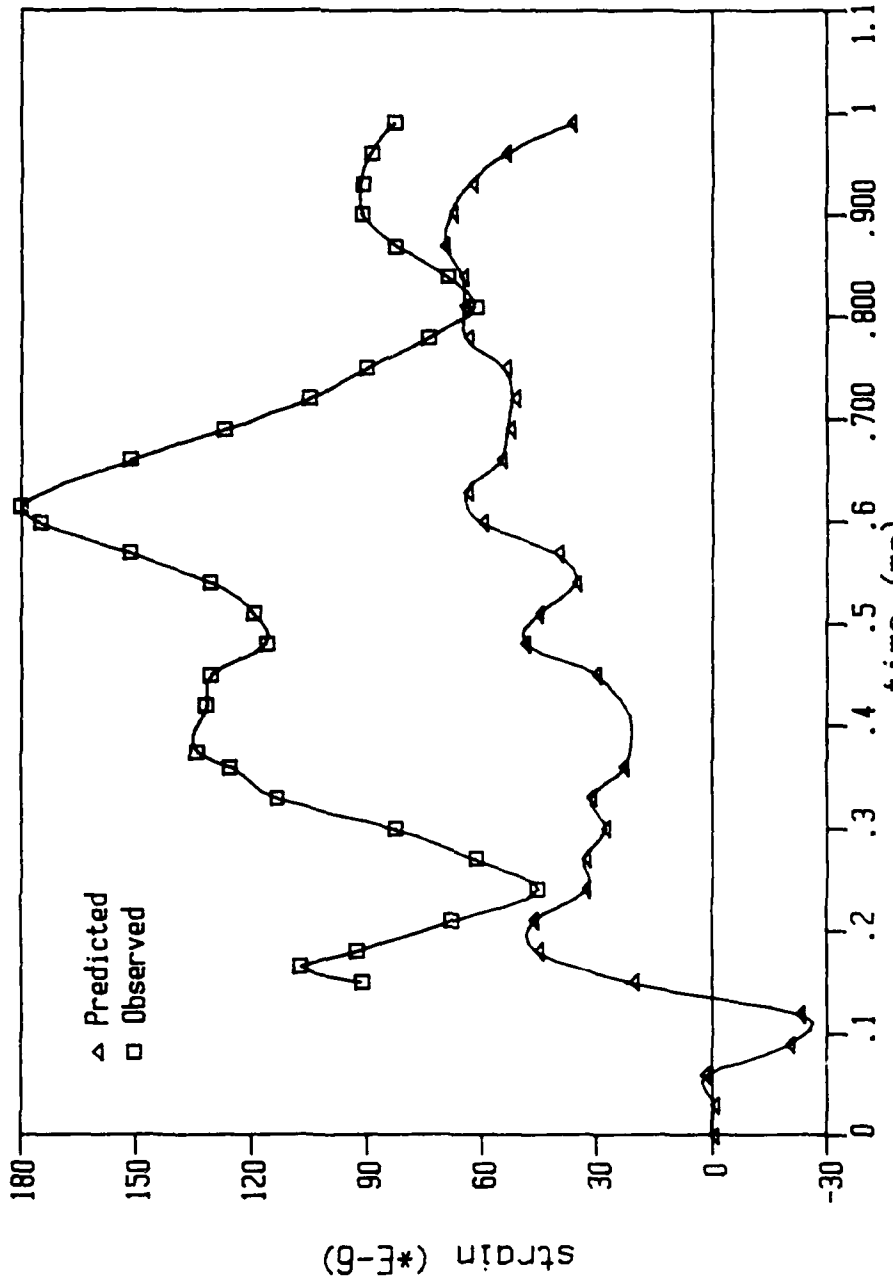

Figure 6.36. Comparison of Predicted and Observed Strains in the Blast Analysis of the Soil-Structure System (gage # 2)

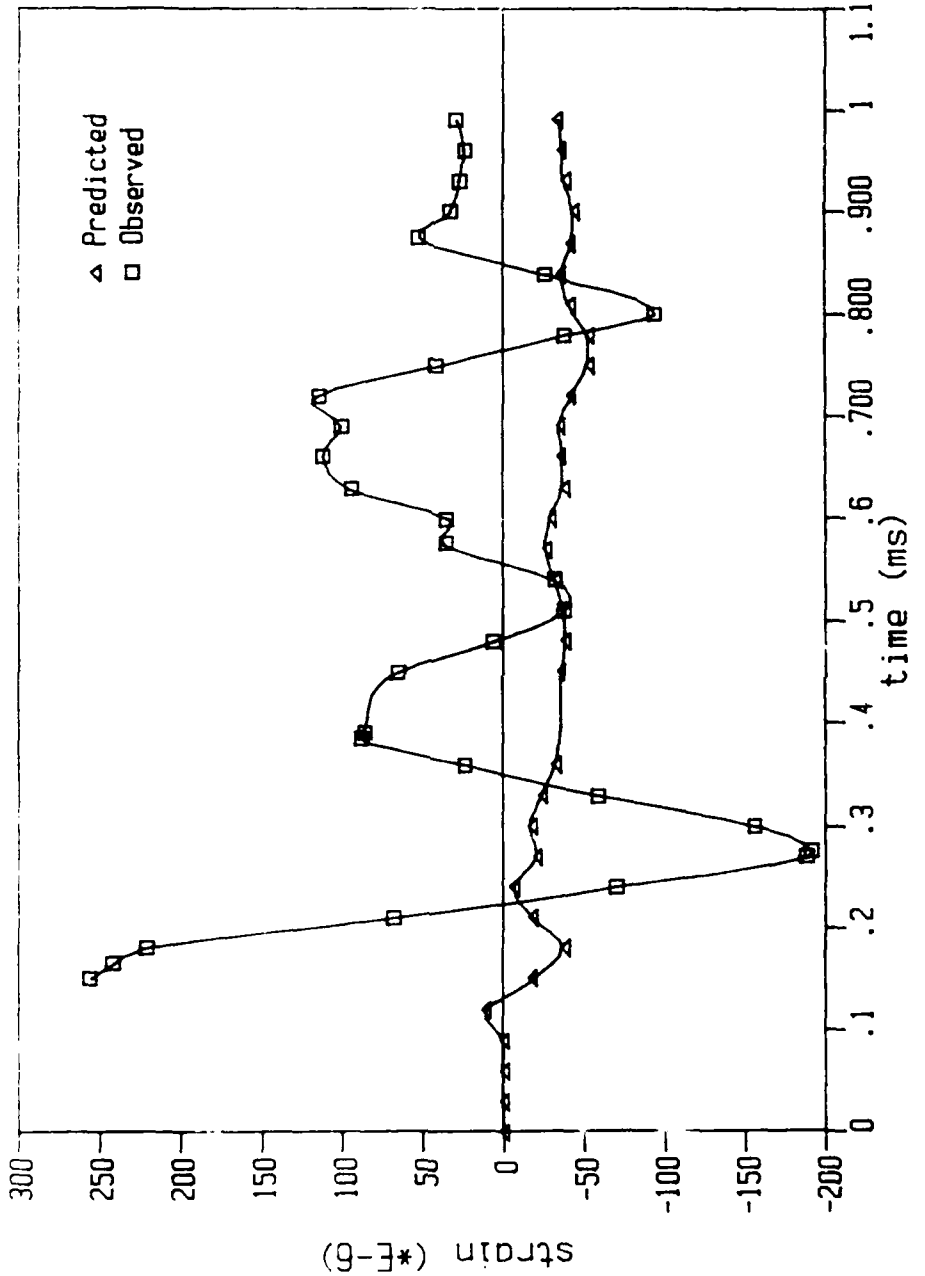

Figure 6.37. Comparison of Predicted and Observed Strains in the Blast Analysis of the Soil-Structure System (gage # 5)

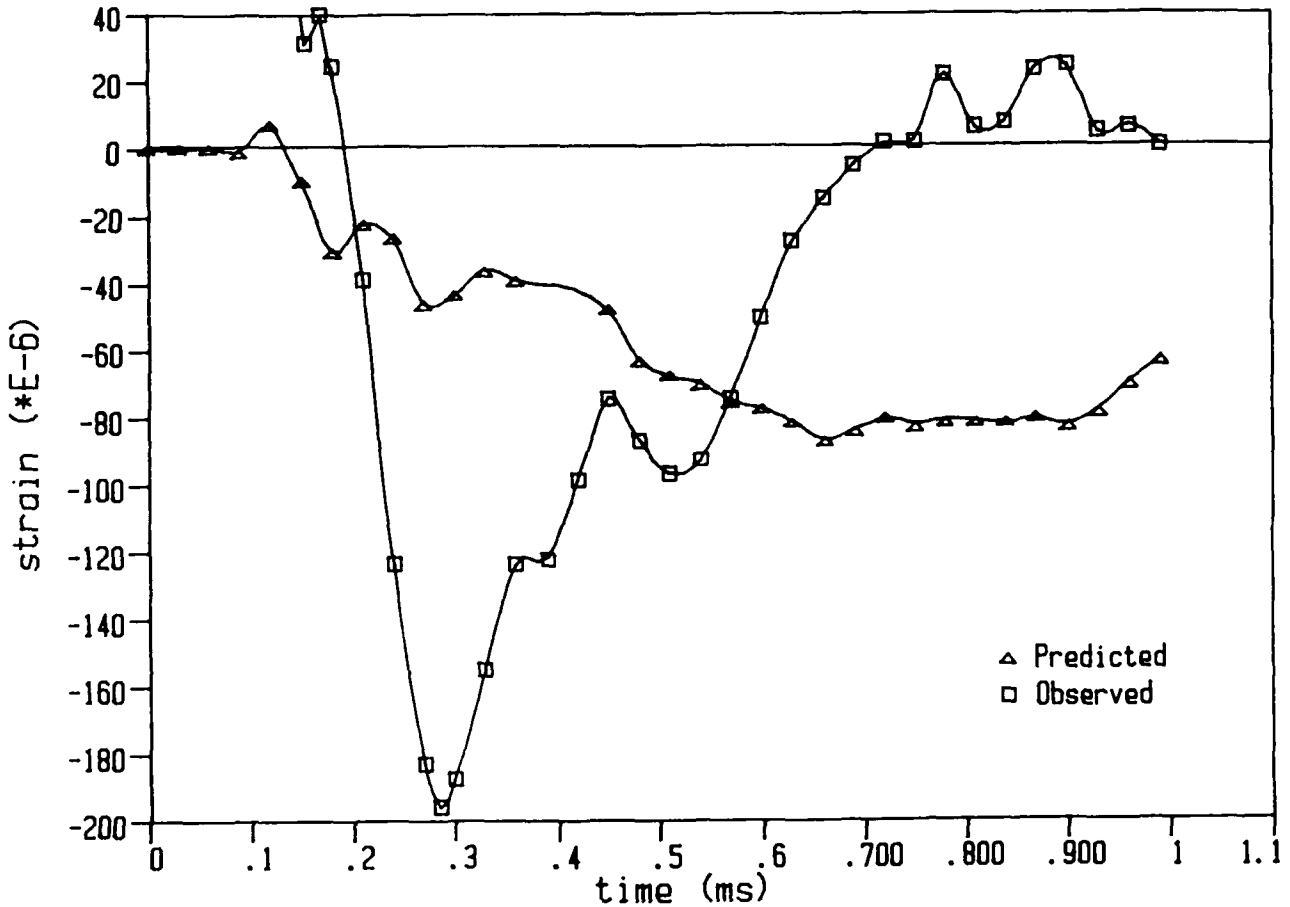

Figure 6.38. Comparison of Predicted and Observed Strains in the Blast Analysis of the Soil-Structure System (gage # 6)

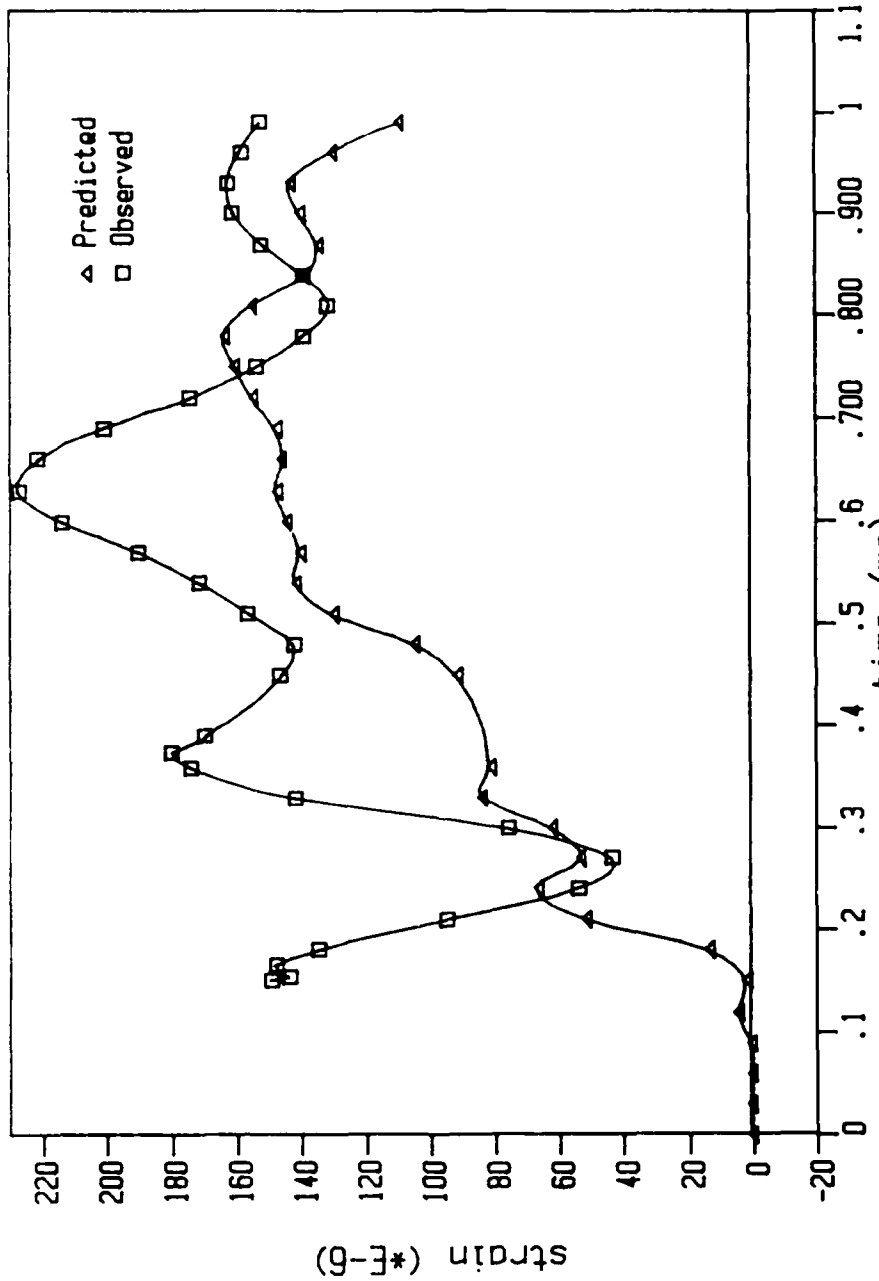

Figure 6.39. Comparison of Predicted and Observed Strains in the Blast Analysis of the Soil-Structure System (gage # 7)

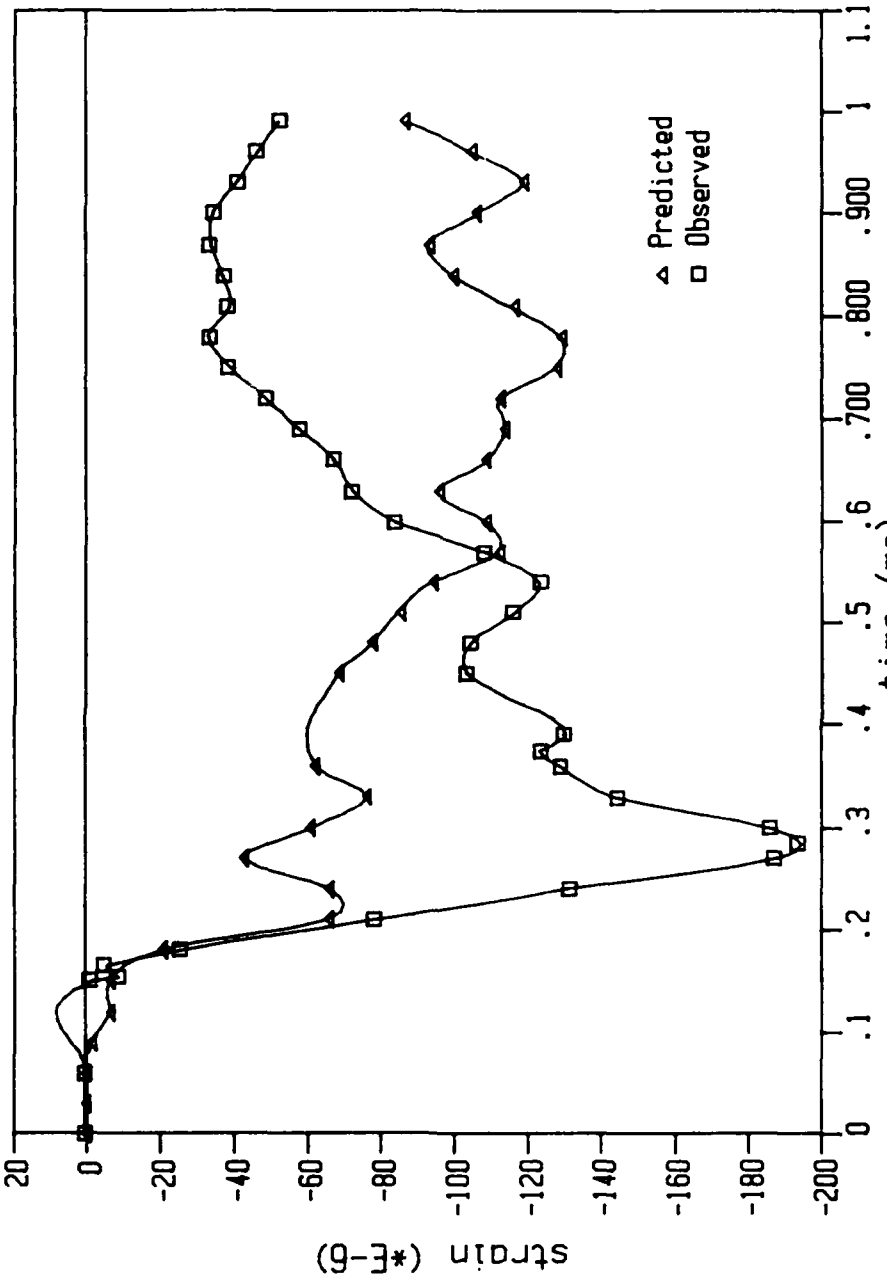

Figure 6.40. Comparison of Predicted and Observed Strains in the Blast Analysis of the Soil-Structure System (gage # 8)

predicted and observed strains are positive indicating tension in these areas. The predicted and observed strains showed a gradual increase with time; however, the peak variation was more pronounced in the observed response.

The analysis predicted the largest stresses in the structure at the bottom slab. This response was surprising because this portion of the structure was the farthest from the detonation. This behavior may be due to the rigidity of the bottom of the soil-structure system. Only 1 inch of soil separated the bottom slab of the structure from the bottom of the bucket. The styrofoam used to absorb the shock wave at the bottom of the soil-structure system was not used in the analysis; therefore, the response of the bottom slab may have been affected by the reflection of the shock wave.

The evaluation of the validity of the numerical model depends on the analysis of the reasons for the differences between predicted and observed values. In general, the causes of these differences can be grouped in two categories; those resulting from experimental errors, and those resulting from the distortion of the numerical model. The problems associated with experimental errors will not be discussed here.

Dynamic modeling in general, and blast modeling in particular, require the consideration of many factors. In this case, the blast analysis is more complicated because the effects of the high gravity environment are not known.

The shock wave due to the explosion in the 60-g environment may very well have different characteristics than the wave at 1-g. The load applied to the soil-structure system in the analysis was determined from curves probably developed at 1-g, and it is not known whether or not this load is appropriate for the high gravity environment. Furthermore, these curves were developed for a spherical charge; however, a cylindrical charge was used in the tests.

Another important factor in the analysis is the choice of the material models. The soil-structure interaction is complex and it is very much dependent on the soil properties. The surrounding soil redistributes the pressure in response to relative displacement of the structure, and this input pressure to the structure depends on the structural geometry, the structural flexibility, the pressure-time history, and the soil characteristics (Balsara, 1970). Yovaish (1984) found that the stresses near the detonation obtained in the nonlinear analysis exceeded those obtained in the linear analysis. This response was due primarily to the nonlinear behavior of the soil. In the nonlinear analysis, the high soil moduli near the detonation transferred the load directly to the structure as a result of the the high stresses in the soil; while, in the linear analysis, the uniform soil modulus distributed the load more evenly over the structure. In the analysis of the scaled soil-structure system, all materials were represented with the same linear model using the properties corresponding to

each type of material. Stresses in the nonlinear range were predicted near the detonation and in the bottom slab of the single bay structure. Although the program NONSAP-C has nonlinear models for concrete and soil, a nonlinear analysis could not be performed due to limitations in computer time and storage.

Another important factor which was not included in the analysis is the effect of the horizontal gravity stresses in the soil mass. It is not known how these stresses affect the behavior of the structure, but they are an important characteristic of the soil.

Another important factor in dynamic analysis is the selection of the integration time step. Previous studies (Clough, Penzien, 1975) have shown a dependency of time step on the following factors:

- rate of variation of the applied loads,
- complexity of damping (not considered in the soil-structure analysis) and stiffness variations throughout the system, and
- period of vibration of the system's predominant response modes.

The time step used in the analysis (0.010 ms) seemed adequate. However, the duration of the first pressure applied on the system (see Table 5.1) was only 0.01062 ms, which is almost the same as the integration time step. Therefore, the time step was large compared to the duration of this pressure load, and it is probable that this load was

not integrated accurately. The inadequate integration of this load is significant because the magnitude of this pressure was the largest applied to the system. In NONSAP-C the load increment per time step is calculated by taking the difference between the applied load at $t + \Delta t$ and the applied load at time t. In the analysis when the first load increment is calculated, the load is already decreasing, and it is close to zero. This fact alone may account for the low stresses obtained in the analysis. A smaller time step should have been used at least for the first 0.020 ms of the analysis. However, problems with the program's performance and with computer time made it impossible.

From the above discussion, it is apparent that further study of the structure's response incorporating nonlinear elements within the system and using smaller time steps is required.

CHAPTER SEVEN
CONCLUSIONS AND RECOMMENDATIONS

Review of Objectives

The major objective of this study was to evaluate the capabilities of the program NONSAP-C to predict

a) the response of a scaled concrete structure subjected to static loads;

b) the response of a scaled concrete structure subjected to dynamic loads; and

c) the response of a scaled buried structure subjected to a blast load in a high gravity environment.

Summary of Results

Static Analysis

The static analyses predicted higher strains than the observed; however, good agreement was observed with respect to the general response of the structure. In the analysis of the reinforced structure, the Chen and Chen model seemed to provide a better response than the Orthotropic Variable-Modulus model.

Dynamic Analysis

In general, the accelerations predicted at the top slab did not agree with those observed. Only the analysis of the reinforced structure with the Orthotropic Variable-Modulus model provided reasonably good agreement with the observed accelerations at the top slab. The differences were attributed to the high stresses developed near the point of load application.

The accelerations predicted in all the dynamic analyses at the center of the inside wall showed reasonably good agreement with those observed. The nonlinear analyses for both the nonreinforced and the reinforced structures provided a better solution than the linear analyses.

Blast Analysis

In general, the magnitudes of the observations from the blast tests were higher than those predicted. The accelerations predicted at the top slab showed good agreement in the magnitudes and frequencies of the response. Predicted and observed peak accelerations were approximately the same; however, they did not occur at the same time. The accelerations predicted at the center of the inside wall showed reasonably good agreement with respect to the frequencies.

The magnitudes of the observed strains were much higher than those predicted; however, good agreement was observed with respect to the general response of the structure.

Compression/tension was predicted were compression/tension was observed. The variation of observed peak strains was more pronounced than the predicted. In general, the predictions showed a gradual increase in the magnitudes of the strains with no definite peak.

Conclusions

1. The program NONSAP-C can safely predict the response of laboratory scaled structures subjected to static loads.
2. The program NONSAP-C can predict the behavior of laboratory scaled structures subjected to simple dynamic loads provided that appropriate integration time steps and material models are used in the analysis.
3. Although the general response of the underground structure subjected to the blast load was predicted with NONSAP-C, uncertainties concerning the load time histories and the effects of the high gravity environment made it difficult to assess whether the program NONSAP-C can accurately predict the response of the underground structure.
4. The definition of the pressure-time history is significant for the appropriate response of the soil-structure system in a high gravity environment.
5. The choice of the material models is significant for the appropriate simulation of stress distribution throughout the soil-structure system.

6. The selection of integration time steps in the analysis of a scaled underground structure is significant for the accurate integration of the pressure-time history of the blast.
7. The analysis of underground structures subjected to blast loads requires the use of large computers that can provide the required cpu time and storage. However, researchers have limited access to such computers which makes the investigation of such structures a difficult task.

Recommendations

1. The analysis of the soil-structure system subjected to a blast load may be improved by introducing nonlinear material models in the areas where nonlinear behavior is expected, provided that computer time and storage are available.
2. The analysis of the soil-structure system should be performed using different time steps to assess the effect of the time step and to obtain an accurate integration of the load and the material models.

APPENDIX A
CALCULATION OF THE MATERIAL CONSTANTS USED IN THE CHEN AND CHEN CONCRETE MODEL

The material constants used in the Chen and Chen concrete model assume different values in the compression and tension-compression regions. They are functions of the ultimate strength of concrete under uniaxial compression (f'_c), uniaxial tension (f'_t), equal biaxial compression (f'_{bc}), and the initial yield of concrete under uniaxial compression (f_c), uniaxial tension (f_t), and equal biaxial compression (f_{bc}).

The equations for calculating these material constants are given below:

For the compression region

$$\frac{A_o}{f'_c} = \frac{(\overline{f_{bc}})^2 - (\overline{f_c})^2}{2(\overline{f_{bc}}) - \overline{f_c}} \quad ; \quad \frac{A_u}{f'_c} = \frac{(\overline{f'_{bc}})^2 - 1}{2(\overline{f'_{bc}}) - 1}$$

$$\frac{(\tau_o)^2}{(f'_c)^2} = \frac{(\overline{f_c})(\overline{f_{bc}})\ (2\overline{f_c} - \overline{f_{bc}})}{3(2\ \overline{f_{bc}} - \overline{f_c})} \quad ;$$

$$\frac{(\tau_u)^2}{(f'_c)^2} = \frac{(\overline{f'_{bc}})(2 - \overline{f'_{bc}})}{3(2\ \overline{f'_{bc}} - 1)}$$

For the tension-compression region

$$\frac{A_o}{f'_c} = \frac{\overline{f_c} - \overline{f_t}}{2} \quad ; \quad \frac{A_u}{f'_c} = \frac{1 - \overline{f'_t}}{2}$$

$$\frac{(\tau_o)^2}{(f'_c)^2} = \frac{(\overline{f_c})\ (\overline{f_t})}{6} \quad ; \quad \frac{(\tau_u)^2}{(f'_c)^2} = \frac{\overline{f'_t}}{6}$$

where (-) denotes the nondimensionalized quantity of the corresponding term with respect to f'_c.

The nondimensionalized quantities were determined as follows

$$\overline{f'_{bc}} = \frac{f'_{bc}}{f'_c} \quad ; \quad \overline{f'_t} = \frac{f'_t}{f'_c}$$

$$\overline{f_c} = \frac{f_c}{f'_c} \quad ; \quad \overline{f_{bc}} = \frac{f_{bc}}{f'_c} \quad ; \quad \overline{f_t} = \frac{f_t}{f'_c}$$

The biaxial compressive strength of concrete, f'_{bc}, was determined as 116% of the ultimate compressive strength of concrete, f'_c (Anderson, et al., 1984); and the initial yield strengths of the concrete (f_c, f_t, f_{bc}) were determined as 45% of the ultimate strength of the corresponding values (f'_c, f'_t, f'_{bc}).

APPENDIX B
MODAL ANALYSIS

The modal analysis of the scaled structure (Figure 1.2) was performed by Dr. M. C. McVay[1] and Habibollah Tabatabai[2]. This analysis was performed using the finite element programs SAP80 (Wilson, Habibullah, 1984) and CAL-80 (Hoit, Wilson, 1983). This programs were run in a IBM-PC AT.

The program SAP80 was used to determine the vibration frequencies (eigenvalues) and the mode shapes (eigenvectors) of the structure. The eigenvalues and eigenvectors were used as part of the input to the CAL-80 program to perform a dynamic analysis on the structure. In this analysis, the structure was loaded at the center of the top slab with an impulsive load of short duration. The analysis was performed with a time step of 0.02 ms, run through 50 time steps. The program calculated the displacements, accelerations, stresses, and moments at the degrees of freedom.

1. Assistant Professor, Dept. of Civil Engineering, University of Florida, Gainesville, Fl 32611.
2. PH.D student, Dept. of Civil Engineering, University of Florida, Gainesville, Fl 32611.

This analysis showed that bending on the structure was essentially in one direction and that the behavior of the structure was essentially plane strain. The bending moment diagrams and the displacements of two lines (Figure B.1) on the top slab of the structure were drawn to illustrate this behavior. Figures B.2 and B.3 show the bending moment diagrams and the displacements of line A-B (Figure B.1) at time steps 25 and 35, respectively. Figures B.4 and B.5 show the bending moment diagrams and the displacements of line C-D (Figure B.1) at time steps 25 and 35, respectively.

The displacements of line A-B showed that this line translates as a whole in the vertical direction with almost no change in the curvature. This type of movement indicates there is no bending in the direction of line A-B, and it is verified by the moment diagram.

On the other hand, the displacements of line C-D showed a curvature in the direction of this line, and this curvature is verified by the change in bending moment across it.

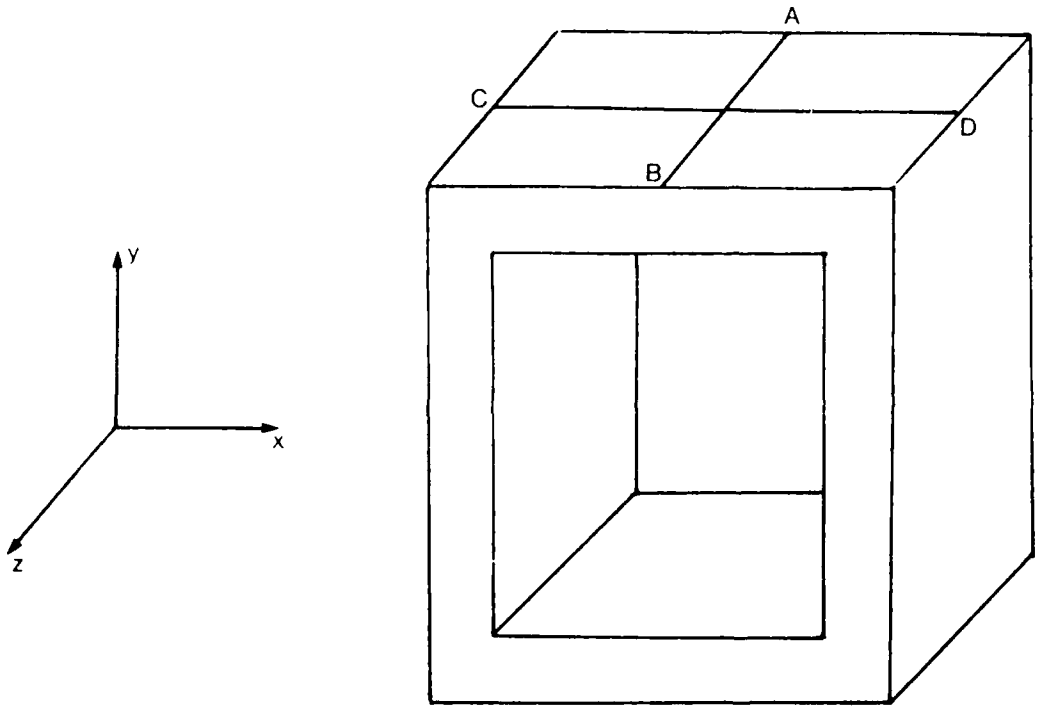

Figure B.1. Lines A-B and C-D on the Top Slap of the Structure

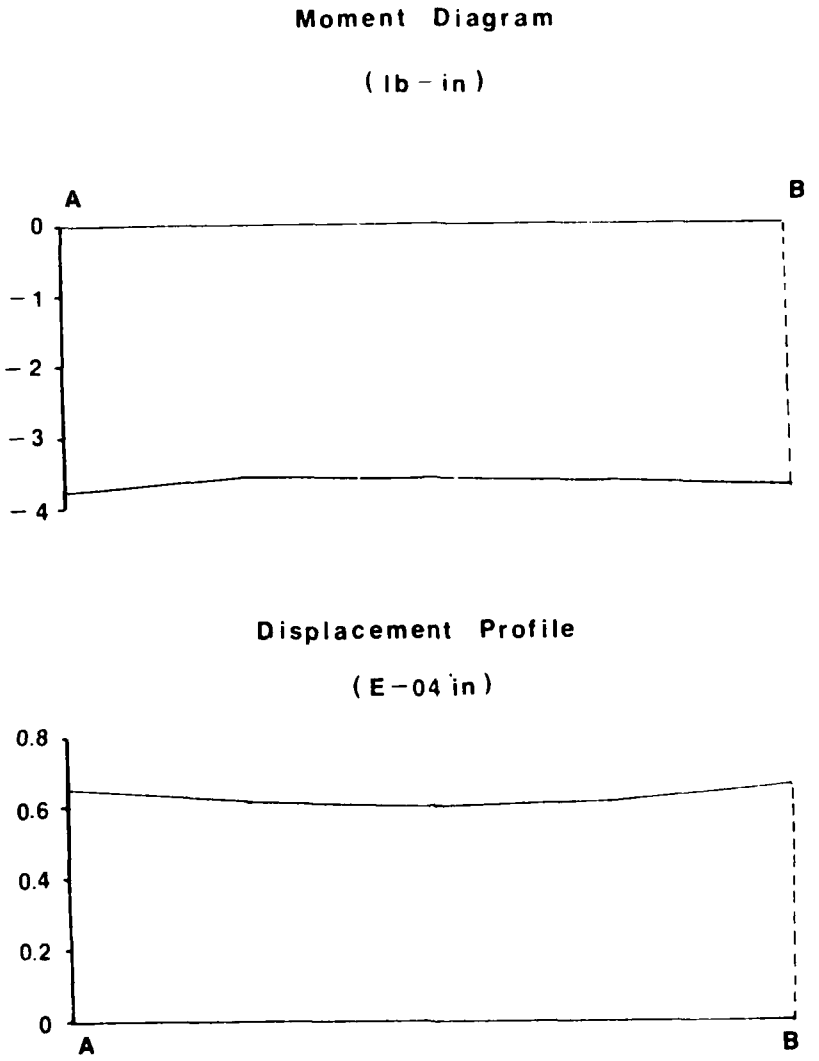

Figure B.2. Bending Moment and Displacement Diagrams of Line A-B at Time Step 25

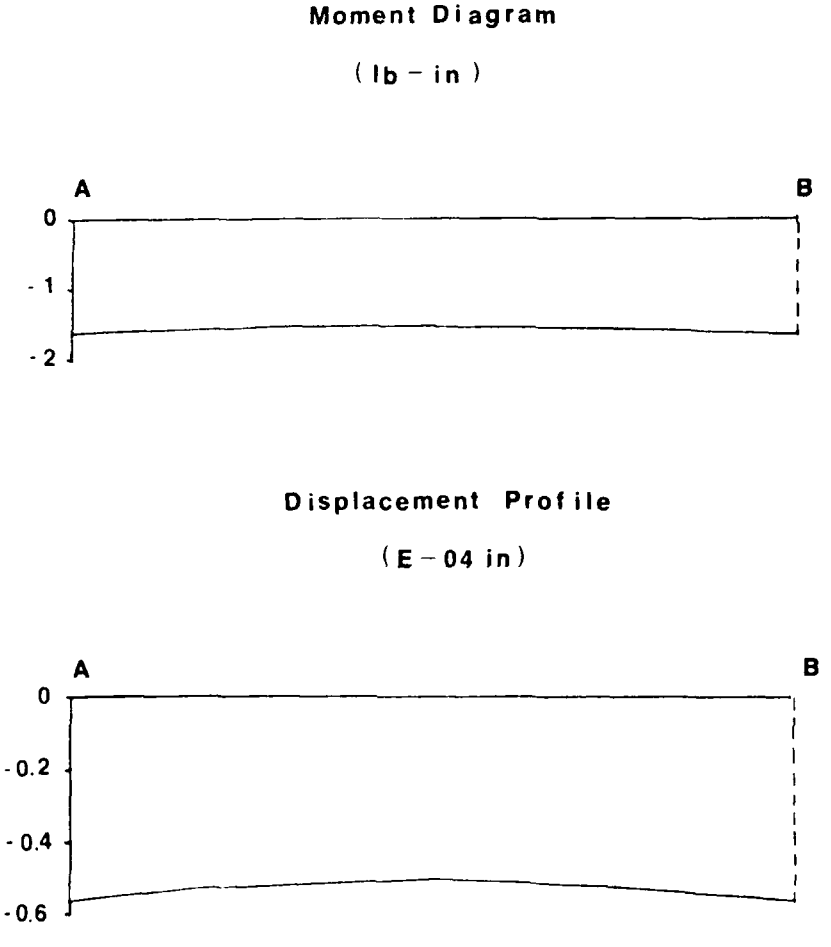

Figure B.3. Bending Moment and Displacement Diagrams of Line A-B at Time Step 35

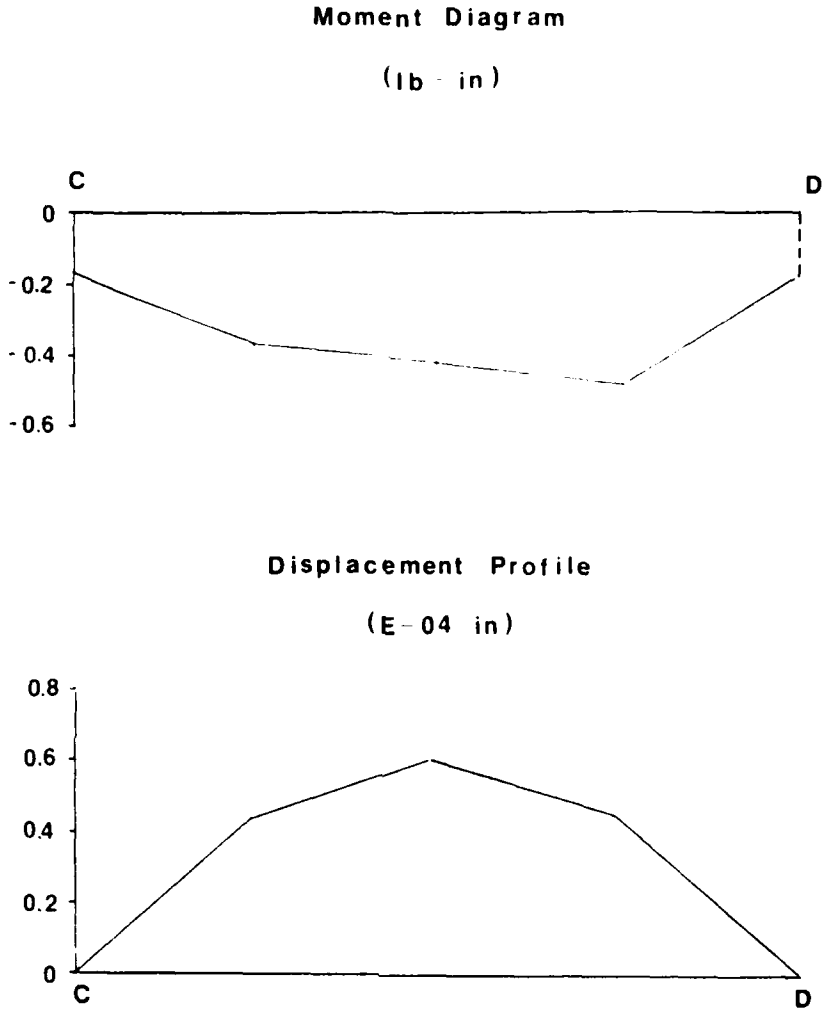

Figure B.4. Bending Moment and Displacement Diagrams of Line C-D at Time Step 25

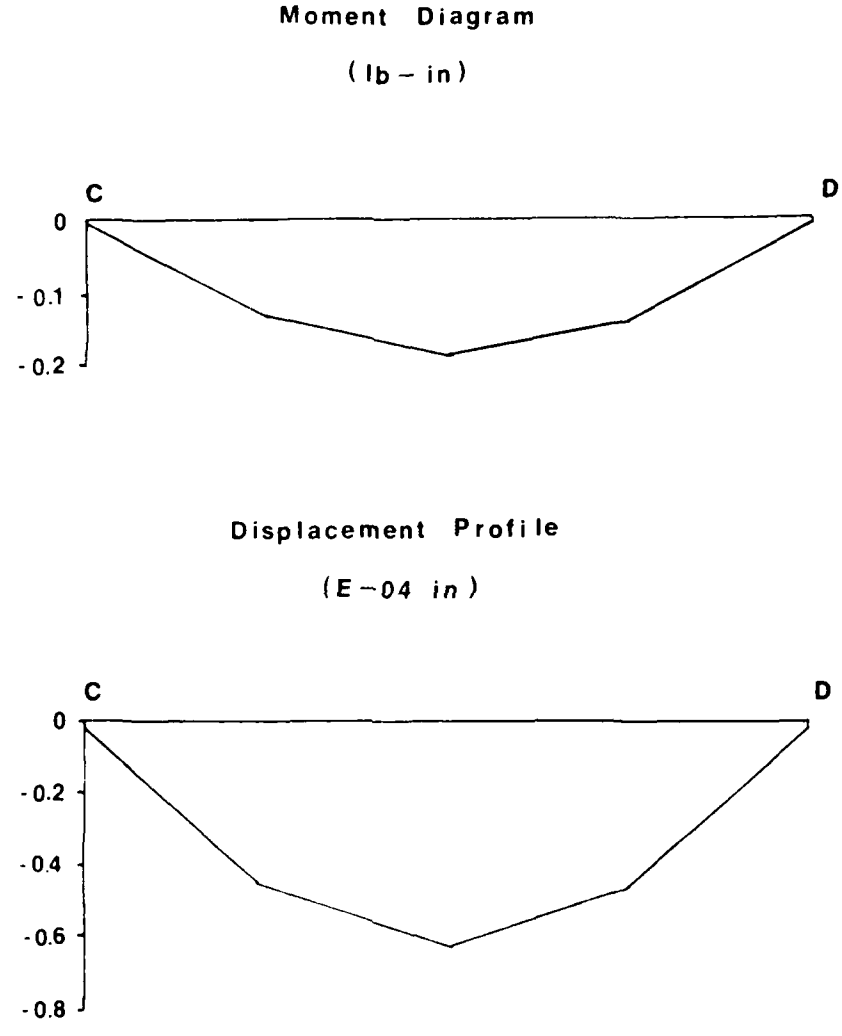

Figure B.5. Bending Moment and Displacement Diagrams of Line C-D at Time Step 35

APPENDIX C
CALCULATION OF THE STEEL REINFORCEMENT

Introduction

The steel was placed in the finite element mesh based in the actual reinforcement used in the laboratory models. The reinforcement in the scaled structures was modeled with Standard Wire Gauges of sizes 28, 24, and 22. In the analyses, the reinforcement was modeled in two different ways according to the material model used for the concrete. Truss bars were used with the Chen and Chen concrete model and the linear model; percentages of steel in the concrete element were used with the Orthotropic Variable-Modulus model.

Truss Bars

The truss bars were placed in the strip as shown in Figure C.1. The location of the bars is approximately at the same location of the reinforcement in the laboratory scaled models. The truss bars were modeled with linear material properties. A cross sectional area was assigned to each bar according to the area of the wire number used in the laboratory models. The areas of the bars along the planes of symmetry were divided by two (one half of the bar is on the symmetric portion of the structure). The cross sectional

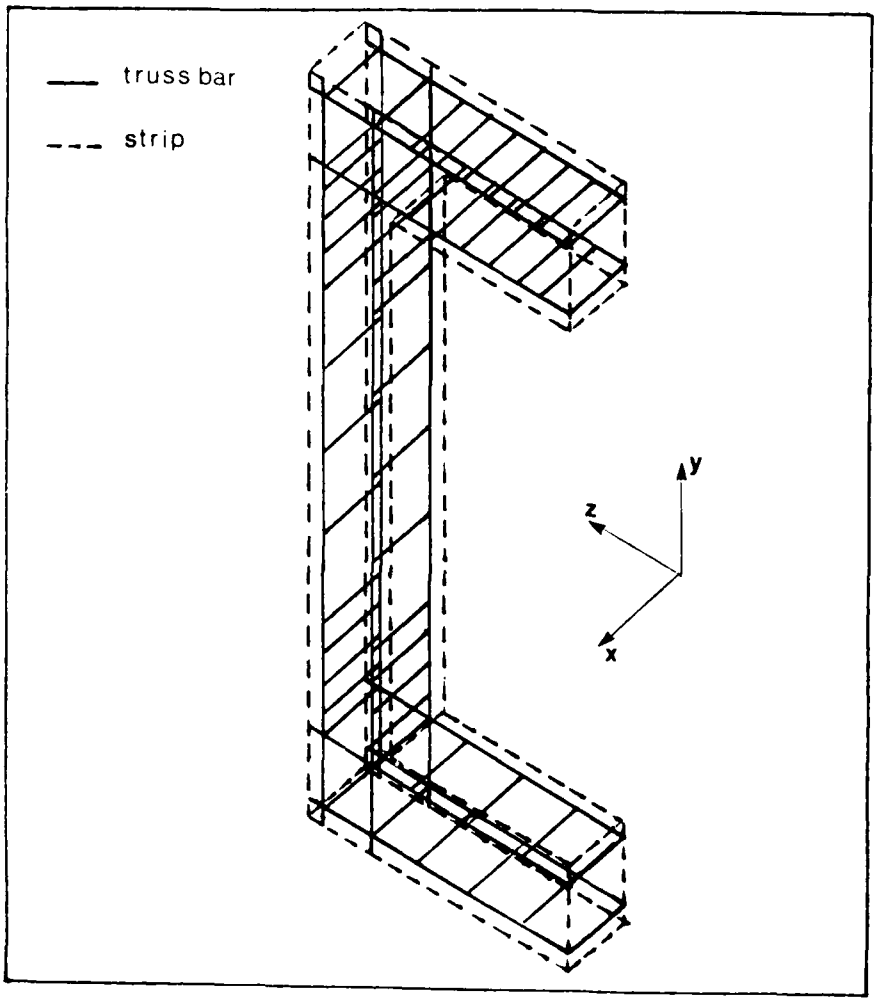

Figure C.1. Location of Truss Bars in the Strip

areas of the bars ard their properties are listed in Table C.1. Refer to Figure C.1 for the orientation of the axes.

Ratios of Steel

The Orthotropic Variable-Modulus model includes the reinforcement in the concrete element as a ratio of the cross sectional area of steel to the cross sectional area of the concrete element. The area of the concrete element used to determine the steel ratios is the area perpendicular to the direction of the wire. These ratios are listed in Table C.2. Figure C.2 illustrates the elements for which steel ratios were specified.

Table C.1. Cross Sectional Areas and Properties of Truss Bars Used With the Chen & Chen and Linear Models

Properties	Element Group	Bar Group	Number of Bars	Direction of Bars	Cross Sectional Area (in^2)
Modulus of Elasticity (psi) 29E+06	Top Slab	1	2	x-direction	2.0774E-04
		2	18	x	4.1548E-04
		3	80	z	9.6364E-04
	Wall	1	128	y	9.6364E-04
Density ($lb \cdot s^2/in^4$) 7.345E-04	Bottom Slab	1	2	x	2.0774E-04
		2	10	x	4.1548E-04
		3	80	z	6.4242E-04

Table C.2. Ratios of Steel Used With the Orthotropic Variable-Modulus Model

Element Group	Element Type	Steel Ratios x-direction	y-direction	z-direction
Top Slab	1	2.07738E-02	0.0	5.4012E-02
	2	0.0	0.0	0.0
	3	4.1548E-02	5.4012E-02	5.4012E-02
Wall	1	2.07738E-02	5.4012E-02	0.0
	2	0.0	0.0	0.0
Bottom Slab	1	1.2465E-02	0.0	5.1394E-02
	2	0.0	0.0	0.0
	3	3.3238E-02	5.4012E-02	5.1394E-02

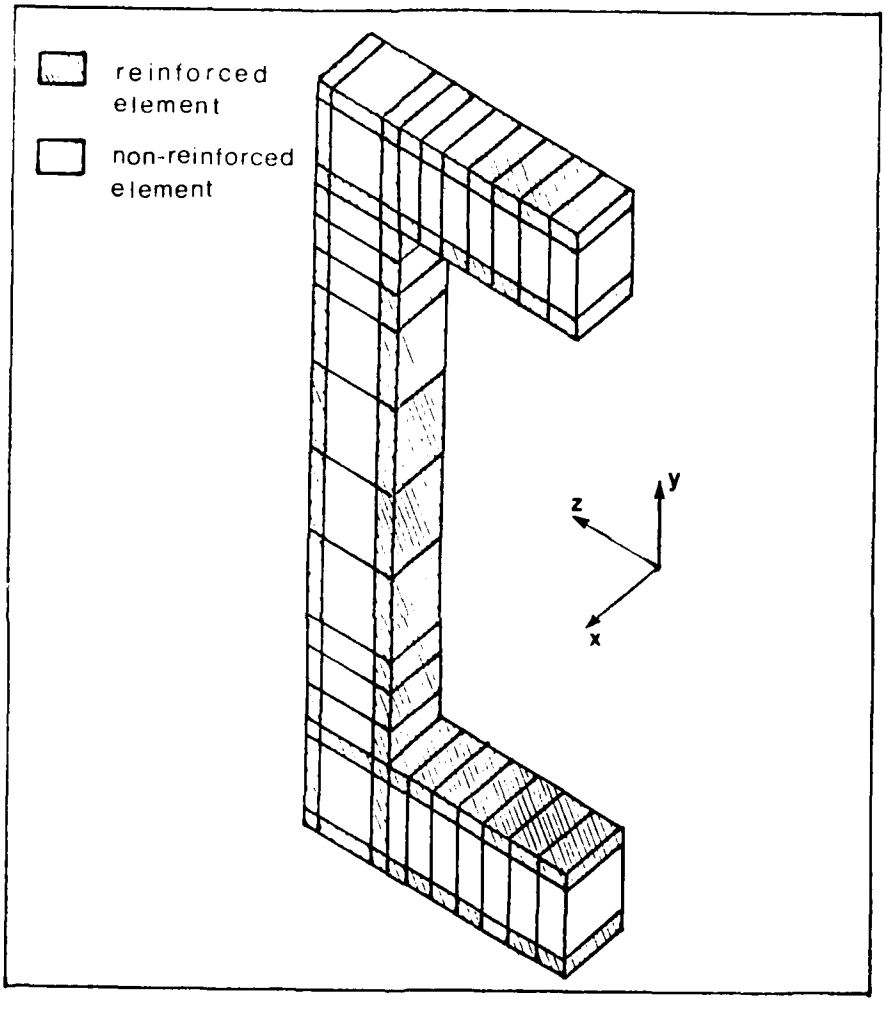

Figure C.2. Elements for Which Steel Ratios Were Specified in the Orthotropic Variable-Modulus Model

BIBLIOGRAPHY

Anderson, C.A.; Smith, P.D.; and Carruthers, L.M., NONSAP-C: A Nonlinear Stress Analysis Program for Concrete Containments Under Static, Dynamic, and Long Term Loadings, NUREG/CR-0416, REV. 1 LA-7496-MS, REV. 1, Los Alamos National Laboratory, Los Alamos, New Mexico, January, 1982.

Belytschko, T., "On the Unconditional Stability of Implicit Algorithm For Nonlinear Structural Dynamics," Journal of Applied Mechanics, Vol. 17, pp. 865-869, December, 1975.

Belytschko, T., "A Survey of Numerical Methods and Computer Programs for Dynamic Structural Analysis," Nuclear Engineering Design, Vol. 37, pp. 23-34, January, 1976.

Chen, A.C.T., and Chen, W.F., "Constitutive Relations for Concrete," Journal of the Engineering Mechanics Division, ASCE, Vol. 101, No. EM4, pp. 465-479, August 1975.

Clough, R.W., and Penzien, J., Dynamics of Structures, McGraw-Hill, New York, 1975.

Cunningham, C.H., Townsend, F.C., and Fagundo, F.E., The Development of Micro-Concrete for Scale Model Testing of Buried Structures, ESL-TR-85-49, Air Force Engineering & Services Center, January, 1986.

Gill, J.J., Centrifugal Modeling of a Subterranean Structure Subjected to Blast Loading, Masters Report, University of Florida, Fall, 1985.

Hoit, M., and Wilson, E., CAL-80 and Simpal: Users Guide, University of Florida, 1983.

Isenberg, J., Adham, S., "Analysis of Orthotropic Reinforced Concrete Structures," Journal of Structural Division, ASCE, Vol. 96, No. ST12, December, 1970.

Melosh, R.J., Utku, S., "Principles for Design of Finite Element Meshes," State-of-the-Art Surveys on Finite Element Technology, American Society of Mechanical Engineers, United Engineering Center, New York, 1983.

Nielsen, J.P., The Centrifugal Simulation of Blast Parameters, ESL-TR-83-12, New Mexico Engineering Research Institute, December, 1983.

Rebora, B., Zimmermann, T., and Wolf J.P., "Dynamic Rupture Analysis of Reinforced Concrete Shells," Nuclear Engineering Design, Vol. 37, pp. 269-297, February, 1976.

Townsend, F.C., McVay, M.C., Bradley, D.M., Cunningham, C.H., Yovaish, D.J., Numerical and Centrifugal Modelling of Buried Structure Response to Near Field Blast, University of Florida Technical Report, No Date.

U.S. Army Engineer Waterways Experiment Station, Fundamentals of Protective Design for Conventional Weapons, Report for Office, Chief of Engineers, U.S. Army, June, 1982.

Wilson, E.L., and Habibullah, A., SAP80 Structural Analysis Programs: A Series of Computer Programs for the Static and Dynamic Finite Element Analysis of Structures, Computers and Structures Inc., Berkeley, California, August, 1984.

Yovaish, D.J., Dynamic Analysis of Buried Structures Subject to High Impulsive Loads of Short Duration, Masters Report, University of Florida, August, 1984.

END

DATE

FILMED

5-88

DTIC